

**EMISSION LINE STUDIES OF
WOLF - RAYET BINARIES**

A Thesis
Submitted For The Degree of
Doctor of Philosophy In the Faculty of Science
BANGALORE UNIVERSITY

B.S. SHYLAJA

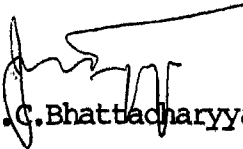
**INDIAN INSTITUTE OF ASTROPHYSICS
BANGALORE
INDIA
1986**

DECLARATION

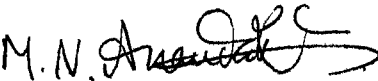
I hereby declare that the matter embodied in this thesis is the result of investigations carried out by me in the Indian Institute of Astrophysics, Bangalore and the Department of Physics, Central College, Bangalore, under the supervision of Prof. M.K.V.Bappu (until his sudden demise in August, 1982), Prof.J.C.Bhattacharyya and Dr.M.N.Ananda Ram.This work has not been submitted for the award of any degree, diploma, associateship, fellowship etc. of any University or Institute.

B.S. Shylaja

B.S.Shylaja
Candidate


J.C.Bhattacharyya

Supervisor


M.N.Ananda Ram

Supervisor

Bangalore

Dated 20th Oct. 1986

ACKNOWLEDGEMENTS

I express my gratitude to late Prof.M.K.V.Bappu, without whose valuable guidance this work would have been impossible. I consider myself fortunate for having his encouragement and inspiration although for a short period only.

I consider it my duty to remember that I was introduced to the field of Astronomy by Prof. J.C.Bhattacharyya. He, after the untimely death of Prof. Bappu in 1982, shouldered the responsibility in the completion of this work. I am indebted to the valuable suggestions and guidance provided by him for the successful completion of this work as well as to Dr.M.N.Ananda Ram, of the Department of Physics, Central College, Bangalore.

As a member of the Indian Institute of Astrophysics, I thank the Director and other staff, who have helped in this work directly and indirectly.

I thank the distinguished members of the Doctoral Committee, Prof. K.N.Kuchela, Prof.P.Paramasiviah, late Prof.N.Madiah, Prof.N.G.Puttaswamy, Prof.N.Devaraj of the Physics Department, Central College and Dr.R.Nityananda of the Raman Research Institute, Bangalore.

I gratefully acknowledge my colleagues, especially Drs. N.Kameswara Rao, R.Rajamohan, M.Parthasarathy, D.C.V.Mallik, C.Sivaram, G.S.D.Babu, T.P.Prabhu and R.K.Kochhar, for their support and continued encouragement in the completion of this work.

Very valuable suggestions during the course of this work were provided by Prof.K.D.Abhayankar & Dr.G.C.Kilambi, Osmania University, Hyderabad, Prof.D.J.Stickland, Oxford, U.K., Prof.R.F.Garrison, David Dunlop Observatory, Ontario, Canada, Prof.C.de Loore, Vrije Universiteit, Brussels, Belgium, Dr.W.Schmutz & Prof.H.Nussbaumer, ETH Zentrum, Zurich, Switzerland.

It is my duty to acknowledge the staff of the Kavalur Observatory, especially Mr.K.Kuppuswamy, Mr.K.Jayakumar, Mr.M.J.Rosario, A.Muniyandi and Mr.M.Appakutty, for their help and cooperation at the telescope. I thank Mr.A.Charles, Mr.F.Gabriel, Mr.V.Chinnappan and Mr.^PA.Santhanam, for their help in making the best use of clear skies with the automated spectrum scanner. Mr.M.N.M.Rao, Mr.A.V.Ananth, Mr.S.Chandramouli and Mr.V.Kutty are acknowledged for help in reducing the data with TDC - 316. Further analysis was carried out with the VAX 11/780, where Dr.S.Giridhar, Mr.Chandramouli and Dr.K.K.Ghosh rendered great help. The drawings incorporated here were prepared by Mr.Muthukrishnan and Mr.Hari Inbaraj, for whom thanks are due. Ms.A.Vagiswari, Ms.Christina Louis and Mr.H.N.Manjunath and other staff of the Library are acknowledged for their kind cooperation.

Assistance at various stages, during the course of this work were provided by Mr.K.Thiyagarajan and the staff of the Faculty Office, Mr.S.Rajasekharan, Mr.M.Batchu, Ms.Meena Krishnan, Ms.B.G.Pramila, for whom I extend my thanks. The final editing by Ms.Sandra Rajiva was immensely helpful.

Thanks are due to Mr.Prabhakar and Mr.Elangovan for help at the copying machine and to Mr.Krishnamoorthy for the binding work.

Finally, I am grateful to my mother Rathnamma, father Ba.Na. Sundara Rao, brothers, Jagadeesha Chandra and Rama Prakash, sisters, Uma Devi and Nethravathi, and brother in law, Abhirama Murthy, for their encouragement and cooperation during the course of this work.

B.S.Shylaja

B.S.Shylaja

CONTENTS

ABSTRACT	1
1. INTRODUCTION	5
1.1 Variability of WR stars	8
1.2 Evolutionary status of WR stars	11
1.3 The atmospheres of WR stars	13
1.4 Need for studying the binaries	17
1.5 Scope of the present investigation	17
2. OBSERVATIONS AND REDUCTIONS	21
2.1 The Instrument	24
2.2 The Instrumental Performance	28
2.3 Standard Stars	30
2.4 Atmospheric Extinction	
2.4.1 Influencing Parameters	32
2.4.2 Comparision with Meterological Data	33
2.5 Instrumental Corrections	41
2.6 Errors	45
3. THE SHORTEST PERIOD BINARY CQ Cep	48
3.1 Observations	52
3.1.1 Reddening Corrections	52
3.1.2 Spectroscopic Studies	53
3.1.3 Light Curves	57
3.1.4 Emission Line Flux	62
3.1.5 Radial Velocity Curves	66

3.2 Correlation between Light and Velocity Curves	66
3.2.1 Helium Lines	66
3.2.2 Nitrogen Lines	73
3.2.3 Carbon Lines	75
3.2.4 Line Blends	79
3.3 Model	79
3.3.1 Light Curve Solutions and the Nature of the Companion	79
3.3.2 Circumstellar Matter	83
4. THE BINARY NATURE OF HD 50896	88
4.1 Observations	90
4.1.1 Spectrophotometry	90
4.1.2 Reddening Corrections	90
4.2 Results	92
4.2.1 Photometry	92
4.2.2 Light Curves	94
4.2.2 Emission Line Flux	94
4.3 Line Flux Variations	99
4.4 Model	106
5. THE MEMBERS OF THE CLUSTER NGC 6231	109
5.1 Observations	111
5.1.1 Spectrophotometry	111
5.1.2 Photometry	111
5.2 Results	116
5.2.1 HD 152270	116
5.2.2 HD 151932	116
5.2.3 Interstellar Reddening	120

5.3 Possibilities of Companion for HD 151932	122
5.4 Atmosphere of HD 151932	126
5.5 Possible Atmospheric Eclipses in HD 152270	126
5.6 Atmosphere of HD 152270	129
6.THE LINE EMITTING REGIONS	131
6.1 Roche Surfaces	132
6.2 Inferences from IR and UV Studies	137
6.3 Comparision with other eclipsing systems	138
6.4 Peculiarities of Some Emission Lines	141
6.4.1 Total flux variations	142
6.4.2 Radial velocities	143
6.4.3 Effects of the companion	146
6.5 Sporadic Events	151
6.6 Evolution	152
7.SUMMARY AND FUTURE PROSPECTS	158
REFERENCES	163
LIST OF PUBLICATIONS	174

To

my beloved father

Sundara Rao

ABSTRACT

The construction of a kinematical and physical picture of a Wolf - Rayet atmosphere was attempted by late Prof. M.K.V. Bappu and the present work is a continuation of the understanding of these atmospheres. The binary systems have been chosen with the idea of seeing the variation of the atmospheric structure as it manifests in the presence of the companion. The simple method of observation of the flux variations was suggested by Prof. Bappu for this study.

Generally the atmospheres of Wolf - Rayet (WR) stars are known to be extended. This was derived from the velocities of the emission and associated absorption lines. Further studies have shown that there is some type of stratification possibly prevalent in these atmospheres.

To study this, the binary systems with WR components are chosen. When the companion passes in front of the primary WR component, atmospheric eclipses are expected to become noticeable. This can be observed as the variation in the total flux of the emission lines under study. Spectrophotometric techniques provide accurate flux estimates and continuum energy distributions as well. The effect of the earth's atmosphere on the measured value of flux and the role played by the minor constituents of the atmosphere will have to be taken into account for this estimation.

For this study, one of the objects chosen was the shortest period binary with WN7 component, CQ Cep. The line profiles have established the complexity of the atmosphere. The eclipse effect

is displayed by only one line - N V line at λ 4603. The radial velocity curves (RV) for different emission lines indicate different orbital solutions. The continuum distribution also does not reveal the identity of the companion. Based on the flux variations, it is possible to arrive at the asymmetric distribution of the line emitting material as a possible cause for non-eclipse effects.

The second object chosen for study is HD 50896, which was considered as single earlier. Recent accurate RV and light variation studies have given it the status of a binary. The emission flux variations, which are reported in this work, reflect the asymmetric distribution of the line emitting material. The nature of the companion becomes indirectly evident, in the distortion of the atmosphere. Fast photometric measurements show variations, which may imply mass transfer and accretion.

The open cluster NGC 6231 has two WR members associated with it, one of them being HD 152270 (WC7 + O). This is an established binary with a period of 8.9 d. The measured flux show possible eclipse effects only for the high excitation lines like C III and C IV. On the other hand, the He I and He II show a scatter implying their non participation in the orbit. The photometric measurements in regions, which avoid the effect of emission lines, show that there is no eclipse of the continuum, as expected from the angle of inclination of the orbit, 39° .

The other member of the cluster, HD 151932 (WN7), considered single, shows irregular variation of flux all through. However,

the photometric variations display a periodicity of about 6 d. Confirmation of this requires better resolution spectra to detect small changes of radial velocity, if any. The existence of a compact companion puts it to the second WR phase in the evolution of a close massive binary and, at the same time, its membership to the cluster becomes doubtful.

From the study of the binaries and suspected binaries, the effect of the companion on the extended atmosphere can be partly understood. The shortest period system, CQ Cep, has the flux variations caused by the asymmetric atmospheric structure, which may be explained by wind dominant Roche surfaces. Similar variations in HD 50896, with a slightly larger period, show that the companion is effective in distorting the line emitting regions. The flux variations of the spectroscopic binary HD 152270 shows that, although the continuum eclipses are not seen, there is a possibility of atmospheric eclipses. Similar study of HD 151932 reveals the important aspect of a possible periodic variation only in the continuum and not of the line flux. This aspect can be established only by more detailed photometric and spectroscopic investigation.

Thus, it appears that there is a general stratification common to all the above mentioned WR systems - the higher excitation lines arising closer to the photosphere. This leads to the distortion of all the emission lines, like N IV, C IV etc for CQ Cep. In HD 50896 such high excitation lines show moderate variations, while He II lines are more distorted. In case of the still longer period binary HD 152270, the eclipse effects are

seen for the higher excitation lines like C III and C IV, and not for the He II and He I lines. When these results are compared with the available information on other binaries, many interesting results emerge. The atmospheric eclipse is evident in many spectroscopic binaries indirectly. Also the behaviour of the $\lambda 4686$ line is different from other He II lines in WN binaries. Similarly the WCs are likely to have the $\lambda 5696$ line of C III as a special case. The results of HD 50896 and HD 151932 show different types of emission and light variations. The possibility of a compact companion in the latter case becomes smaller, especially when the results on another system with suspected compact companion, HD 76536, are compared. Finally, the evolution of the WR phase in binaries and the possible effect on the atmospheric structure are discussed, from which it appears that although the subgroups of WRs are heterogeneous, the stratifications in their atmospheres, in general, are similar.

1. INTRODUCTION

The Wolf-Rayet stars, abbreviated as WR stars, are characterised by broad emission lines of helium, oxygen, carbon and nitrogen, at various stages of ionization. They are broadly classified into two groups. The first group is associated with OB stars and the second with planetary nebulae. The latter group objects are generally found in the disk of the Galaxy and are separated out by their galactic distribution and proper motions.

The WRs are further classified into various subgroups on the basis of the relative strengths of nitrogen or carbon lines of different excitation as well as helium and oxygen line intensities. The notation of WC, for those with strong lines of carbon, and that of WN, for those with strong lines of nitrogen are used for separating them into two sequences. In the earliest classification scheme by Beals (1938), no attention was paid to the absorption lines in the spectra of some WR stars. Later Hiltner & Schild (1966) modified the choice of different groups of emission lines for purposes of classification. They recognised subgroups WN4 to WN8 and WC5 to WC9, based on the corresponding line strengths of nitrogen and carbon lines. The lines from the highest ionization levels are stronger in WN4 and WC5, and relatively weak in WN8 and WC9. Although this classification was not quantitative, it was implied that the general level of excitation level increases as one goes from subgroups 4 to 8. WN was further subdivided into WNA and WNB; WNA has relatively narrow emission line and strong continuum while in WNB the lines are broad.

Smith (1968a) reclassified these subgroups taking into account both nitrogen and helium lines, in case of WN, and carbon, helium and oxygen in case of WC (Table 1.1).

The association of WRs with young clusters and Associations is expected to restrict them to the spiral arms of the Galaxy, like the Cygnus-Orion arm, Sagittarius-Carina arm, Vela spur and Perseus arm and none towards the anticentre direction. However, in the most recent and exhaustive catalog of van der Hucht et al. (1981), where all identified galactic WRs down to 16th magnitude are listed, their distribution is not found to be restricted to the galactic plane, as was thought earlier. The new, high space velocity stars included in the list make it a complicated distribution.

The luminosities, temperatures and other physical parameters of WRs are not easy to determine because of the observational difficulties and lack of satisfactory models. The relation between the two subgroups also is not known definitely. Two stars of the same subgroup do not show identical energy distributions. However, with some WRs being the members of open clusters and a large number of them in the neighbouring galaxies of the Large Magellanic Cloud (LMC) and the Small Magellanic Cloud (SMC) identified, it has been possible to derive the range of luminosities and effective temperatures (Smith, 1968b).

Recently, Massey (1985) has discussed the distribution of WRs in the Galaxy and also in the local group of galaxies. He has shown that WRs can effectively be used as probes of massive star contents in other galaxies, by emission line surveys.

Table 1.1. Classification of Wolf-Rayet Stars (Smith, 1968b)

WN types	Nitrogen ions	Other criteria	
WN 9	N III present, N IV weak or absent	He I, lower Balmer series P Cyg	
WN 8	N III \gg N IV	He I strong P Cyg, N III λ 4640 \approx He II λ 4686	
WN 7	N III $>$ N IV	He I weak P Cyg, N III λ 4640 $<$ He II λ 4686	
WN 6	N III \approx N IV, N V present but weak		
WN 5	N III \approx N IV \approx N V		
WN 4.5	N IV $>$ N V, N III weak or absent		
WN 4	N IV \approx N V, N III weak or absent		
WN 3	N IV \ll N V, N III weak or absent		
WN 2	N V weak or absent	Strong He II	

WC types	Carbon ions λ 5696 C III / λ 5805 C IV	Carbon, oxygen ions λ 5696 C III / λ 5592 O V	Other criteria
WC 9	C III $>$ C IV	O V weak or absent	C II present
WC 8.5	C III $>$ C IV	O V weak or absent	C II not present
WC 8	C III \approx C IV	O V weak or absent	
WC 7	C III $<$ C IV	C III \gg O V	
WC 6	C III \ll C IV	C III $>$ O V	
WC 5	C III \ll C IV	C III $<$ O V	
WC 4	C IV strong, C III weak or absent	O V moderate	

1.1 Variability of WR stars

Many of the WRs were identified as light variables and spectrum variables. From a study of these systems, it was found that four of them show eclipses - V444 Cyg(4.2d), CQ Cep(1.64d), CX Cep(2.1d) and HD 211853 (6.6d) - the orbital periods are indicated in parenthesis. The case of CV Ser is strange because it has eclipses recorded prior to 1970 (Hjellming & Hiltner, 1963) and later the eclipses were not detected at all (Cowley et al., 1971).

Some objects like HD 50896, HD 96548, HD 164270 and MR 87 were known to be definitely variables, while some like HD 76536, HD 104994, MR 80 and HD 165763 were suspected to be variables (cf. Underhill, 1968).

The presence of absorption lines in the spectrum of some WRs, noted in the classification scheme itself, and in some cases the associated variability, made it possible to postulate the OB companion to these stars. This led to the discovery of the WR spectroscopic binary, V444 Cyg, as early as in 1939 (Wilson, 1939). Later many other systems displaying variations in spectral features were discovered and the absorptions were generally associated with the companion. Niemela (1973) pointed out the H absorption line behaviour in the binary HD 92740, suggesting a velocity curve that goes with the WN component itself. This phenomenon, in CQ Cep (McLaughlin & Hiltner, 1941) made it difficult to identify the spectral type of the companion. Lately it has been found that many, in the subgroup WN7 to WN9, display absorption lines. Therefore the conclusive

evidence on the binary nature should be derived from the observations of periodic phenomena like radial velocity (RV) or light variations. Many WRs with absorption features in their spectra have been investigated by Massey (1980, 81), Massey & Conti (1981a, b, c) and Massey, Conti & Niemela (1981) in a series of papers. Thus only twenty out of the 159 galactic WRs are established as binaries in the catalog of van der Hucht et al. (1981). As mentioned earlier, only four of them show eclipses (Table 1.2).

An inspection of this Table shows that the binary nature predominantly appears among the subgroups WN4 to WN7 and WC6 to WC8 only. The other interesting point is that the orbits are generally circular, except the long period ones, like γ^2 Vel (P=78.5d), HD 190918 (P=112.8d) and HD 92740 (P=80.4d), and those with small mass functions like HD 50896 and HD 197406. Further, it may be seen from the observed mass functions that the range of masses of WN is different from that of WC.

The difference between the WN and WC groups has been attempted to be understood in terms of the ionization, excitation and structural differences among them rather than the chemical compositions. Underhill (1968) attributes the differences mainly to the temperatures. However, there are some unexplained features. The similarity of the C III and N III ionization levels and the dissimilar spectra of some subgroups make it difficult to draw any conclusion. The infra red measurements (Hackwell et al., 1974; Cohen et al., 1975) have shown that there is an infra red excess of energy at 10μ , which

Table 1.2 Binaries with Wolf-Rayet components from van der Hucht et al. (1981).

WR #	HD	P days	Sp Type	f(M)	$\frac{M \sin^3 i}{M_{\odot}}$	i	$\frac{M_{WR}}{M_{\odot}}$	$\frac{M_{WR}}{M_2}$	e
21	90657	8.2	WN4	10.4	9.5	45	25	0.43	0.0
31	94546	4.9	O4-6	12.4	21.1		58	0.34	0.0
127	186943	9.55	WN4	3.9	8	70	24	0.52	0.0
133	190918	112.8	O9V	1.24	9-11	25	13	0.26	0.43
151	CX Cep	2.13	WN4.5	5.4	17-21	50	25	0.43	0.0
6	50896	3.76	O9.5I	0.015	0.7		35	(6.9)	0.34
139	193576	4.21	WN5	12.4	12	72	12-16	0.39	0.0
136	192163	4.5	SB1	0.0002	10		31	(29)	?
141	193928	21.64	WN6	4.9	26			(0.55)	0.0
153	211853	6.69	SB1	16.1		50-60	10-25	0.22	0.0
47	311884	6.34	O	14.4	40	70	45-114	0.84	0.0
22	92740	80.35	WN6	1.67	47		50	2.67	0.55
155	211884	1.6	O5V	5.1	64	40	60	1.19	0.0
148	CG Cep	4.32	O?	0.025	24		19	0.11	0.11
145	AS 422	22	WN7	7.7	23				
			SB1		19				
			WN						
			WC						
BINARIES WITH WC COMPONENTS									
48	113904	18.34	WC6	9.9					0.0
42	97152	7.89	O9.5I	3.7	3.6	35	20	0.59	0.0
11	152270	8.89	WC7	2.7	6.1	25	34	0.36	0.0
79	68273	78.5	O7V	13.7	1.8	70	20	0.54	0.40
113	168206	29.71	WC7	15.0	5.0	60	26	0.37	0.0
			O5		17		30		
			WC8		32		38		
			O9I		11		11-14		
			WC8		22		30		
			O8V						

is characteristic of free-free emission. They also have shown that WC 8 to 9 subgroups show cool blackbody emission with temperatures ranging from 800 to 1800° K. Therefore, the origin of this circumstellar dust, which appears selectively in some subgroups only, also is another problem. Many WN subgroups show the lines of carbon as well; while the WC subgroups show little or no nitrogen. Therefore, the classification may be termed as based on predominant ions, which are 'well developed' in each subgroup (Smith, 1973).

Conti (1982) classifies the subgroups on the basis of elemental abundances, as follows; WN subtypes result from the evolution of stars in which the CNO equilibrium products are observed on the stellar surface. These include helium and nitrogen and diminished carbon and oxygen. WC subtypes result from the appearance of products of helium burning in which carbon and oxygen are enhanced at the expense of helium and nitrogen. It may be remembered that the central stars of planetary nebulae, which represent the final stages of evolution, are rich in carbon and oxygen, as a consequence of their evolution.

1.2 Evolutionary Status of WR stars

The WRs are accounted for by various scenarios, which are generally centered on one aspect of evolution. The binary mass exchange phenomenon was suggested by Paczynski (1973) for the formation of the WR phase of the more massive component. Conti (1982) discussed the similarities of the WN and Of objects suggesting an evolutionary connection between the two. The detection of dust shells surrounding certain subtypes led Chiosi

et al. (1978) to postulate a post red giant phase corresponding to the WR phenomenon. Maeder (1983) has put forward the argument of chemical mixing being responsible for the WR phenomenon. He also has shown that the time spent by a massive star as a red supergiant and as a WR object is dependant on the metallicity.

Appenzeller (1970) has derived the vibrational instability of massive stars, which is discussed in the context of H II regions by Conti & Massey (1981). The nebulae are thought to be dominated by the effects of a few, very massive, unstable objects with WR spectra.

In the case of binaries, two WR phases of almost equal durations have been postulated (Tutukov & Yungelson, 1979; de Loore & De Greve, 1975; van den Heuvel, 1976).

OB + OB -----> WR + OB -----> C + OB -----> C + WR

The Roche lobe overflow (RLOF) provides a strong means of mass loss in binaries. The evolutionary calculations of de Loore (1980) show that the first phase corresponds to the more familiar (WR+ OB) phase, which can be detected as double line spectroscopic binaries. The following supernova explosion of the WR component gives a pair (Compact star + OB). This eventually evolves into (Compact star + WR) as a runaway single line spectroscopic binary. Following this scheme, it appears that the frequency of the (WR + Compact) systems might be similar to that of (WR + OB) systems. Therefore, it becomes important to find out whether the single stars are truly

single, or (WR + C) systems, or (WR + OB) systems, in which the OB companion is masked. It was possible to detect the other three phases of the scenerio, namely binaries with both OB components, WR + OB systems and OB + Compact systems. Even the following phase of WR + Compact may be considered as detected, when one includes the possibility of runaway pulsars as binaries (Radhakrishnan, 1985).

The detection of (WR + C) phase needs high resolution spectra in optical, supplemented by UV and IR data, as has been done for (OB + C) systems (Garmany et al., 1980). Indirect evidences like low mass functions from radial velocity (RV) curves, peculiarities in light curves, larger values of $|z|$, the distance from the galactic plane, associated nebula or ring, are probably useful here. Table 1.3 lists the possible candidates for (WR + C) phase (cf. Moffat, 1981). It may be noticed that there is a preponderance of low excitation subgroups of WN, excepting the case of HD 164270, which is WC9. Many of the candidates like HD 50896, HD 192163 and HD 197406 have more than one of the four properties mentioned above as indirect evidences. The derived masses of the WR components are as large as those derived for those in (WR + OB) systems.

1.3 The Atmospheres of WR Stars

Beals (1938) made the first attempt to study the WRs in great detail. Noting that the spectral line profiles resemble that of novae, he postulated the expanding atmosphere hypothesis. Such an expanding atmosphere is known to exist for many other systems like the novae, supernovae, the P Cygni type

Table 1.3
WR+ COMPACT SYSTEMS WITH LOW MASS

HD	Sp. Type	Assoc. H II	Z (pc)	P (d)	e	K (km s ⁻¹)	M _{WR} /M _⊙
50896	WN5	S308	-356	3.8	0.34	36	12
192163	WN6	NGC 6888	+ 53	4.5	0.3	20	27
193077	WN6(+OB)	S109	+ 29	2.3	0.0	16	51
97950	WN6(+OB)	NGC 3603	- 68	3.8	0.0	54	(5)
38268	WN6(+OB)	30 Dor	-	4.4	0.0	43	(7)
197406	WN7	-	+799	4.3	0.11	90	(1.3)
96548	WN8	RCW 58	-342	4.8	0.0	10	71
86161	WN8	282.2-2.0	-181	10.7	0.0	6	104
209 BAC	WN8	S 80	+264	2.4	0.0	13	68
177230	WN8	-	-824	1.8	0.0	22	35
164270	WC9	-	-228	1.8	0.0	20	41

stars and the supergiants. Bappu (1951a) has shown that all emission lines originate in these extended atmospheres and their profiles reflect the complexity of the dynamics prevalent in these atmospheres. He studied the line profiles of many WR stars and derived the colour temperatures, assuming their formation in an extended shell.

As mentioned earlier, it was observed that some WRs show absorption lines in their spectra. It was also found that these absorption lines arise in a region different from those of emission lines. This was shown by Bappu (1973) as an inverse relation between the velocities of these absorption components and the corresponding excitation potential of the upper level. This relation implies the material accelerating outwards. Such weak absorptions were detected for C IV lines as well (Giridhar & Bappu, 1978) and for many more systems (Moffat & Seggewiss, 1978; Niemela & Sahade, 1980).

Based on a detailed study of the WN7 stars, Moffat & Seggewiss (1977) show that the N V lines with average velocity of -55 kms^{-1} are formed closer to the star's surface than He II (-155 kms^{-1}), N IV (-200 kms^{-1}) and He I (-670 kms^{-1}). The line of He I at $\lambda 3888$ is different from others: it displays a flat topped profile and the velocity is more negative (-1200 kms^{-1}). Therefore, it is more likely that H absorption lines are not formed in the 'extended envelope', where the emission lines originate, but they are formed closer to the photosphere (Sahade, 1981). This further requires that the atmospheres be transparent to such photospheric lines, which is not true in

many cases. Sahade (1981) mentions about the following exceptions:

1. HD 193077, WN5, which displays absorption features and is apparently single.
2. θ Muscae, (WC6 + O9.5-B0), which also shows absorption features.

Thus, the variability of line profiles can be intrinsic and need not necessarily have any relation to the binary nature. In case of the binaries, which are established for duplicity by other techniques, the profile variation can be used as a tool to understand the nature of the companion, which, in many cases is not possible otherwise. The non periodic intrinsic variations are likely to be present in binaries as well. For single systems, such variations can be associated with the asymmetry and inhomogeneity of the atmosphere.

Generally, the observations of WRs are difficult because of the faintness of the objects. Further, they are available together as a group in selected regions of the sky. Hence a derivation of any periodic variation can lead to anomalies. A more detailed examination (Vreux, 1985) of such derivations from light variations shows that all derived periods are aliases of shorter periods. The true period in most cases turned out to be about 0.45d and a non-radial pulsation explanation has been offered. Therefore, it appears likely that many stars grouped as (WR + C) systems, are single.

1.4 Need for Studying Binaries

Bappu (1951a) had mentioned that the study of binaries offer wider scope for understanding the peculiarities, because a variable phenomenon discloses more of its nature than a steady one. Eclipsing systems provide still better chances as seen in case of ζ Aur, where the eclipse effects of the extended atmosphere of the K star by the B companion can be observed. When any spectral line changes its profile, this can be interpreted in terms of the geometry of the situation.

Of the many binaries listed in Table 1.2, only V444 Cygni has been well studied (Kuhi, 1967; Ganesh et al., 1968). When the companion passes in front of the primary, WN5, atmospheric eclipse effects are expected to become noticeable. However, the tidal effects dominated the situation and it was not possible to study the atmospheric structure. Ganesh et al. (1968) showed that the different emission lines yield different types of orbital solutions, which may reflect the effect of the companion on the extended atmosphere. Such results emphasize the need of the study of binaries in great detail.

1.5 Scope of the Present Investigation

The variability of the total flux as measured from the ground based telescopes can be used as a tool for understanding the emission line behaviour in binaries. The binaries are CQ Cep and HD 50896. Further, two more systems HD 151932 and HD 152270 which are members of a cluster are studied for possibility of a companion in one case and for possible atmospheric eclipses in the other case.

The second chapter describes the instrument and the reduction procedure. A detailed study of the extinction due to earth's atmosphere in the context of astronomical observations also is presented. The method of derivation of absolute flux also is described. A comparison of the extinction measures with the meteorological measurements of ozone and water vapour content is made to understand the effect of these on the earth's atmospheric extinction.

Each system, that is studied in this work is presented as a separate chapter. The Chapter 3 deals with the study of CQ Cep, which is chosen because of the short orbital period (1.64d). This was studied spectroscopically by many investigators and the complexity of the emission and absorption lines were discussed. In this work, all the lines in the visible region, which were easily identifiable, have been studied for flux variations. This is supplemented with the data from the collection of recorded spectra by Bappu. The technique of spectrophotometry used here also provides monochromatic magnitudes at different wavelengths so that the emission-line-effect-free light curves can be constructed. Since none of the emission or absorption lines depict the movement of the companion, the identification of the companion has been sought through energy distribution studies. This situation of no contribution either to line flux or to the continuum is sought to be resolved in this Chapter.

The fourth Chapter describes the study of HD 50896, which was considered to be single till Firmani et al. (1979) established its duplicity. The emission line variations in

different seasons have been studied to understand the asymmetry in the atmospheric structure, which is possibly due to the presence of the companion. The signature of the companion is sought for in the flux and continuum measurements.

The fifth Chapter deals with the two members of the open cluster NGC 6231, HD 151932 and HD 152270. They were chosen for the following reasons: It was thought that HD 151932 was a binary because of the excess reddening it displays (Bappu, 1973). A possible period of 3d had been derived by Struve (1944). However, this was disputed by Seggewiss (1974a), who showed that the interstellar lines also had similar variations of velocity. The other system of HD 152270 is known to be a spectroscopic binary of period about 9d. In this case although the angle orbital inclination is not favourable for eclipses of the continuum, atmospheric eclipses are anticipated. This will help in understanding the atmospheric stratification.

The sixth Chapter discusses the result of all these systems, to understand the effect of the companion on the extended atmosphere. The asymmetric wind dominant Roche surfaces are used to explain the flux variations. The peculiarities of some spectral lines, in particular He II λ 4686, are discussed and compared with the available information for all binaries. The possibilities and the effects of compact companion are discussed; in this context the results on the system HD 76536 are presented to search for the suspected companion. Some sporadic events common to all systems are discussed. All these aspects are made use of to understand the possible atmospheric

stratification. This can throw some light on the evolutionary scenerios proposed for the evolution of the WR stars in general and the binaries with WR components, in particular.

The seventh and final Chapter discusses the usefulness of the technique of spectrophotometry in the study of such systems with extended atmospheres. A possible extension of this technique to other systems of interest also is briefly narrated.

2. OBSERVATIONS AND REDUCTIONS

Eversince the recording of spectrum of celestial bodies was developed, the need for the determination of absolute flux of radiation was felt. The earliest attempts were for the comparison of flux from stars with black body sources. The most direct method of recording flux is to place a detector behind the slit of the spectrograph. The technique of photography is very widely used but the serious disadvantages are those of limited range of intensity and the plate calibration accuracy. The non-linearity of the plate response with reference to the intensity also is very well known.

After the advent of photoelectric detectors in astronomical applications, very accurate flux measures have been made available. These measures are always made relative to standards and the accuracy achieved is about 1% (Oke, 1965). When one compares the photoelectric and photographic techniques, the linearity of the response of the photoemissive cathode immediately becomes evident. Although time resolution is lost in this, because only one of the regions of the spectrum can be recorded at a time, the higher quantum efficiency increases the accuracy. Another advantage is the higher precision, that can be obtained by increasing the exposure time, which is not possible with the photographic detectors (Code & Liller, 1962). Special detectors can increase the wavelength of operation from UV to IR.

The earliest record of such scanner applications is that of Dunham and Bruch (cf. Wright, 1962), who produced the solar Ca II

line profiles. This technique was used by Hall (1936) with an objective grating to scan the spectra of stars in the wavelength range of 4500 to 10,300 Å. Later developments of the instrument involved the movement of the slit to scan the spectrum. Further sophisticated versions employed the movement of the dispersive element, like the prism or the grating, and a stationary detector behind the exit slot.

Variety of applications other than the measurement of energy distribution have been attempted. The three parameter system of spectral classification based on the magnitude of Balmer discontinuity D , its position λ and the gradient ϕ , in the blue by Chalonge (cf. Wright, 1962) is a very important application. Walravens (cf. Wright, 1962) have classified the stars according to luminosity and spectral type by means of a photoelectric spectrum analyzer. The study of the line profiles using photoelectric techniques is considered to be as efficient as the photographic technique as shown by Wright (1962).

The type of dispersive element that is adopted in such a photoelectric spectrum scanner is decided by the desired application. For measurement of colour, Trodahl et al. (1973) used a semicircular wedge. They covered a range of 4000 to 8000 Å for measuring the colour indices relative to standard stars. This scheme of stellar classification employed prisms. The continuum energy distribution studies and line profile analyses can be done with only gratings, which have the advantage of linear dispersion and wavelength independent reflecting surface.

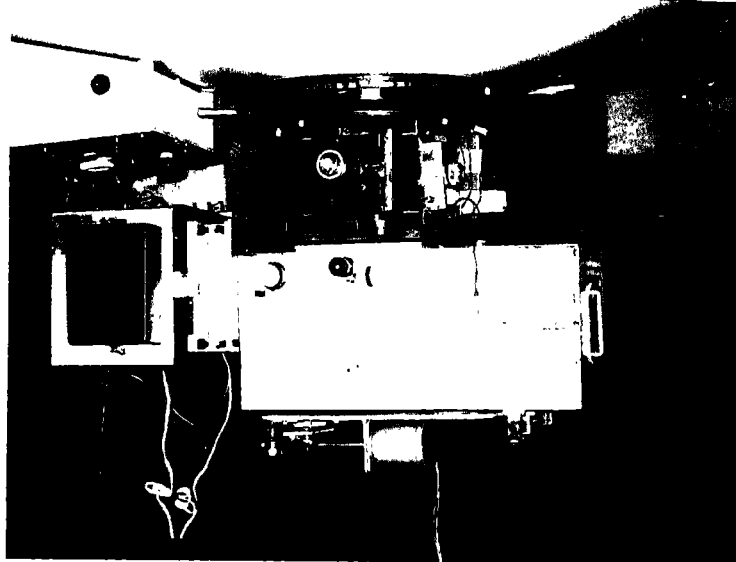


Figure 2.1a The automated spectrum scanner at the Cassegrain focus of the 102cm reflector.

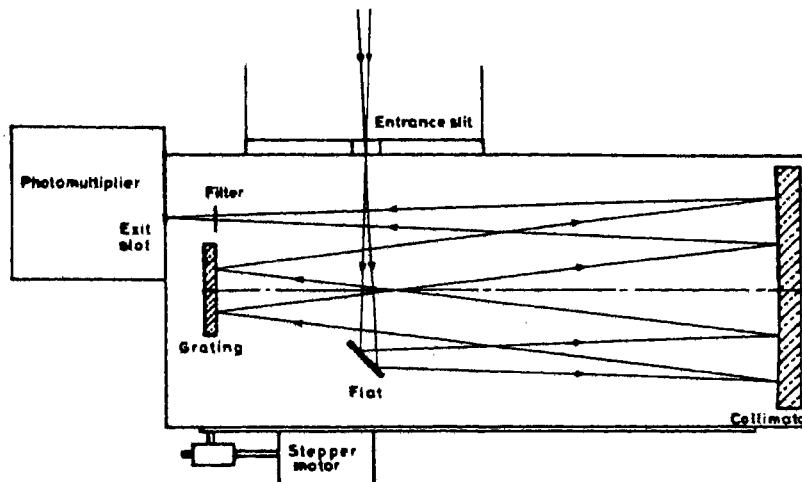


Figure 2.1b Schematic diagram of the scanner.

2.1 The Instrument

Various arrangements of optical elements for photoelectric spectrophotometry have been discussed by Code & Liller (1962) in great detail. The basic principle is to measure a sample of uniform width of each wavelength region. The selection of sample is achieved by rotating the grating so that the exit slot sweeps through the spectrum. The detector behind the slot records the different samples sequentially.

The 102 cm reflector of Kavalur Observatory has the provision for mounting a scanner at the Cassegrain focus (Bappu, 1977). The instrument has the optical system of Ebert-Fastie type as shown in Figures 2.1 a & b. The collimator is a spherical mirror of one meter radius and matches with the f/13 beam from the secondary mirror of the telescope. Circular as well as rectangular slits at the entrance are available. Generally, the circular one of 800μ is used, which corresponds to the 13 arcsec of the sky. The plate scale at the Cassegrain focal plane is $16 \text{ arcsec mm}^{-1}$

The $600 \text{ lines mm}^{-1}$ grating blazed at 7600 \AA , yielding a dispersion of 25 \AA mm^{-1} at the exit slot was used. The resolution, r , of the equipment may be calculated, in \AA as,

$$r = \frac{50 a F}{g n f}$$

where,

a = stellar image diameter in arcsec,

F/f = ratio of focal length of telescope to spectrograph collimator,

g = number of grooves per mm of the grating,

n = order of the spectrum (cf. Oke, 1965)

For the case with $600 \text{ lines mm}^{-1}$ grating and first order, the resolution works out to be about 3 Å for seeing conditions of the order of 2 arcsec. However, for better S/N ratio the exit slot is opened to larger dimensions. Although there is a provision to open to almost 6mm, it was usually kept at a lower value. A reading of 40 on the circular scale was usually considered reasonable, where each division corresponds to about 0.5 Å, in the first order. This results in a channel dispersion of almost 10 Å and a resolution of nearly 20 Å in first order; these values are 5 Å and 10 Å in the second order respectively. The exit slot was sometimes opened to 100 divisions ($\sim 50 \text{ Å}$ in first order) for very faint objects.

The rotation of the grating is achieved by a stepper motor with 200 steps per revolution. Each step corresponds to one channel, i.e. about 10 Å in first order. The position of the grating can be read out to an accuracy of one channel by a dial gauge. The calibration of this dial gauge is done with the help of a laboratory source, which is a mercury lamp in this case.

There is a provision to isolate the red region from the second order blue wavelengths by introducing a filter just before the exit slot. The filters that are generally used are W 25 or OG1 for the red region and BG 12 or BG 14 for isolating the second order blue region. GG 13 was used in the first order visual region.

The output from the photomultiplier was fed to an amplifier and discriminator, whose basic function is to amplify the small PMT output current of the order of nA and $\mu \text{ A}$. One of the

requirements of such an amplifier is the high input impedance. The discriminator converts the output from the amplifier to voltage levels compatible with a digital counter. This technique of pulse counting has the advantage of longer integrations, which is not possible with the conventional DC techniques. The pulse amplifier discriminator (PAD) has a very high input impedance. This unit was tested on a UBV photometer and the gain was so adjusted that it does not saturate for reasonably high pulse rates, at the same time attempting to achieve maximum efficiency for faint light levels. This procedure, called the 'dead time correction', essentially ensures that the pulses are not missed during counting, especially when the pulse rate is very high. This type of optimized gain adjustment and the smaller band widths employed in our work prevented the attainment of saturation even when stars as bright as γ Gem ($m_v = 1.93$) were observed.

The detector was generally the S20 surface. During the observing seasons of 1980-81 and 1981-82, the refrigerated EMI 9558B tube was used. The tube EMI 9804B also was occasionally used, for only the blue region. For the season of 1982-83 and later, a new EMI 9658R was made available, with a built-in PAD from 'Products for Research'. This could be fitted to either a thermo-couple cooled chamber or a dry ice cooled chamber. Suitable Fabry lenses were mounted onto these chambers. In 1985 another detector, RCA 31031, with a better response in the long wavelength region also was available. This was especially useful in deriving the continuum distribution up to almost 9500 Å.

The pulses from PAD served as input to an on-line computer

TDC-12 (4k, 12 bits, 2 μ s), where rapid counting was possible. There was provision for two modes of operation. The first one, called the sequential mode, permitted a continuous scanning of the spectrum, to a maximum of 200 channels (2000 Å in first order). The second mode, called the random mode, would scan only certain wavelength bands, which may be specified in terms of channel numbers, through mercury lamp calibration. This mode was particularly useful in monitoring faint sources, where avoiding regions of very little interest, total observing time was saved. While observing the red regions, the unwanted (earth's) atmospheric absorptions also may be avoided by this mode. However, this has the serious disadvantage that the backlash of the motor would shift the region of interest in to a gap, after several number of observing runs. This demands the recalibration with the mercury, all too often.

The time spent at each channel, during a scan, could be chosen from 1 ms to 999 ms. This choice was mainly decided by sky conditions. The faintness of the source (star) decided the total number of scans per observing run. This meant that while a total duration of 4 to 5 minutes was sufficient for a brighter star ($m_v = 6$) in the blue region, about 15 to 20 minutes were needed for a fainter star ($m_v \sim 10$). The total time spent at each channel varied from 1 to 10 seconds.

The counts were monitored at fixed time intervals (one or two minutes) at the end of which, the maximum and minimum counts were printed on a line printer. The scanning could be continued or halted on an inspection of these values. The spectrum can then be printed out as a table with running channel number, on

command.

The computer TDC-12 was later replaced by a microprocessor controlled photon counting system. This equipment mimicked the performance of TDC-12 with several additional features. The size of the memory was increased to (16k ROM + 4k RAM) so that larger wavelength coverage was possible at a stretch. An oscilloscope displayed the building up of the spectrum, scan after scan, making the monitoring easier. Apart from this, the maximum and minimum counts were also displayed. The most important addition was the built-in clock, which facilitated the printing of the times of the beginning and ending of each observing run.

2.2 The Instrumental Performance

The instrument has already found a variety of applications from comets to stars (Sivaraman et al., 1977; Bappu et al., 1978; Shylaja & Prabhu, 1979; Babu & Shylaja, 1981, 1982 a & b, 1983; Shylaja, 1983, 1984, 1985; Shylaja & Babu, 1985). Applications to Wolf-Rayet stars in particular has been discussed by Bappu (1977).

For the present study, the blue region has been observed in the second order, so that emission lines are resolved. The red region has been covered in the first order. Some sample scans showing stars of different spectral types are shown in Figures 2.2 (blue). The figures include one nova, where even the violet absorption edge is clearly identifiable, in spite of the poor resolution. In case of peculiar A stars, the depression at 5200 Å is striking in the scans even before any correction is applied.

It may be immediately seen that the instrument is suited for

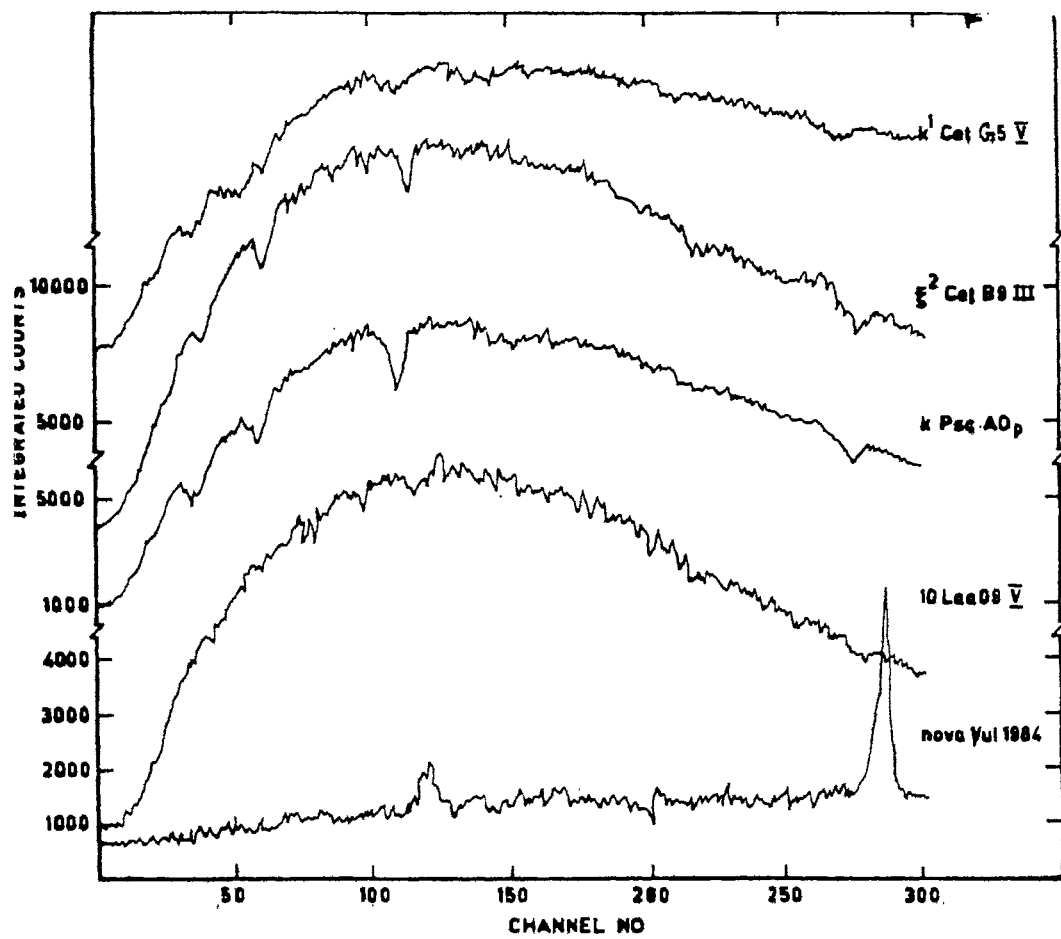


Figure 2.2 Sample scans of the scanner in the blue region.

the study of broad band emission and absorption features.

2.3 Standard Stars

To determine the absolute energy distribution of a star, the observed scan should be corrected for various contributions from sky conditions, telescope optics, detector sensitivity and noises generated in the process. For this purpose α Lyrae is chosen as the primary standard. Many lists of the secondary standards are available in literature (Oke, 1964; Hayes, 1970; Breger, 1976). Generally these standards are all of spectral type A and B, and are not calibrated in the regions of convergence of the Balmer and Paschen lines i.e. 3600 to 4000 A and 8200 to 8600 A. To overcome this difficulty many O type standards (Kuan & Kuhi, 1976) and late type stars (Fay et al., 1975; Taylor, 1982) are made available. The list of standards used in the present study are compiled in Table 2.1.

On the same night atleast three standards were monitored to cover a range of hour angles. They were chosen to be of spectral type similar to that of program stars. The procedure adopted for obtaining these scans was as follows

1. Mercury lamp to fix up the wavelength region
2. Standard star #1 blue region
3. Sky near std.star in blue region
4. Std. star #1 in red region
5. Sky near std star, red region
6. Program star #1 blue region
7. Sky near prog.star blue region
8. Prog.star #1 red region
9. Sky near prog. star red region

Table 2.1 List of standards used in the present study.

NAME	HR NO.	MAGNITUDE	B-V	SP. TYPE
ξ^2 Cet	718	4.28	-0.06	B9 III
γ Gem	2421	1.93	0.00	A0 IV
27 CMa	2745	4.66	-0.19	B3 IIIe
η CMa	2827	2.45	-0.08	B5 Ia
ζ Pup	3165	2.25	-0.26	O5 I
η Hya	3454	4.30	-0.20	B3 V
θ Crb	4468	4.70	-0.08	B9.5 V
109 Vir	5511	3.72	-0.01	A0 V
η Sge	7574	6.23	+0.01	O8f
58 Aql	7596	5.61	0.10	A0 III
ϵ Aqr	7950	3.77	0.00	A1 V
λ Cep	8469	5.04	+0.25	O6 If
10 Lac	8622	4.88	-0.20	O9 V
29 Psc	9087	5.10	-0.12	B7 III

10. Std. star #2 in red region

11. Std star #2 in blue region

and so on.

Care was taken to observe the program star as close to the meridian as possible. The calibration of the dial gauge was checked 3 to 4 times during the night with the help of the mercury lamp.

2.4 Atmospheric Extinction

2.4.1 Influencing parameters

The model suggested by Hayes & Latham (1975) has been used to determine the nightly extinction coefficients based on the observations of standard stars as follows

Consider a monochromatic beam of wavelength λ entering the atmosphere from outside, at a zenith angle z , with reference to the observer. The intensity as measured by the observer is decided by the optical depth τ of the atmosphere as,

$$I(\lambda, \tau) = I(\lambda, 0) \exp[-\tau(\lambda, z)] \quad (1)$$

neglecting the angular effects.

The optical depth is defined as,

$$\tau(\lambda, z) = \kappa(\lambda) X(z) \quad (2)$$

where $\kappa(\lambda)$ is the extinction coefficient and $X(z)$ is the airmass.

The optical depth at zenith distance zero is

$$\tau(\lambda, 0) = \kappa(\lambda) \quad (3)$$

Hence, (1) can be rewritten as,

$$I(\lambda, \tau) = I(\lambda, 0) \exp[-\kappa(\lambda) X(z)]$$

$$\frac{\partial}{\partial X} \ln I(\lambda, \tau) = -\kappa(\lambda) \quad (4)$$

Therefore, a plot of the airmass versus the natural logarithm of the measured intensity gives the slope as $\kappa(\lambda)$,

the extinction coefficient. The knowledge of the intensity prior to the entry into the atmosphere $I(\lambda, 0)$, is not necessary.

The extinction is caused by various factors. The main contributors are, Rayleigh scattering by molecules, molecular absorption and aerosol scattering. The Rayleigh absorption is defined as,

$$A_{\text{Ray}}(\lambda, h) = 9.4977 \times 10^{-3} \times \frac{1}{\lambda^4} \left[\frac{(n-1)_{\lambda}}{(n-1)_{\lambda=1}} \right]^2 \exp \left(\frac{-h}{7.996} \right) \quad (5)$$

where n is the refractive index at λ , in microns, h is the altitude of the place, i.e. the Observatory.

The absorption due to ozone may be expressed as,

$$A_{\text{oz}}(\lambda) = 1.11 T_{\text{oz}} k_{\text{oz}}(\lambda) \quad (6)$$

where T_{oz} is the thickness of ozone in atmo.cm, which is independent of the altitude of the place.

The aerosol scattering is caused by the smaller particles ($0.1 \mu < \text{diameter} < 10 \mu$) and this contribution may be estimated as,

$$A_{\text{aer}}(\lambda, h) = A_0 \lambda^{-\alpha} \exp(-h/H) \quad (7)$$

Ozone is known to absorb in two bands (Allen, 1976). One in the UV region with the peak at 2700 Å and the other is in the visible region with the peak at ~ 6000 Å. Therefore, the region in the range, $3800 < \lambda < 5000$ Å can be considered to be solely due to the aerosols and using (7) the coefficient α can be calculated, if corresponding data are available.

2.4.2 Comparison with Meteorological Data

In the present analysis, we analysed these atmospheric data in the following way. Four nights' data on very clear nights were chosen for this purpose (Table 2.2). The total absorption was

Table 2.2 Data used for extinction analysis and results.

Date	Prog star	Std star	z	A	B	α	Abs. due to ozone %	Ozone measures atmo cm
1980 Oct 29	ϵ Aqr	γ Gem.	24.73	0.063	0.0141	1.33	15	269
1981 Feb 27	η Hya	γ Gem.	30.03	0.050	0.0132	1.31	12	246
1983 Feb 4	ϵ Cet	ζ Pup	23.93	0.051	0.0158	1.14	6	243
1984 Dec 13	β Leo	ζ Pup	26.96	0.075	0.0142	0.92	7	241

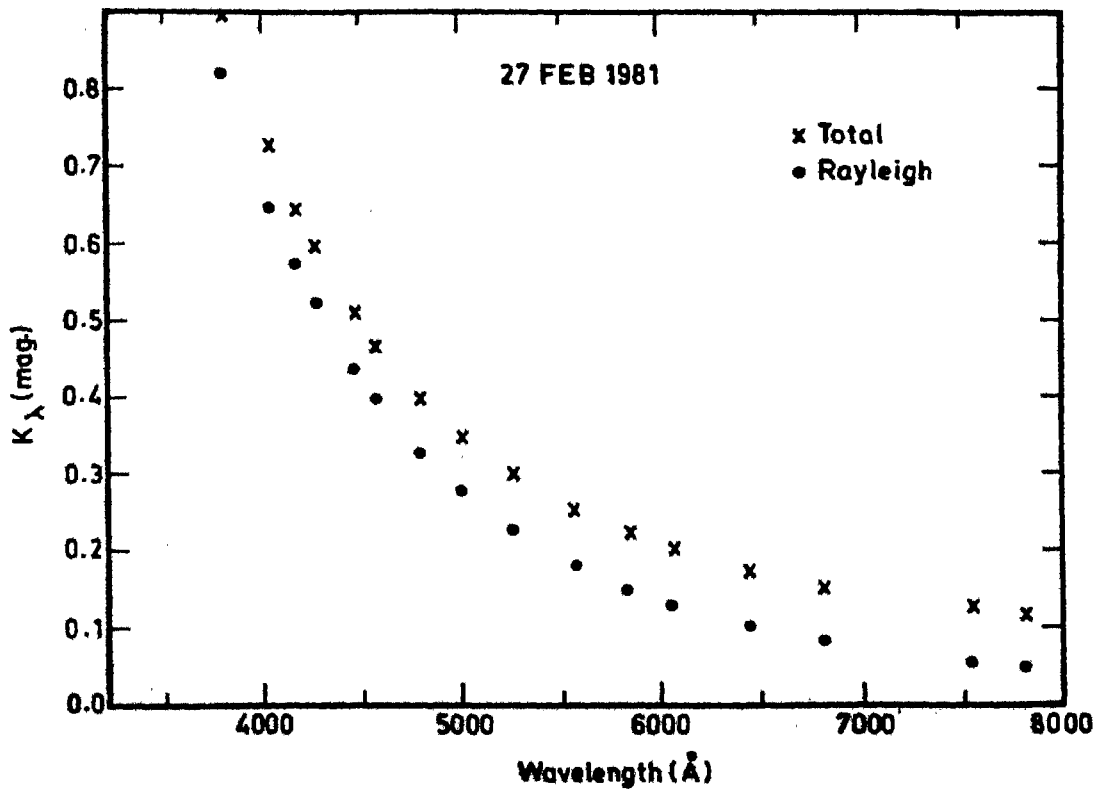


Figure 2.3 The measured total absorption and that due to pure Rayleigh scattering per air mass, given as $K(\lambda)$ in magnitudes.

calculated from a set of standard stars. The variation of this absorption on one such night is shown in Figure 2.3. Following van den Bergh & Henry (1963) this absorption was fitted in to the coefficient as,

$$k(\lambda) = A + B/\lambda^4 \quad (8)$$

where λ is in microns.

The Figure also shows the effect of pure Rayleigh scattering. This was subtracted from the total absorption to get the contribution from other sources (Tug et al., 1977; Hayes & Latham, 1975). This accounts for the vertical shift between the two curves in Figure 2.3 i.e. the term A in equation (8). This residual absorption, when plotted on an expanded scale, shows a general increase in the region of ozone absorption (Figure 2.4). The ozone absorption coefficient from Allen (1976) also is shown in the Figure.

To check these effects, the data from India Meteorological Department on ozone measurements and T - ϕ grams were obtained. It is possible to measure the amount of precipitable water content in the following way.

Consider the water vapour contained in an air-column of thickness dz and let its density be ρ_v . Then the water vapour content is given by $\rho_v dz$. If we extend this to the entire column of air to a height z , we get,

$$W = \int_0^z \rho_v dz \quad (9)$$

The pressure in the element dz is given by,

$$dp = -\rho g dz \quad \text{or,} \quad dz = -\frac{1}{\rho g} dp \quad (10)$$

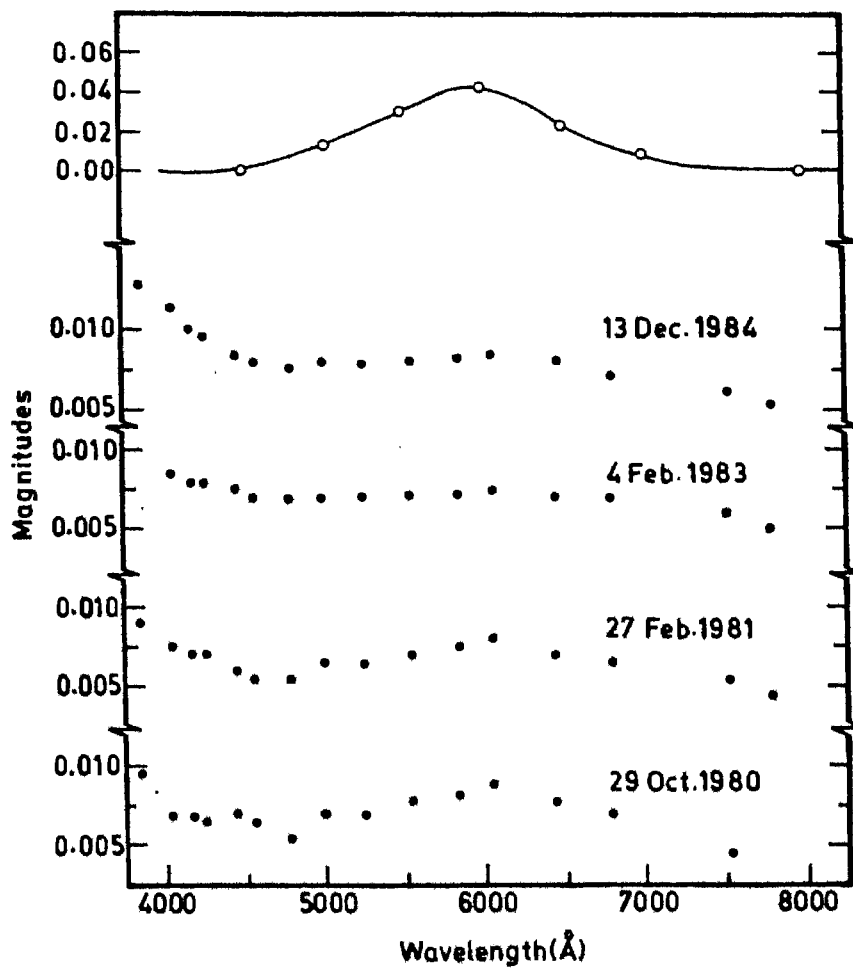


Figure 2.4 Residual absorptions after removing the Rayleigh effect. The ozone absorption coefficient (Allen, 1976) also is shown in the top curve.

where ρ is the density of the particles.

Therefore, the total water vapour content is given by,

$$W = \frac{P}{P_0} \int \frac{\rho_v}{\rho} \frac{1}{g} dp \quad (11)$$

The term q is called the specific humidity, which is defined as the ratio of the water vapour to that of air (dry air + moisture). Then the total water vapour content in a column where the pressure varies from p_0 to p is,

$$W = \frac{1}{g} \bar{q}(p_0 - p) \quad (12)$$

where \bar{q} is the mean specific humidity at that level. From the superposition of 'isohygrics', i.e. the curves of equal water vapour content, on the T- ϕ grams, it is possible to read out the mixing ratio, for every 50 mb of pressure. This mixing ratio, defined as the ratio of mass of water vapour to mass of dry air is assumed to be differing from the mean specific humidity by a small fraction such as 0.1. Hence, we can measure the quantity for every 50 mb difference of pressure and compute the precipitable water vapour content from equation (11). When this is added over the entire air-column we get the total water vapour content.

These measurements are made from the balloon borne apparatus twice in a day at 5:30 am and 5:30 pm IST from selected places only. The nearest places for Kavalur were Bangalore (latitude: 12° 55', altitude: 921m) and Madras (latitude: 13° 04', altitude: 7m). It was decided to compare the measurements made from Bangalore. Table 2.3 includes all these measures obtained from IMD for

Table 2.3 Comparison of water vapour measurements.

Precipitable water measurements			Water vapour absorption measurements		
Date	Time UT	Amount cm	Name of star	Time UT	Absorption %
1980 Oct 29	12:00	1.46	ε Aqt HR 2216	13:45	65
				14:10	56
1981 Feb 27	12:00	0.96	γ Cen, HR 1732	17:55	38
				18:03	42
1983 Feb 4	0:00	0.80	ξ ² Cet	14:18	47
	12:00	1.37			
1984 Dec 13	0:00	0.47	ξ Pup ρ Leo	23:38*	42
				23:55*	46

* Times of Dec 12

Table 2.4 Am stars observed on the same night.

Name HR #	Sp type	δ (1984)	z	θ(eff)
73 Vir 5094	A4m	-19 40	46	0.64
λ Vir 5359	Am	-13 19	39	0.50
60 Hya 5591	Am	-28 00	49	0.59
5762	Am	-19 38	40	0.53
5875	Am	- 3 48	25	0.50

these four selected dates. From stellar measurements, it is possible to estimate the absorption at the 7100 Å band, after establishing the continuum energy distribution of the star. Such measurements made as close to the balloon launch times as possible also are included in Table 2.3. No apparent relation between the two is evident.

In order to understand the variation of water vapour content, the measurements made on the same night were analyzed. Stars of similar spectral type, at similar zenith distances, observed on the same night were used for this analysis. Table 2.4 lists these stars, whose effective temperatures have been estimated (Shylaja et al., 1985). The variation in the water absorption band at 7100 Å can be easily seen (Figure 2.5). This is also an important reason, other than the differences in times of observations and also in geographical locations of water vapour measures, for not finding any relation in the corresponding quantities in Table 2.3.

The solar irradiance measures of Dunkelman & Scolnik (1959) used the practical measures of ozone to show the effect of absorption. They showed that the Huggins band absorptions in the region $3000 < \lambda < 3400$ Å, show a relationship with ozone measures.

For the above mentioned four nights of observation, the ozone measures were obtained from IMD. The nearest locations of these measurements were Kodaikanal (latitude: $10^{\circ} 14'$, altitude: 2343 m) and Pune (latitude: $18^{\circ} 41'$, altitude: 559 m). These values of ozone measurements are included in Table 2.2. It may be seen that there is a general increase in the ozone content from both measures during 1980. However, significant variations in ozone content in

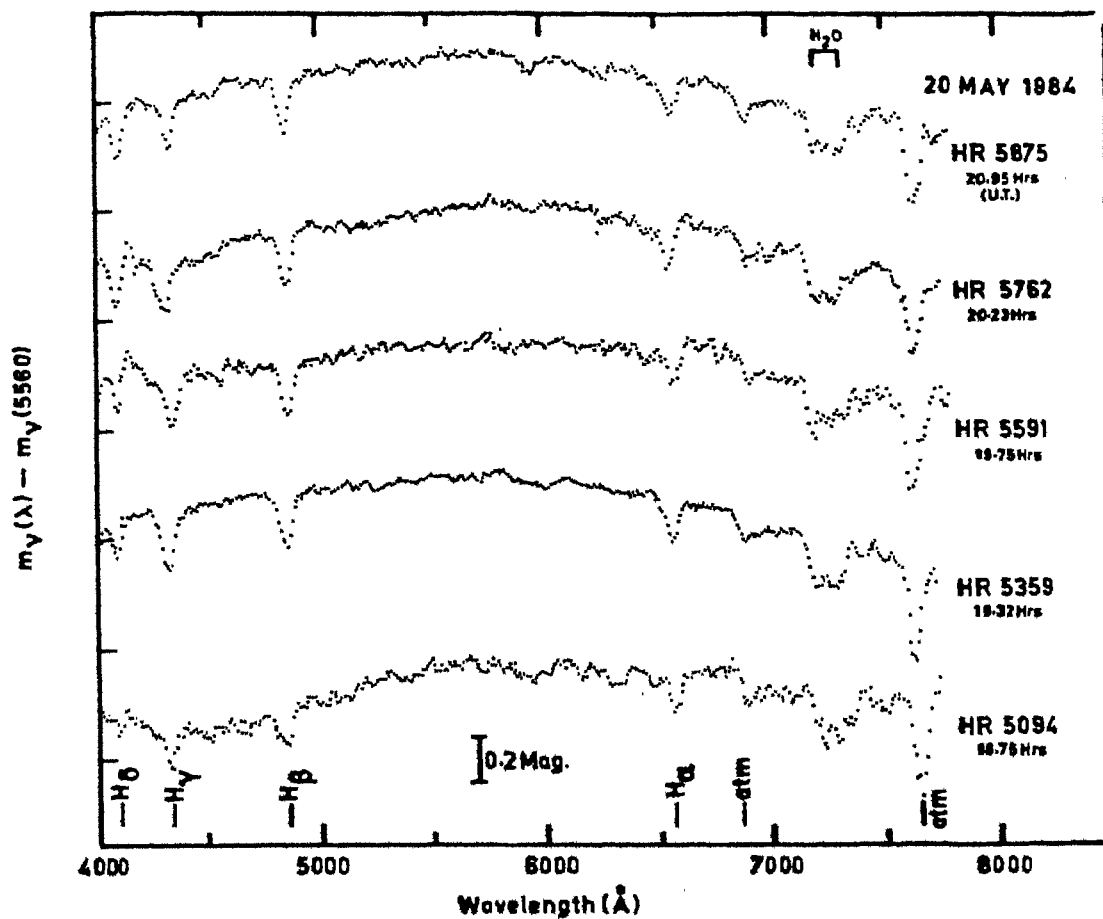


Figure 2.5 Energy distributions of five stars of similar spectral type as observed on the same night at similar zenith distances. The difference in H₂O absorption with UT is noticeable. Details of observations are in Table 2.4.

time scales as small as a few hours are reported (cf. Hayes & Latham, 1975) and the meteorological measurements may represent only a mean value.

This comparative study definitely shows that within the accuracies achieved here, equation (8) is valid. It may also be remembered that Dunkelmann & Scolnik (1959) have shown that the mean extinction curve lies 15% above the Rayleigh curve. Hence the term A can be used to evaluate the constant α in equation (7) from the residual absorption measures in the region $3800 < \lambda < 5000$ Å. These values of α also are included in the Table 2.2. Similar studies by de Vou Couleurs (1965) have shown that the volcanic eruptions of Mt. Agung on the island of Bali (114° E 9° S), were effective in changing the value from 0.8 to 1.2 in 1963, at McDonald Observatory (104° W 30° N).

The values of A and B for different nights and seasons have been tabulated in Table 2.5 and shown in Figure 2.6 as well. The fluctuations in B are quite small and yields the average value around 0.014. The large variations in the value of A are real, as the variations in particle density and other contributors show, from the above discussions.

On occasions when the sky conditions did not permit the determination of A and B, a comparison star of known energy distribution, monitored immediately after or before the program star, was used, to derive the absolute flux.

2.5 Instrumental Corrections:

At the 12 wavelengths listed by Hayes (1970) for continuum measurements which are free of any effect from emission or

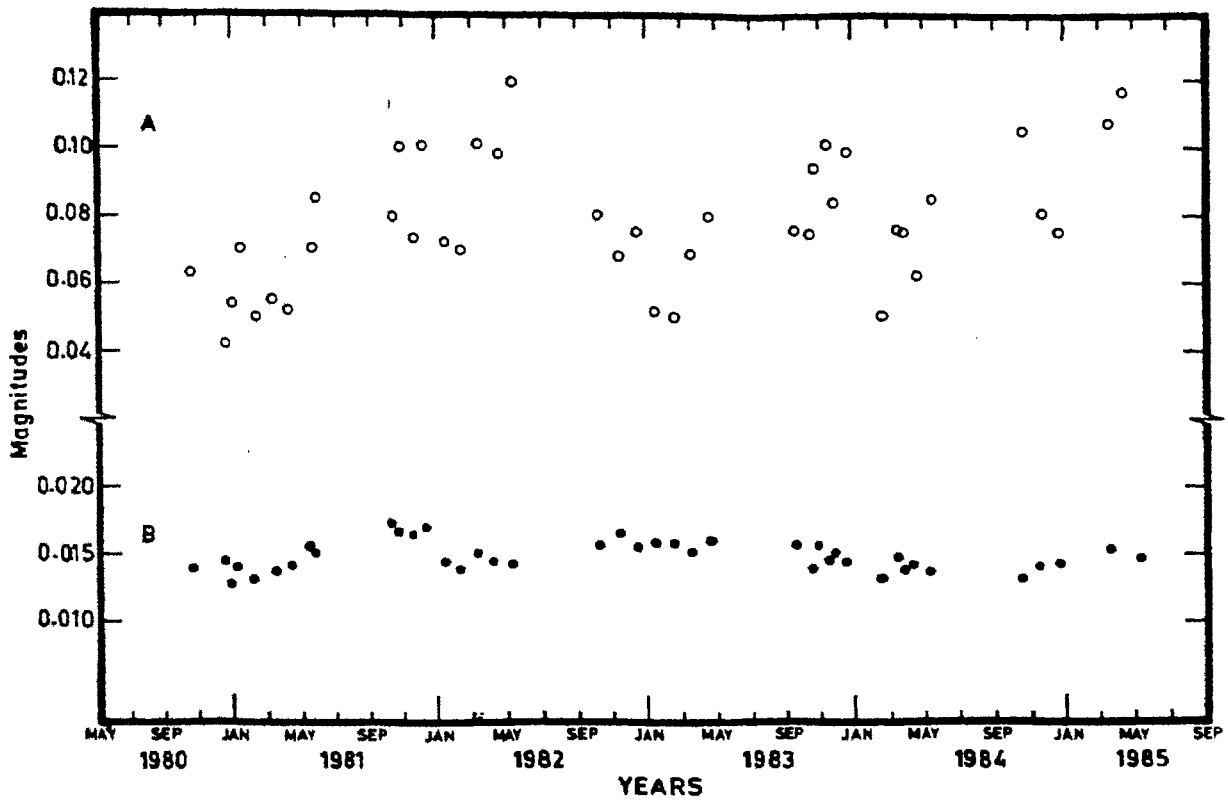


Figure 2.6 The variation of coefficients A and B during 1980-85.

Table 2.5 The extinction coefficients A and B during 1980-85.

	B	A		B	A
Oct 80	0.0141	0.063	Jan 83	0.0160	0.052
Dec 80	0.0145	0.042	Feb 83	0.0158	0.051
Dec 80	0.0127	0.054	Mar 83	0.0153	0.069
			Apr 83	0.0161	0.080
Jan 81	0.0135	0.070	Sep 83	0.0157	0.076
Feb 81	0.0132	0.050	Oct 83	0.0140	0.095
Mar 81	0.0138	0.055	Oct 83	0.0156	0.075
Apr 81	0.0140	0.052	Nov 83	0.0145	0.101
May 81	0.0155	0.070	Nov 83	0.0152	0.085
May 81	0.0150	0.085	Dec 83	0.0145	0.095
Oct 81	0.0174	0.080			
Oct 81	0.0170	0.100	Feb 84	0.0132	0.050
Nov 81	0.0165	0.074	Mar 84	0.0146	0.076
Dec 81	0.0170	0.101	Mar 84	0.0140	0.070
			Apr 84	0.0142	0.062
Jan 82	0.0145	0.072	May 84	0.0138	0.085
Feb 82	0.0138	0.070	Oct 84	0.0132	0.105
Mar 82	0.0151	0.101	Nov 84	0.0141	0.080
Apr 82	0.0145	0.098	Dec 84	0.0142	0.075
May 82	0.0143	0.120			
Oct 82	0.0157	0.080	Jan 85	0.0160	0.092
Nov 82	0.0165	0.068	Mar 85	0.0152	0.108
Dec 82	0.0155	0.075	May 85	0.0148	0.116

absorption lines, the observed counts were averaged over three channels and corrected for sky contribution. This is then converted to magnitude as, $m_{\text{obs}}(\lambda) = -2.5 \log n^*$

where n^* is the the number of counts per second per A. The airmass X is known to be a function of the zenith distance z as,

$$X = \sec z - 0.0018167 (\sec z - 1)^2 - 0.002875 (\sec z - 1)^3 - 0.0008083 (\sec z - 1)^4 \quad (13)$$

from Hardie (1962). Neglecting second order terms, X can be replaced by $\sec z$ itself. From a knowledge of the constant B , the extinction coefficient, the instrumental magnitudes of the particular night at any wavelength can be derived as,

$$m_{\text{ins}} = m_{\text{obs}} - k_{\lambda} \sec z \quad (14)$$

where $k_{\lambda} = B/\lambda^4$. These would be the magnitudes observed if the instrument was kept above the atmosphere. These are normalized at 5000 A as,

$$m_{i\lambda} = m_{\text{obs}} - k_{\lambda} \sec z - m_{\text{obs}}(5000) \quad (15)$$

These are compared with known energy distributions in case of standard stars, which are also normalized at 5000 A, and the instrumental corrections are derived as,

$$\text{cor}(\lambda) = m_{\text{lit.}} - m_{i\lambda} \quad (16)$$

Figure 2.7 shows sample of observed curve, instrumental magnitude, literature magnitude (known energy distribution) and derived corrections.

These corrections are to be applied to the program stars. The procedures for derivation of instrumental magnitude for program star is exactly similar to that of standard stars till equation (16). For the normalized magnitude the corrections are applied from (17) as,

$$m_{\text{prog}} = m_i + \text{cor}(\lambda) \quad (17)$$

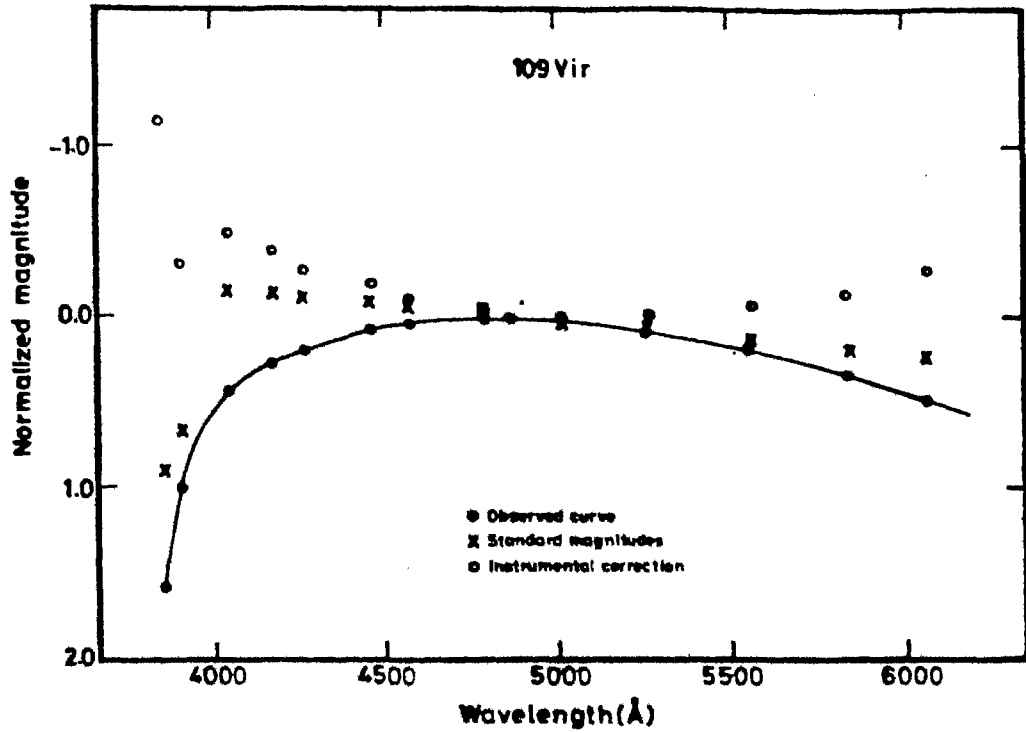


Figure 2.7 A sample of observed curve, Instrumental correction and absolute magnitude (normalised).

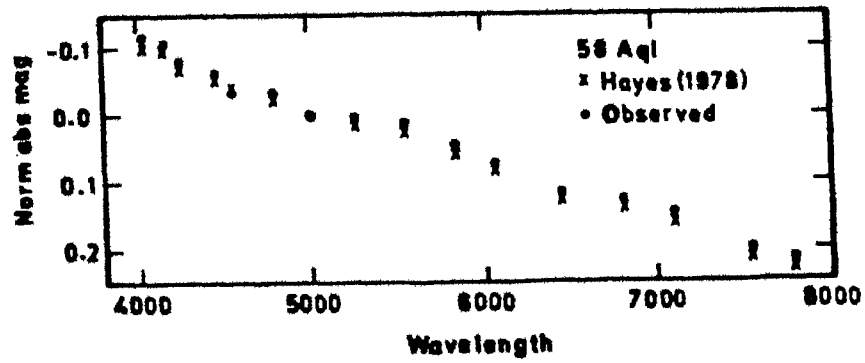


Figure 2.8 Energy distribution of 58 Aql obtained using 109 vir as standard star.

When the corrections from equation (17) are derived for selected wavelengths only, they can be interpolated to all other intermediate wavelengths. The curves in Figure 2.7 shows that this interpolation does not introduce any considerable error especially when the points are closely spaced.

The normalized magnitudes thus obtained are converted in to flux as,

$$m_{\nu} = -2.5 \log F_{\nu} + \text{const.} \quad (18)$$

which can be in units of ergs/cm²/sec/Å or ergs/cm²/sec/Hz, depending on the value of the constant, since

$$m_{\lambda} = -2.5 \log F_{\lambda} + \text{const.} \quad (19)$$

The constant is -48.615 for (18) and -21.146 for (19), based on the definition of the energy of the primary standard α Lyrae, as 3.58×10^{-20} ergs/cm²/sec/Hz (Hayes & Latham, 1975).

Figure 2.8 shows the comparison of the energy distribution known from other sources for 58 Aql, with the derived values using 109 Vir as the standard star.

2.6 Errors

The source of errors can be either optical or electrical. Bad seeing conditions lead to inaccurate flux determinations. Under such circumstances the diaphragm was opened to 1000 μ . This, however, reduces the accuracy by raising the general sky background. Similarly, changing sky conditions in a night give erratic values for the extinction coefficients. Again, on such occasions the comparison star monitored immediately before or after the program star was used for deriving the instrumental corrections from a mean value of the extinction coefficient.

Electrical noise can be photon noise or the digitising

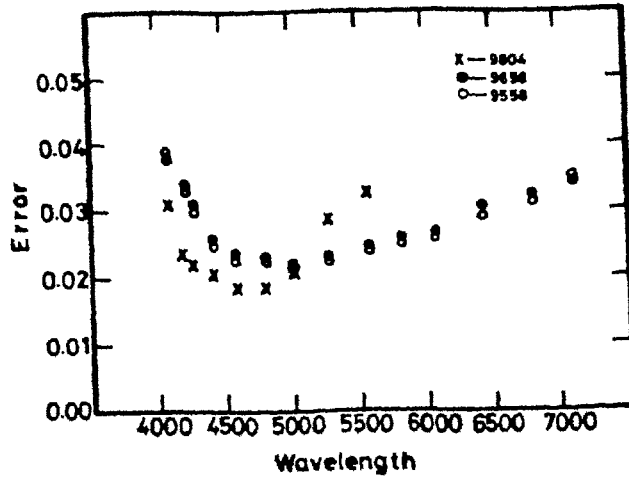


Figure 2.9 Errors for different photomultiplier tubes.

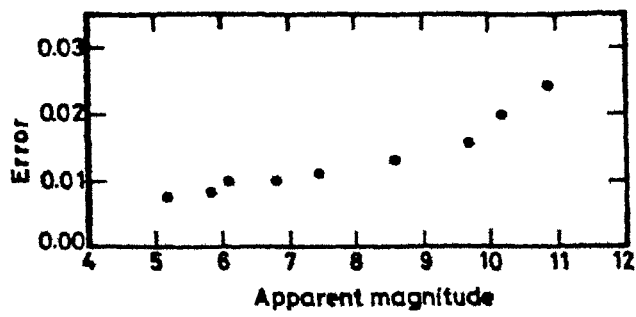


Figure 2.10 Variation of error with apparent magnitude.

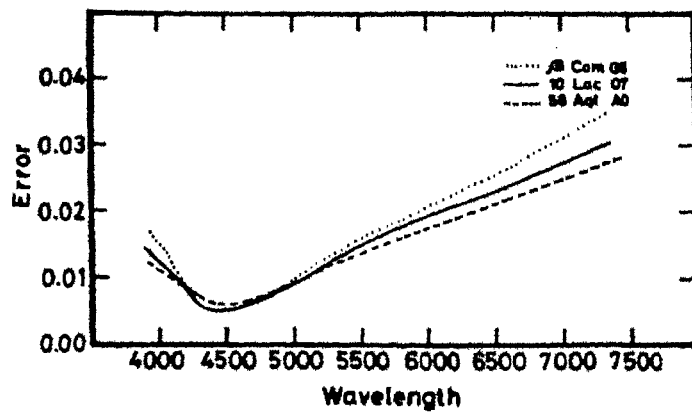


Figure 2.11 Variation of error with spectral type.

noise. The photon noise decreases with the number of integrations over the same channel. This may be represented by $(N_j)^{-1/2}$, where N_j is the number of photons in channel j . The digitising noise has been found to be proportional to the pulse output from the discriminator (Lynds & Aitkens, 1965). It is shown that the signal to noise ratio is,

$$S/N = (6Tt)^{1/2} F$$

where t = time interval spent at each channel during a single run, called the counting interval, here,

T = total time

= Nt , where N is the total number of scans,

F = frequency of the output of the PAD.

Since, this is also proportional to $F = (N)^{1/2}$, it is better to integrate over a long duration. However, this increases T and therefore one has to go in for a compromise.

The errors have been determined treating star of known energy distributions as unknown program star. The error as a function of wave length, is basically decided by the response of the photomultiplier tube, as demonstrated by the Figure 2.9. The faintness of the source also is partly responsible for errors (Figure 2.10). It is thus essential to choose a comparison of similar magnitude range. A difference in spectral type also is likely to introduce errors as shown (Fig.2.11); here the standard chosen was of spectral type A to derive the energy distribution of stars of spectral type O and G.

3. THE SHORTEST PERIOD BINARY CQ CEPHEI

CQ Cep (HD 214419 = BD +56° 2818) is an eclipsing system with a period of 1.64d. One component is a WN7 star and the companion is probably a massive early type star (van der Hucht et al., 1981).

The binary nature of CQ Cep was discovered by McLaughlin & Hiltner (1941) from prismatic survey plates at a dispersion of 150 \AA mm^{-1} . Based on radial velocity (RV) measurements from six spectra, they derived a period of 6.5d. They attributed the weak absorptions to a companion of class O8. However, they noted that one of the plates showed velocities of absorption lines matching with the movement of the WN7 component itself.

Further spectroscopic studies by Hiltner (1944) with better dispersion spectra yielded a period of 1.6410d. Again, there was no signature of the companion in the spectra. The absorption velocities depicted the movement of the WN7 component as was noted earlier also. Generally the helium lines of He I and He II showed violet absorption edge. The other striking changes were of line profiles and strengths. He obtained the radial velocity curves for the 4058 \AA line of N IV (eccentricity, $e = 0.0$, amplitude, $K = 295 \text{ kms}^{-1}$) and also for the $\lambda 4686$ line of He II ($e = 0.35$; $K = 160 \text{ kms}^{-1}$). Another feature he noticed was that the He I lines at 3888, 4026 and 4471 \AA , were always associated with violet absorption components and it appeared that they were split into two components only on plates obtained on November 13 and 14, 1943.

Gaposchkin (1944) derived photographic light curves making

use of the data from Hiltner, which showed asymmetric minima. Thus this was established as an eclipsing system. A large number of plates were used for this purpose and the long base line of 44 years improved the period to 1.641271d. He also suggested a possible secular change in the period.

The photoelectric light curves were first produced by Hiltner (1950), in the continuum at 3550 Å and 5300 Å, and also at 4686 Å with 73 Å pass band. These light curves and the radial velocity solutions obtained earlier, yielded the information that the deeper and the narrower minimum corresponded to the eclipse of the component. The minima at 3550 Å were 0.1 mag deeper than those at 5300 Å. He also observed that there was no change of polarization with orbital phase.

Another interesting finding by Hiltner was the behaviour of the 4686 Å line of He II, whose maxima were observed at phases corresponding to conjunctions from the other light curves, i.e. the intensities were more at phases corresponding to the eclipse and transit of the components. Hence the light curve of this line was almost like a mirror image of the continuum light curves.

Bappu (1951) studied the line profiles of various emission lines. More detailed investigations (Bappu, 1951a, b & 1952) showed that many other lines also followed the behaviour of the 4686 line. Bappu & Sinhal (1955, 1959) carried out the narrow-band photometry of this system and obtained the light curves at 4860 and 5410 Å, which looked similar to that of the λ 4686 light curve obtained by Hiltner.

Broadband photometry in the optical region have been

continued by various investigators (Tchugainov, 1960; Gusseinzade, 1969; Semeniuk, 1968; Khaliullin, 1974; Kartasheva, 1976; Cherepashchuk & Khaliullin, 1976; Antokhina et al., 1982 and Walker et al., 1983). They all have pointed out the similar shape of the light curve at different wavelengths. Semeniuk (1968) studied the times of minima till 1967 and arrived at a possible shortening of the period. Cherepashchuk & Khaliullin (1976) and Antokhina et al., (1982) arrived at a value for the mass loss as $1.10 \times 10^{-10} M_{\odot} \text{ yr}^{-1}$, based on the period changes. This aspect of period change has been discussed by Stickland et al. (1984) in detail, who proceed to show that after 1960s the period seems to have remained constant at 1.641246d.

The infra red (IR) observations of this system were first obtained by Hackwell et al. (1974) and they showed that the observed IR excess can be explained by free-free emission in the gas. The IR light curves have been derived by Stickland et al. (1984) and they clearly demonstrate the decrease of the light curve amplitude at longer wavelength regions indicating the contribution from the free-free emission.

Detailed spectroscopic investigations were taken up by Bappu & Viswanadham (1977) and Giridhar (1978), who found that the emission lines showed marked difference in behaviour. Both the amplitude and eccentricity derived from these radial velocity curves were different. The line profile variation also have been studied. Leung et al. (1983) carried out more detailed observations and confirmed that the radial velocity curves were disparate. The measurements of absorption components of the 3888Å line of He I line by Niemela (1980) has shown the indication of

the movement of the companion; but this is yet to be confirmed by more detailed studies.

Hiltner (1950) attempted to explain the behaviour of the emission line of He II at λ 4686 by assuming that although the nitrogen lines are produced more or less symmetrically, the He II lines are produced throughout a common envelope surrounding both the stars. Khaliullin (1973) had observed photometrically in four wavelength bands (two emissions and two continua). He had attempted to model the variation by combining an assumed variation of the absorption due to secondary. However, no evidence of such absorptions were found subsequently by Stickland et al. (1984), although Niemela (1980) found for only one He I line.

In a recent study of the variation of the radial velocities and light curves, Leung et al. (1983) arrived at a mass ratio of 0.75 for the components. The smaller amplitude of the λ 4686 RV curve has been related to the ejection of hot λ 4686 emitting material with a strong radial velocity component directed towards the observer at phase 0.8.

The most recent and exhaustive study of CQ Cep is by Stickland et al. (1984). They have analyzed the data obtained by IUE, UBVJKL photometry as well as the radial velocity measurements in the optical from Hiltner's plates of 1944. They obtained a total of 18 continuum light curves covering the wavelength range from 0.13 to 0.3 μ m. Their conclusions may be summarized as,

1. The light curve solutions indicate that half the amplitude of

light variation is produced by ellipticity effects and the other half by geometric effects.

2. None of the spectral features is an indicator of the companion's presence or motion.

3. The companion does not modify the overall expected variation of excitation, velocity characteristics and in this respect resembles any other single WN7 atmosphere.

4. The luminosity ratio implied by the light curves is not consistent with allowable radii and separation values, unless their masses and temperatures are considerably raised.

In all these investigations, the continuum and line variations of this system, as a function of phase, have been studied for only λ 3550, 5300, 4790, 6300 Å and the two lines of He II at λ 4686 and λ 6562, in the visible region. Our main interest in observing this system was to obtain light curves in all major emission lines in the optical region systematically. Such data combined with spectroscopic information, which already exists both in UV and optical, is likely to give a better insight and may lead us to unravel at least some of the mysteries of this system.

3.1 Observations

The spectrophotometric observations were obtained with the automated spectrum scanner, as described in Chapter 2. The list of standards used also are included in Table 2.1.

3.1.1 Reddening corrections

The affiliation of CQ Cep to the Cep OB1 Association has been confirmed by Stickland et al. (1984) from the observed strengths of interstellar lines in the UV spectrum obtained at

high resolution. Therefore, a distance of more than 3 kpc will introduce interstellar reddening effects in the energy distribution. Here, the reddening corrections are estimated by comparing it with 10 Lac (O7 V), whose reddening corrections are known (Hua et al., 1982) at wavelengths selected so as to be free of emission line contaminations. Similar corrections have been derived by Kuhl (1966), Hua et al. (1982) and Stickland et al. (1984). The latter derived the reddening corrections from the 2200 Å depression and using Seaton's curve for reddening. The dereddened energy distributions are compared in Table 3.1 and are shown in Figures 3.1a & b, where samples at three different phases are plotted. It may be seen that our values agree more closely with those of Stickland et al. (1984), which are represented by crosses in the Figures.

3.1.2 Spectroscopic studies

For spectroscopic measurements, the collection of spectra by Bappu was made use of. They were obtained at Mt. Wilson 60" telescope in 1951-52. The spectra fall into two classes:

1. Blue spectra covering a range of wavelength λ 4000 to 5000 Å at a dispersion of 75 \AA mm^{-1} at 4340 Å on IIaO baked plates.
2. Red spectra covering the range of λ 5100 to 6700 Å at a dispersion of 160 \AA mm^{-1} at 5500 Å on 103-aF plates.

The intensity profiles for a few lines were provided by Bappu, from which some intensity measurements were possible. For the other lines the radial velocities were measured. For some lines the RV measurements are already published (Bappu & Viswanadham, 1977; Giridhar, 1978). The remaining lines like the

Table 3.1 Dereddened energy distribution for CQ Cap.

Wavelength	Stickland et al. 1984	Hua et al. 1982	Kuhi 1966	This Work
4037	-	-0.727	-	-0.682
4150	-0.65	-	-0.30	-0.680
4168	-	-0.688	-	-0.604
4255	-0.61	-0.523	-0.27	-0.604
4420	-0.42	-	-0.19	-0.572
4460	-	-0.523	-	-0.525
4560	-	-0.437	-	-
4786	-0.13	-0.165	-0.06	-0.150
5000	0.00	0.000	0.00	0.000
5130	0.02	-	-0.02	0.018
5263	0.19	-	0.08	0.185
5300	0.29	-	-	0.315
5556	0.30	-	0.10	0.425
5840	-	0.485	-	0.615
5950	0.68	-	-	0.705
6056	-	0.665	-	0.795
6431	-	0.828	-	1.112
6790	-	0.985	0.53	1.200
6806	1.17	-	-	1.205

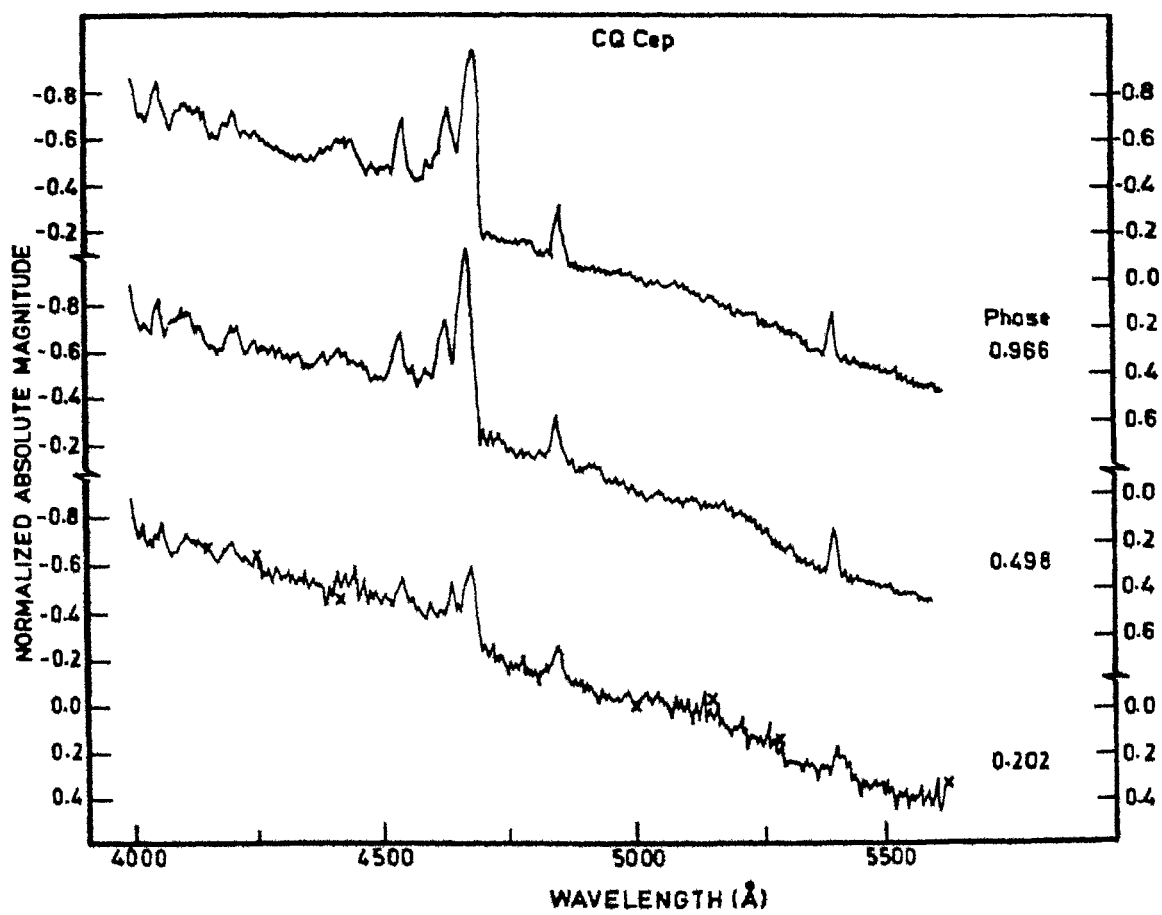


Figure 3.1 Samples of energy distribution at three epochs.
 (a) blue region

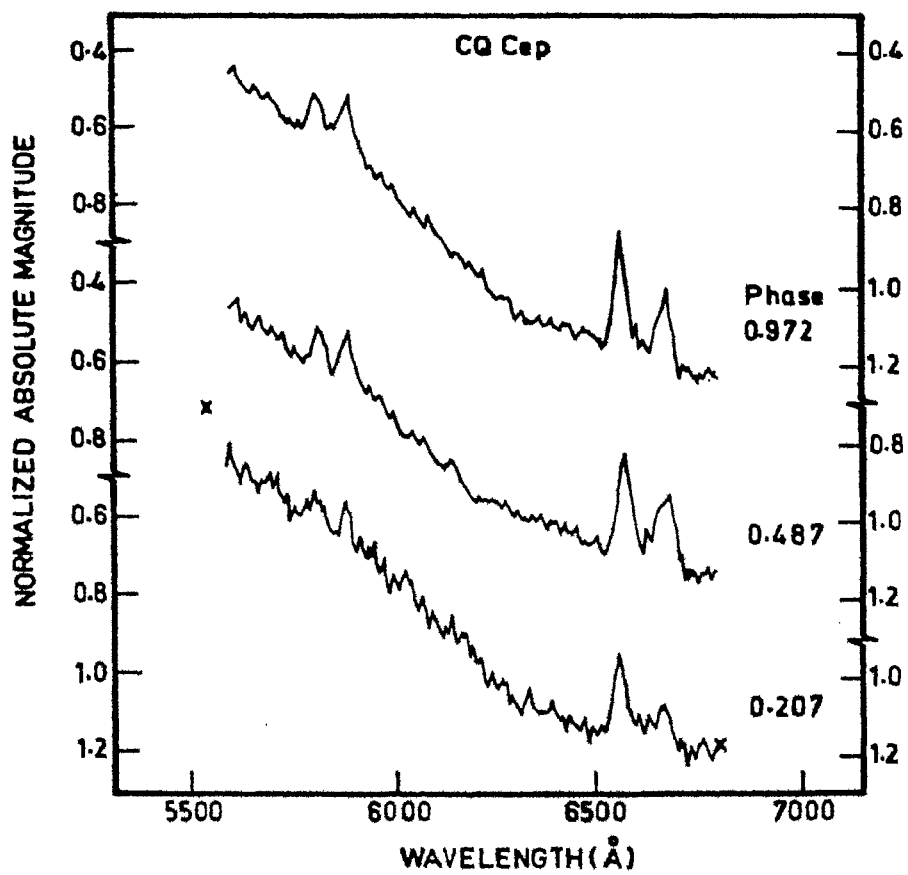


Figure 3.1(b) red region.

He II lines at λ 4860, λ 6562, N III at λ 4640, N V at λ 4603 and He I at λ 5876 and 4471 were measured. For the N V line at λ 4603 it was possible to measure both emission as well as absorption velocities, whereas for the He I line λ 5876, it was possible to measure only the absorption velocity.

The intensity tracings were available for the He II line at 4686, 4860, 5410 and the N IV line at λ 4058.

3.1.3 Light Curves

From the observed energy distributions at various phases, it was possible to construct the monochromatic light curves, as well as to derive the orbital variations of emission flux of different lines. Based on the broadband photometry from various investigators, Walker et al. (1983) and Stickland et al. (1984) have analyzed the behaviour of the orbital period, in the last few decades. It appears that the period is constant during the last 45 years. Khaliullin (1973) derived a mean period combining Hiltner's data with his own and the ephemeris derived by him are similar to those of Semeniuk (1968). We have adopted the ephemeris

$$T_{\min} = 24432456.668 + 1.641246E$$

of Semeniuk (1968) for our studies.

Eight wavelengths were selected to be free of emissions and the light curves were constructed (Table 3.2). These are shown in Figures 3.2 a & b. They all generally resemble the 5300 Å light curve of Hiltner (1950).

The errors in these magnitude measures varied from season to season. In 1982, the error at quadratures and conjunctions never exceeded + 0.05 mag. In 1983 and 1984 the errors were slightly

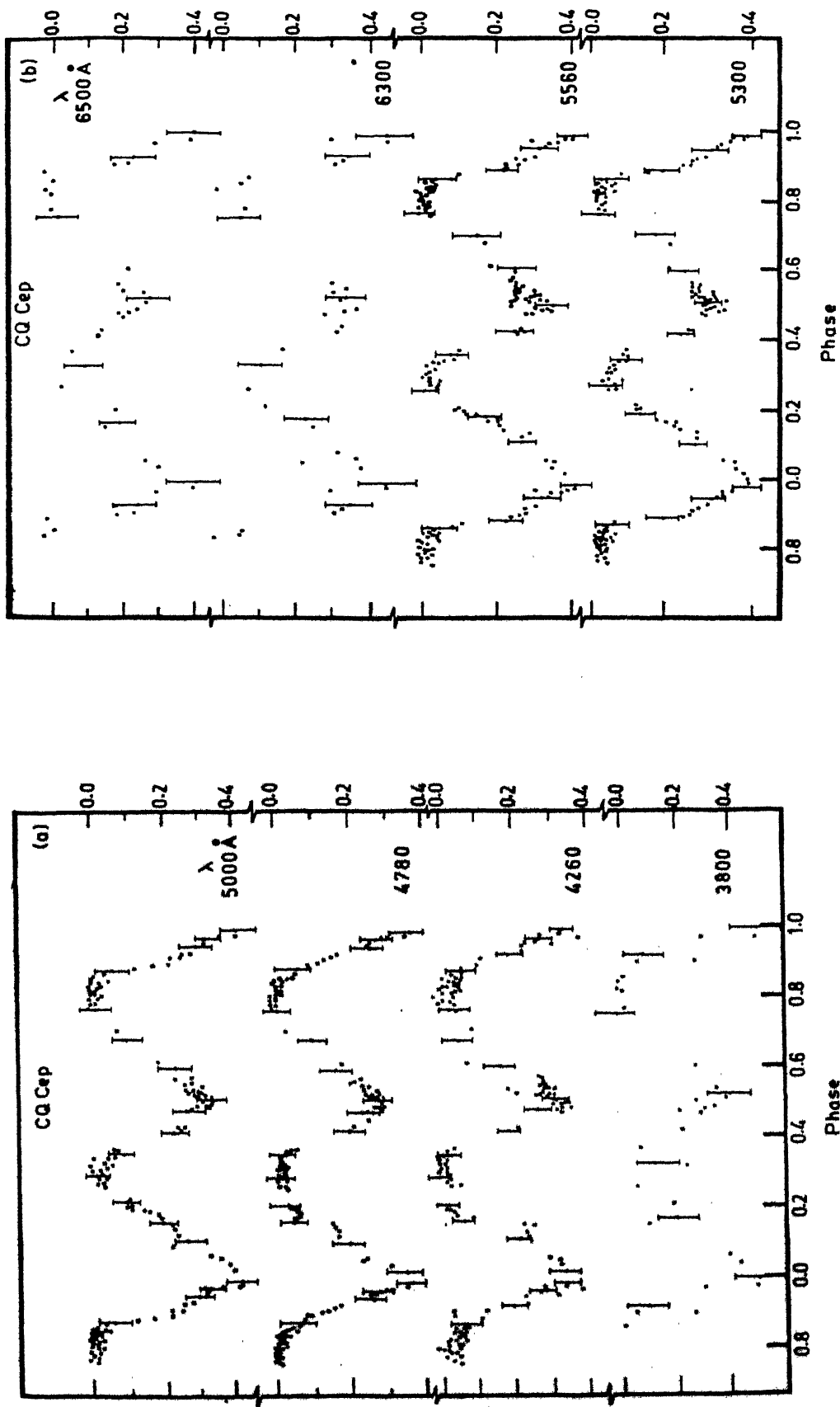


Figure 3.2 Monochromatic light curves of CQ Cep

Table 3.2

MONOCHROMATIC MAGNITUDES OF CG CEP

WAVELENGTH PHASE	4260 ANG	4780 ANG	5000 ANG	5300 ANG	5560 ANG	6300 ANG	6500 ANG	3800 ANG
0 018	0.354	0.356	0.408	0.419	0.398	-	-	-
0 038	0.342	0.316	0.398	0.392	0.365	0.392	0.324	0.347
0 053	0.340	0.236	0.378	0.392	0.371	-	-	-
0 059	0.312	0.251	0.348	0.357	0.353	0.386	0.286	0.312
0 107	0.232	0.204	0.283	0.276	0.281	-	-	-
0 124	0.257	0.181	0.253	0.280	0.280	-	-	-
0 135	0.255	0.179	0.251	0.278	0.300	-	-	-
0 146	0.269	0.169	0.240	0.232	0.235	-	-	-
0 157	0.240	0.153	0.215	0.226	0.225	0.262	0.070	0.090
0 167	0.077	0.056	0.208	0.222	0.215	0.247	0.288	0.319
0 170	0.097	0.059	0.203	0.197	0.180	-	-	-
0 182	0.057	0.068	0.178	0.172	0.175	-	-	-
0 187	0.052	0.071	0.158	0.167	0.165	-	-	-
0 192	0.041	0.051	0.123	0.129	0.135	-	-	-
0 197	0.037	0.056	0.108	0.120	0.130	-	-	-
0 202	0.032	0.046	0.118	0.126	0.110	-	-	-
0 207	0.035	0.041	0.108	0.117	0.112	0.136	0.267	0.312
0 264	0.075	0.019	0.043	0.037	0.022	0.086	0.050	0.055
0 277	0.057	0.014	0.031	0.027	0.040	-	-	-
0 277	0.031	0.042	0.034	0.058	0.059	-	-	-
0 283	0.041	0.039	0.053	0.030	0.038	-	-	-
0 288	0.011	0.036	0.020	0.075	0.068	-	-	-
0 294	0.012	0.025	0.043	0.035	0.035	-	-	-
0 300	0.031	0.041	0.011	0.000	0.020	-	-	-
0 306	0.010	0.016	0.028	0.036	0.029	-	-	-
0 312	0.013	0.032	0.047	0.042	0.039	-	-	-
0 318	0.031	0.041	0.063	0.057	0.041	-	-	-
0 321	0.012	0.031	0.001	0.057	0.050	-	-	-
0 321	0.042	0.021	0.041	0.034	0.027	-	-	-
0 332	0.031	0.029	0.013	0.057	0.065	0.126	0.112	0.105
0 339	0.010	0.029	0.050	0.062	0.045	-	-	-
0 345	0.020	0.019	0.070	0.086	0.080	-	-	-
0 351	0.033	0.031	0.091	0.091	0.094	-	-	-
0 357	0.036	0.041	0.083	0.092	0.110	-	-	-
0 363	0.032	0.231	0.073	0.077	0.092	-	-	-
0 369	0.057	0.066	0.111	0.089	0.112	0.182	0.075	0.067
0 420	0.207	0.211	0.243	0.237	0.274	0.332	0.156	0.182
0 429	0.230	0.214	0.253	0.262	0.295	0.337	0.161	0.173
0 429	0.230	0.214	0.253	0.262	0.295	0.337	0.161	0.173

Table 3.2 contd.

MONOCHROMATIC MAGNITUDES OF CG CEP (CONTD)								
WAVELENGTH PHASE	4260 ANG	4780 ANG	5000 ANG	5300 ANG	5560 ANG	6300 ANG	6500 ANG	3800 ANG
0 474	0.350	0.241	0.258	0.257	0.259	0.296	0.226	0.248
0 477	0.340	0.291	0.293	0.307	0.305	0.333	0.211	0.248
0 478	0.287	0.271	0.288	0.307	0.310	0.346	0.240	0.251
0 478	0.354	0.259	0.271	0.265	0.263	-	-	-
0 483	0.352	0.276	0.345	0.345	0.338	-	-	-
0 487	0.352	0.279	0.309	0.312	0.321	0.377	0.253	0.273
0 489	0.340	0.291	0.348	0.362	0.358	-	-	-
0 495	0.361	0.294	0.328	0.322	0.355	-	-	-
0 498	0.372	0.292	0.335	0.332	0.360	-	-	-
0 510	0.337	0.286	0.348	0.312	0.310	0.338	0.286	0.307
0 513	0.287	0.289	0.316	0.317	0.308	-	-	-
0 514	0.331	0.273	0.341	0.366	0.356	-	-	-
0 517	0.292	0.269	0.331	0.310	0.303	-	-	-
0 519	0.281	0.294	0.308	0.320	0.318	0.350	0.292	0.317
0 519	0.312	0.280	0.343	0.338	0.331	-	-	-
0 523	0.317	0.266	0.310	0.302	0.309	-	-	-
0 526	0.231	0.265	0.287	0.287	0.315	-	-	-
0 527	0.320	0.286	0.328	0.337	0.318	-	-	-
0 530	0.297	0.284	0.298	0.266	0.272	-	-	-
0 535	0.336	0.292	0.323	0.329	0.327	-	-	-
0 536	0.302	0.250	0.316	0.276	0.269	-	-	-
0 537	0.206	0.249	0.274	0.287	0.280	0.321	0.280	0.290
0 540	0.297	0.250	0.324	0.325	0.323	0.356	0.219	0.280
0 543	0.320	0.261	0.271	0.266	0.265	-	-	-
0 549	0.312	0.241	0.296	0.286	0.278	-	-	-
0 555	0.305	0.262	0.242	0.267	0.267	-	-	-
0 561	0.300	0.226	0.248	0.292	0.287	0.320	0.206	0.217
0 568	0.290	0.240	0.293	0.270	0.268	-	-	-
0 601	0.185	0.171	0.246	0.247	0.270	0.315	0.334	0.215
0 610	0.087	0.186	0.181	0.202	0.200	-	-	-
0 675	0.072	0.112	0.108	0.207	0.190	-	-	-
0 705	0.107	0.036	0.078	0.167	0.163	-	-	-
0 767	0.047	0.006	0.003	0.009	0.010	-	-	-
0 779	0.022	0.009	0.018	0.009	0.010	0.069	0.019	0.025
0 780	0.064	0.003	0.011	0.025	0.028	-	-	-
0 787	0.050	0.000	0.003	0.022	0.030	-	-	-
0 792	0.033	0.014	0.026	0.025	0.025	-	-	-

Table 3.2 contd.

WAVELENGTH PHASE	MONOCHROMATIC MAGNITUDES OF CO CEP (CONTD)							
	4260 ANG	4780 ANG	5000 ANG	5300 ANG	5560 ANG	6300 ANG	6500 ANG	6800 ANG
0 502	0 000	0 007	0 031	0 030	0 043	-	-	-
0 303	0 062	0 002	0 318	0 029	0 040	-	-	-
0 809	0 060	0 015	0 007	0 007	0 015	-	-	-
0 811	0 031	0 015	0 013	0 007	0 010	-	-	-
0 315	0 065	0 031	0 005	0 011	0 013	-	-	-
0 820	0 021	0 020	0 024	0 026	0 029	-	-	-
0 821	0 074	0 028	0 002	0 015	0 015	-	-	-
0 828	0 033	0 016	0 035	0 052	0 059	0 095	0 009	0 015
0 828	0 047	0 016	0 011	0 002	0 000	-	-	-
0 833	0 073	0 016	0 000	0 008	0 055	0 000	0 001	0 005
0 334	0 064	0 021	0 016	0 030	0 038	-	-	-
0 838	0 067	0 010	0 031	0 045	0 052	-	-	-
0 840	0 073	0 031	0 026	0 022	0 030	-	-	-
0 842	0 071	0 016	0 003	0 002	0 040	-	-	-
0 846	0 067	0 035	0 021	0 022	0 025	0 069	0 000	0 005
0 847	0 050	0 021	0 055	0 056	0 058	-	-	-
0 850	0 074	0 021	0 033	0 012	0 032	-	-	-
0 857	0 073	0 029	0 043	0 035	0 035	0 080	0 021	0 021
0 857	0 046	0 041	0 013	0 022	0 043	-	-	-
0 863	0 082	0 051	0 043	0 032	0 060	-	-	-
0 871	0 082	0 071	0 074	0 071	0 100	-	-	-
0 879	0 120	0 072	0 135	0 152	0 120	-	-	-
0 888	0 121	0 079	0 183	0 192	0 222	-	-	-
0 897	0 047	0 101	0 228	0 242	0 250	-	-	-
0 905	0 044	0 126	0 228	0 262	0 280	0 325	0 001	0 021
0 911	0 137	0 146	0 265	0 272	0 285	0 347	0 046	0 057
0 917	0 212	0 163	0 268	0 282	0 290	-	-	-
0 926	0 247	0 180	0 293	0 312	0 320	0 366	0 059	0 077
0 948	0 245	0 265	0 313	0 322	0 335	-	-	-
0 954	0 330	0 259	0 326	0 337	0 353	-	-	-
0 960	0 286	0 271	0 335	0 352	0 358	-	-	-
0 966	0 302	0 283	0 343	0 352	0 382	-	-	-
0 972	0 299	0 314	0 371	0 385	0 405	-	-	-
0 972	0 400	0 301	0 323	0 377	0 315	0 305	0 311	0 242
0 979	0 354	0 359	0 421	0 417	0 420	0 459	0 420	0 435
0 986	0 357	0 371	0 426	0 424	0 422	0 457	0 324	0 438

higher - at quadratures it was + 0.06 mag and at conjunctions +0.08 mag. On some occasions, when the error exceeded + 0.1 mag, the observations were not included in the light curve at all. However, it is possible that these represent the intrinsic variations of the system.

3.1.4 Emission line flux

The flux of some lines of He I, He II, N III, N IV, N V and C IV were measured from these energy distributions. Many lines appear as blends - the most complicated being the region λ 4600 to 4700 A. The line of N V at λ 4603 is associated with an absorption throughout the orbit. The emissions of N III at λ 4640 and He II at λ 4686, which follow this line immediately, are very strong. In our spectrophotometric scans, it was barely possible to resolve these three emissions (resolution 10 A per channel). A smooth curve was drawn to represent approximate gaussian profiles of these lines. The continuum was fixed by the points at λ 4460 and 4790 A. The area, within the profile, above the continuum only was measured. The errors in the flux arise mainly because of the assumed gaussian profiles. Such errors are indicated in the corresponding plots. Strong lines like the N IV at λ 4058 and the He II at 4860 have least errors because they are free of any blends. At the same time intrinsically weak emissions like C IV at λ 5808 show larger errors.

It was also found that at phases near 0.25 and 0.75, the errors were larger. The scan, in general, looked noisy probably because the linestrengths also diminished at these phases. At phases close to 0.75, sometimes, it was not possible to measure

Table 3.3 Emission line Fluxes

	PHASE	MIV 3058 x10-9	NV 4603 10-11	NI II 4810 10-9	He II 4840 10-9	He II 5410 10-9	CIV 5808 10-10	He I 5876 10-10	He II 4562 10-10	He I 6678 10-10	Blnd 4100 10-9	Blnd 4540 10-9	Blnd 4200 10-9
3440003													
4941.109	0.972	110.0	29.0	204.0	304.0	203.0	132.0	48.0	182.0	95.0	-	-	-
4942.141	0.601	108.0	72.0	103.0	384.0	103.0	114.0	102.0	140.0	90.0	-	-	-
5253.180	0.823	68.0	92.0	24.0	371.0	24.0	35.0	18.0	117.0	62.0	246.0	163.0	114.0
5253.196	0.842	163.0	102.0	58.0	410.0	58.0	-	-	-	-	219.0	199.0	184.0
5253.209	0.850	75.0	78.0	88.0	322.0	88.0	-	-	-	-	282.0	160.0	93.0
5253.219	0.857	34.0	93.0	127.0	478.0	127.0	-	-	-	-	163.0	184.0	59.0
5253.231	0.863	63.0	74.0	84.0	431.0	84.0	-	-	-	-	180.0	136.0	84.0
5253.244	0.871	72.0	72.0	87.0	484.0	87.0	-	-	-	-	170.0	207.0	63.0
5253.257	0.879	74.0	68.0	79.0	490.0	78.0	-	-	-	-	158.0	190.0	110.0
5253.272	0.888	83.0	64.0	74.0	623.0	74.0	-	-	-	-	167.0	177.0	148.0
5253.286	0.897	146.0	58.0	77.0	587.0	77.0	-	-	-	-	234.0	274.0	79.0
5253.299	0.905	175.0	44.0	147.0	490.0	147.0	92.0	63.0	190.0	72.0	196.0	153.0	98.0
5254.091	0.917	84.0	53.0	162.0	432.0	162.0	-	-	-	-	137.0	140.0	87.0
5254.144	0.920	160.0	78.0	87.0	373.0	87.0	136.0	88.0	93.0	90.0	273.0	150.0	200.0
5254.158	0.929	208.0	84.0	97.0	470.0	97.0	104.0	102.0	189.0	119.0	257.0	109.0	138.0
5254.239	0.978	180.0	68.0	106.0	468.0	106.0	127.0	90.0	219.0	133.0	266.0	179.0	201.0
5254.254	0.987	182.0	42.0	92.0	416.0	92.0	141.0	77.0	199.0	115.0	256.0	132.0	125.0
5254.272	0.998	180.0	59.0	115.0	407.0	115.0	132.0	-	-	-	177.0	176.0	96.0
5254.409	0.526	132.0	75.0	83.0	440.0	83.0	-	-	-	-	196.0	230.0	82.0
5254.080	0.911	70.0	42.0	151.0	533.0	151.0	-	92.0	150.0	75.0	113.0	209.0	52.0
5254.106	0.926	115.0	48.0	158.0	480.0	158.0	106.0	109.0	203.0	102.0	209.0	239.0	50.0
5254.107	0.537	162.0	80.0	114.0	490.0	114.0	77.0	110.0	223.0	125.0	286.0	198.0	79.0
5314.096	0.948	124.0	42.0	162.0	428.0	162.0	-	-	-	-	163.0	60.0	42.0
5314.106	0.954	72.0	47.0	132.0	323.0	132.0	-	-	-	-	202.0	80.0	203.0
5314.116	0.960	94.0	38.0	180.0	487.0	180.0	-	-	-	-	192.0	224.0	220.0
5314.129	0.966	98.0	29.0	184.0	416.0	184.0	-	-	-	-	134.0	168.0	207.0
5314.238	0.972	140.0	22.0	196.0	402.0	196.0	-	-	-	-	150.0	177.0	187.0
5314.147	0.979	122.0	18.0	177.0	410.0	177.0	137.0	122.0	240.0	135.0	201.0	104.0	187.0
5314.158	0.986	149.0	22.0	170.0	412.0	170.0	147.0	110.0	233.0	140.0	163.0	94.0	137.0
5447.171	0.107	90.0	62.0	130.0	332.0	50.0	-	-	-	-	201.0	134.0	125.0
5447.217	0.135	92.0	72.0	-	330.0	-	-	-	-	-	97.0	83.0	106.0
5449.235	0.146	72.0	106.0	-	260.0	-	-	-	-	-	102.0	110.0	77.0

Table 3.3 contd.

	PHASE	NIV 4038 110-9	NV 4603 10-11	MSII 4848 10-9	MSII 4850 10-9	MSII 4852 10-10	CIV 5808 10-10	MSI 5874 10-10	MSII 4562 10-10	MSI 6078 10-10	MSI 4100 10-9	MSI 4360 10-9	MSI 4500 10-9
2440 200													
2449 234	0.197	113.0	113.0	-	290.0	-	24.0	82.0	180.0	83.0	102.0	110.0	97.0
2451 071	0.264	70.0	78.0	139.0	320.0	39.0	37.0	51.0	81.0	92.0	73.0	99.0	62.0
2451 091	0.277	98.0	52.0	123.0	247.0	48.0	-	-	-	-	50.0	38.0	39.0
2451 100	0.283	68.0	74.0	113.0	338.0	83.0	-	-	-	-	68.0	55.0	49.0
2451 128	0.294	82.0	64.0	108.0	296.0	98.0	-	-	-	-	101.0	75.0	68.0
2451 129	0.300	92.0	78.0	92.0	282.0	62.0	-	-	-	-	92.0	118.0	101.0
2451 159	0.304	63.0	82.0	131.0	277.0	31.0	-	-	-	-	104.0	92.0	82.0
2451 149	0.312	81.0	52.0	78.0	311.0	38.0	-	-	-	-	76.0	63.0	64.0
2451 158	0.318	113.0	106.0	106.0	340.0	60.0	-	-	-	-	96.0	110.0	43.0
2451 148	0.324	65.0	78.0	83.0	387.0	68.0	-	-	-	-	87.0	88.0	62.0
2451 194	0.339	93.0	92.0	90.0	290.0	30.0	-	-	-	-	90.0	117.0	71.0
2451 203	0.345	126.0	63.0	84.0	326.0	64.0	-	-	-	-	128.0	95.0	101.0
2451 212	0.351	103.0	60.0	120.0	300.0	60.0	-	-	-	-	140.0	140.0	101.0
2451 222	0.357	113.0	72.0	109.0	342.0	109.0	-	-	-	-	-	-	-
2451 232	0.363	142.0	114.0	173.0	380.0	118.0	-	-	-	-	155.0	170.0	113.0
2451 242	0.369	106.0	82.0	120.0	357.0	120.0	77.0	123.0	172.0	70.0	-	-	-
2460 093	0.124	80.0	102.0	-	298.0	-	-	-	-	-	114.0	104.0	82.0
2460 093	0.762	87.0	91.0	55.0	345.0	58.0	40.0	85.0	70.0	45.0	69.0	73.0	97.0
2460 102	0.767	74.0	107.0	-	260.0	-	-	-	-	-	32.0	44.0	84.0
2460 123	0.789	50.0	88.0	64.0	297.0	64.0	-	-	-	-	42.0	49.0	72.0
2460 134	0.787	-	102.0	-	312.0	-	-	-	-	-	34.0	38.0	64.0
2460 141	0.803	-	110.0	52.0	300.0	52.0	-	-	-	-	-	-	-
2460 171	0.809	48.0	78.0	-	275.0	-	-	-	-	-	75.0	64.0	109.0
2460 181	0.813	60.0	102.0	-	372.0	-	-	-	-	-	84.0	69.0	85.0
2460 191	0.821	50.0	68.0	-	354.0	-	-	-	-	-	92.0	98.0	136.0
2460 202	0.828	55.0	97.0	32.0	302.0	32.0	-	-	-	-	-	-	-
2460 212	0.834	79.0	92.0	-	302.0	-	-	-	-	-	108.0	103.0	77.0
2460 221	0.840	94.0	75.0	-	294.0	-	-	-	-	-	99.0	124.0	118.0
2460 231	0.846	88.0	104.0	28.0	343.0	28.0	28.0	62.0	68.0	60.0	115.0	110.0	185.0
2476 092	0.510	204.0	68.0	158.0	455.0	148.0	109.0	198.0	192.0	120.0	211.0	201.0	176.0
2476 104	0.517	173.0	62.0	152.0	407.0	152.0	-	-	-	-	-	-	-
2476 114	0.523	134.0	78.0	120.0	350.0	120.0	-	-	-	-	-	-	-

Table 3.3 contd.

JD ↓	PHASE	NIV 4058 x10-9	NV 4603 10-11	NIII 4640 10-9	HeII 4686 10-9	HeII 4860 10-9	HeII 5410 10-9	CIV 5808 10-10	HeI 5876 10-10	HeII 6502 10-10	HeI 6678 10-10	Blnd 4150 10-9	Blnd 4540 10-9	Blnd 4200 10-9
2440000														
5676.124	0.530	192.0	51.0	135.0	422.0	105.0	-	-	-	-	-	231.0	176.0	128.0
5676.135	0.536	180.0	72.0	101.0	464.0	101.0	-	-	-	-	-	-	-	-
5676.146	0.543	193.0	69.0	102.0	401.0	102.0	-	-	-	-	-	-	-	-
5676.156	0.549	190.0	101.0	132.0	355.0	132.0	-	-	-	-	-	-	-	-
5676.166	0.555	180.0	91.0	106.0	388.0	106.0	-	-	-	-	-	210.0	162.0	86.0
5676.176	0.561	146.0	81.0	83.0	418.0	83.0	73.0	125.0	152.0	210.0	105.0	-	-	-
5676.187	0.568	161.0	84.0	94.0	382.0	94.0	-	-	-	-	-	-	-	-
5945.535	0.675	95.0	102.0	-	412.0	-	-	-	-	-	-	41.0	109.0	31.0
5945.585	0.705	122.0	83.0	-	395.0	-	-	-	-	-	-	35.0	70.0	22.0
5963.252	0.476	192.0	42.0	-	434.0	165.0	120.0	121.0	132.0	180.0	117.0	152.0	178.0	126.0
5963.257	0.478	251.0	51.0	158.0	421.0	153.0	-	-	-	-	-	210.0	207.0	185.0
5963.317	0.514	251.0	96.0	147.0	350.0	147.0	-	-	-	-	-	177.0	155.0	214.0
5963.326	0.519	176.0	115.0	52.0	380.0	122.0	-	120.0	187.0	220.0	115.0	245.0	215.0	190.0
5963.339	0.527	205.0	98.0	135.0	325.0	135.0	-	-	-	-	-	-	-	-
5963.352	0.535	193.0	90.0	110.0	360.0	110.0	-	-	-	-	-	-	-	-
5963.360	0.540	220.0	90.0	120.0	385.0	98.0	59.0	120.0	175.0	182.0	110.0	135.0	79.0	58.0
5964.144	- 18	190.0	28.0	95.0	320.0	141.0	62.0	-	-	-	-	212.0	198.0	150.0
5964.176	- 38	178.0	58.0	99.0	380.0	108.0	75.0	99.0	160.0	227.0	122.0	201.0	205.0	188.0
5964.202	- 53	162.0	52.0	102.0	360.0	122.0	102.0	-	-	-	-	-	-	-
5964.211	- 99	195.0	85.0	120.0	375.0	92.0	60.0 ⁸	90.0	155.0	215.0	104.0	176.0	192.0	140.0
6037.113	0.477	-	-	-	-	-	-	101.0	120.0	207.0	99.0	-	-	-
6047.186	0.610	116.0	68.0	-	388.0	-	-	-	-	-	-	110.0	151.0	60.0
6048.092	0.167	-	-	-	-	-	-	35.0	105.0	152.0	57.0	-	-	-
6048.158	0.207	-	-	-	-	-	-	31.0	80.0	122.0	45.0	-	-	-

the emission flux because the emission was buried in noise. Such measurements are not included in the flux plots (Figures 3.3 to 3.8). Table 3.3 lists all the measured flux.

3.1.5 Radial Velocity Curves

The radial velocities were measured with the Abbe Comparator. The central portion of the emission line was chosen for the measurement. Because of the broad features, the errors are larger, especially in case of N III 4640 Å. The errors are generally 40 to 60 kms^{-1} . These curves were solved by Lehmann-Filhes method and all solutions, including those obtained by others, are tabulated in Table 3.4. The individual velocity curves appear with flux plots (Table 3.5 & Figures 3.3 to 3.8). It appears reasonable to assume that the measures of Stickland et al. (1984) and Leung et al. (1983) are more accurate by virtue of the method of measurement and solution.

3.2 Correlation between light and velocity curves

3.2.1 Helium lines

The lines of He II that are studied are at λ 4686, 4860, 5410 and 6562 Å.

The strongest line in the spectra is the He II line at 4686. Figure 3.3a shows the measured intensities and flux. It also includes the radial velocity measurements of Bappu & Viswanadham (1977), who derived an orbital solution with eccentricity $e = 0.31$ and the velocity for the center of mass as $\gamma = 118 \text{ km s}^{-1}$. They also studied the line profiles, which are narrow and sharp at minima and broad and rounded at quadratures. The Figure 3.3a clearly shows the enhancement of flux and intensity at phases near 0.0 and 0.5. This is confirmity with the

Table 3.4
ORBITAL SOLUTIONS FROM RV CURVES FOR CQ CEP

LINE	γ	K	e	w	Ref
HeII 4686	+117.5	148.2	0.31	323	1
	+133.8	164.0	0.26	356.4	2
4860	+196.0	221.9	0.35	286	6
	± 11.4	± 12.2	± 0.02	± 18	
	+198.2	235.8	0.36		2
5411	+176.0	230.1	0.095	335	3
6562	+206.0	212.0	0.233	331	6
	± 10.2	± 12.5	± 0.03	± 19	
NIII 4640	-114.0	127.8	0.014	316	6
	± 8.2	± 10.4	± 0.019		
	-114.3	127.0	0.0		2
NIV 4058	-60.8	312.7	0.035	96.7	1
	-53.4	297.4	0.0		2
	-60	310			4
	-85	285			5
NV 4603e	+159.6	286.0	0.041	295	6
	± 7.2	± 6.4	± 0.017		
	+153	280			4
NV 4603a	-216.1	307.5	0.035	298	6
	± 5.8	± 7.3	± 0.018		
	-220	299			4

References to the Table
1 Bappu & Viswanadham, 1977
2 Stickland et al., 1984
3 Giridhar, 1978
4 Leung et al., 1983
5 Niemela, 1980
6 This work

Table 3.5

RADIAL VELOCITIES OF CQ CEP

PHASE	HeII 4860	NV 4603e	NV 4603a	NIII 4640
0.014	+180	+ 80	-204	-105
0.087	+ 22	- 35	-315	-160
0.138	- 31	-115	-406	-168
0.232	- 85	-135	-515	-190
0.264	-110	-140	-495	-188
0.280	-132	-110	-485	-177
0.351	- 94	- 15	-452	-175
0.433	+ 45	+ 50	-295	-135
0.476	+188	+145	-240	-128
0.606	+352	+320	- 75	- 85
0.645	+435	+410	- 45	- 60
0.676	+462	+445	+ 35	- 57
0.687	+445	+450	+ 58	- 52
0.844	+401	+380	+ 45	- 72
0.878	+322	+315	- 75	- 75
0.944	+252	+205	-155	-105

earlier studies (Hiltner, 1950); Khaliullin, 1973; Bappu & Viswanadham, 1977). The two maxima are of unequal magnitudes, the one near phase 0.0 is stronger. Also it may be noticed that the maxima do not coincide with phases 0.0 and 0.5, but are slightly shifted. This shift was seen by Hiltner (1950) also, but in an opposite direction. It may also be seen from the Figure 3.2 a & b, that the falling edges of the minima are not smooth. Similar effect is probably reflected in the flux measures. A similar effect was seen by Walker et al. (1983), who studied the eclipses in a great detail.

The 4860 line of He II is shown in Figure 3.3b for intensities, radial velocities and flux. Although the general behaviour is similar to $\lambda 4686$ line, it may be seen that the flux at phases 0.0 and 0.5 are of similar magnitude and they do not show a sudden increase like the 4686 line itself. Also the variation is smoother and the flux at phase 0.75 are smaller compared to those at phase 0.25. The amplitude of the radial velocity curve is slightly larger than that of $\lambda 4686$ and this curve gives an orbital solution of $e = 0.36$ and $\gamma = 196 \text{ km s}^{-1}$. The line profile given by Bappu & Viswanadham (1977) show that the violet absorption cuts into the emission wing at some phases especially after the secondary minimum. To study this all the plates were checked for the behaviour of this line. It appears that $\lambda 4860$ line has got a variable structure, which was noted by Hiltner (1950) also, with multiple components. The effect of the absorption in the violet wing appears to be more prominent at phases close to 0.75, but it appears that there is an

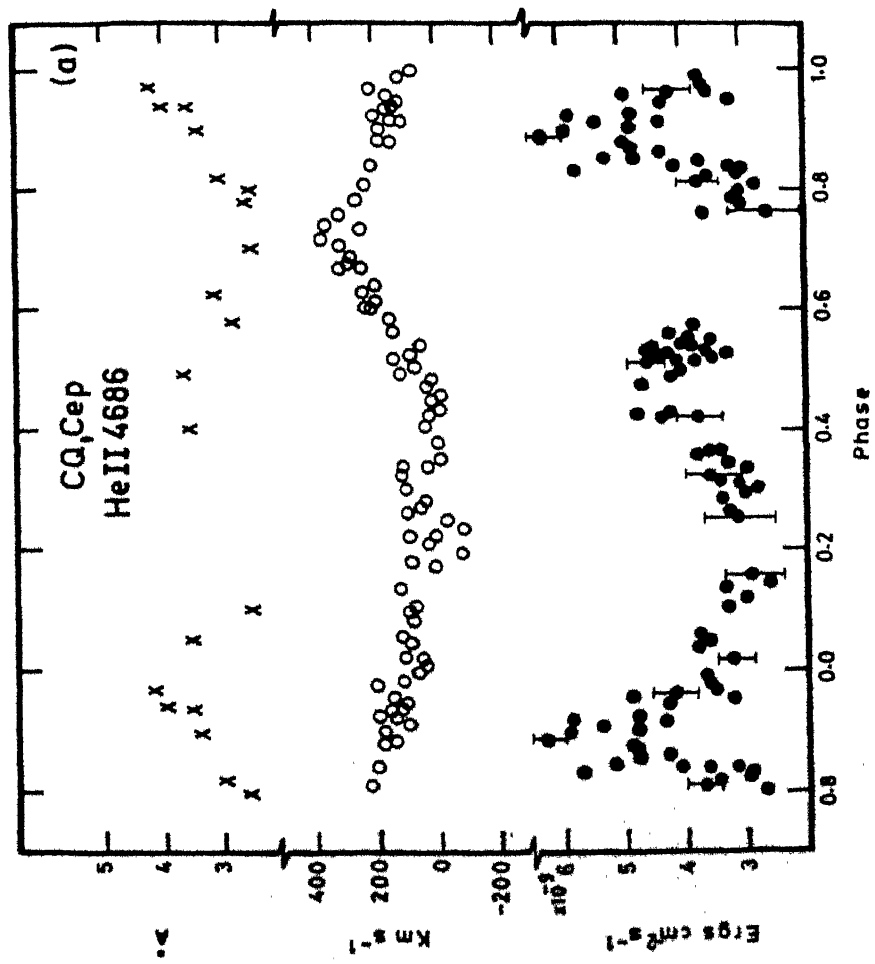
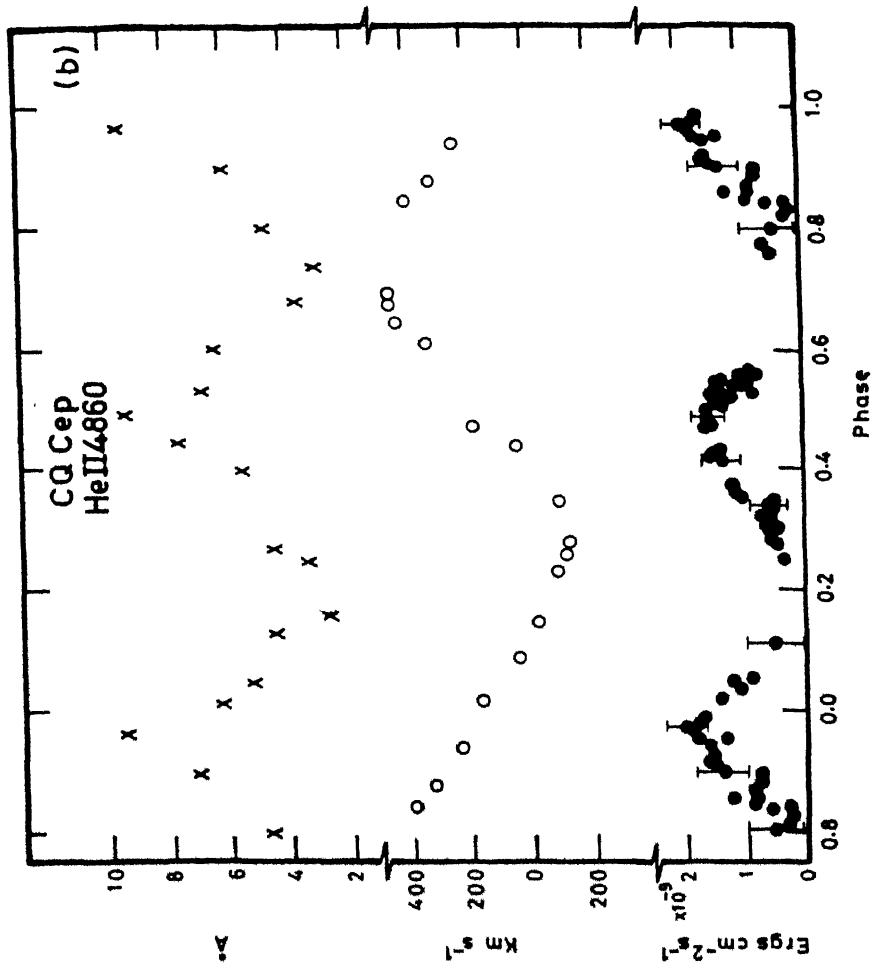


Figure 3.3 Flux variations of various He II emission lines Radial velocity (unfilled circles) and emission equivalent widths (crosses) also are included (a) λ 4686.

Figure 3.3 (b) 4860

absorption component which moves with the emission. Since this component is weak at all phases, it was not possible to measure this line very precisely.

Figure 3.3c shows the flux and intensities of 5410 Å line of He II. The radial velocities from Giridhar (1978) also are included; the orbital solution from this RV curve may be quoted as $e = 0.1$ and $\gamma = 176 \text{ km s}^{-1}$. The line profiles also have been studied by her and they appear to be generally symmetrical, with an indication of a violet absorption edge just after secondary minimum. The enhancement of flux close to phases 0.0 and 0.5 are very smooth, as are the intensity measures as well.

The radial velocities and flux of the He II line at 6562 Å are shown in Figure 3.3d. This RV curve gives an orbital solution of $e = 0.31$ and $\gamma = 206 \text{ km s}^{-1}$. The density tracings of some spectra to include this region are shown in Figure 3.9a, which clearly demonstrates the variation of the structure of the line. Like the $\lambda 4860$ line, this also shows the violet absorption edges soon after the secondary minimum, whereas at phases just after the primary minimum such effects are barely detectable. However, spectra with better dispersion can resolve this phenomenon.

Among the He I lines, it was possible to study those at 5876 and 6678. Figure 3.9a includes the region of $\lambda 6678$ as well. It may be seen that the line profile varies throughout the orbit, making the radial velocity measurements very difficult. Sometimes, it appears as though the line is split into two components. Figure 3.9b shows the structure of the $\lambda 5876$ line. It may be noticed that the violet absorption edge is very strong and it appears throughout the orbital cycle, whereas the emissions

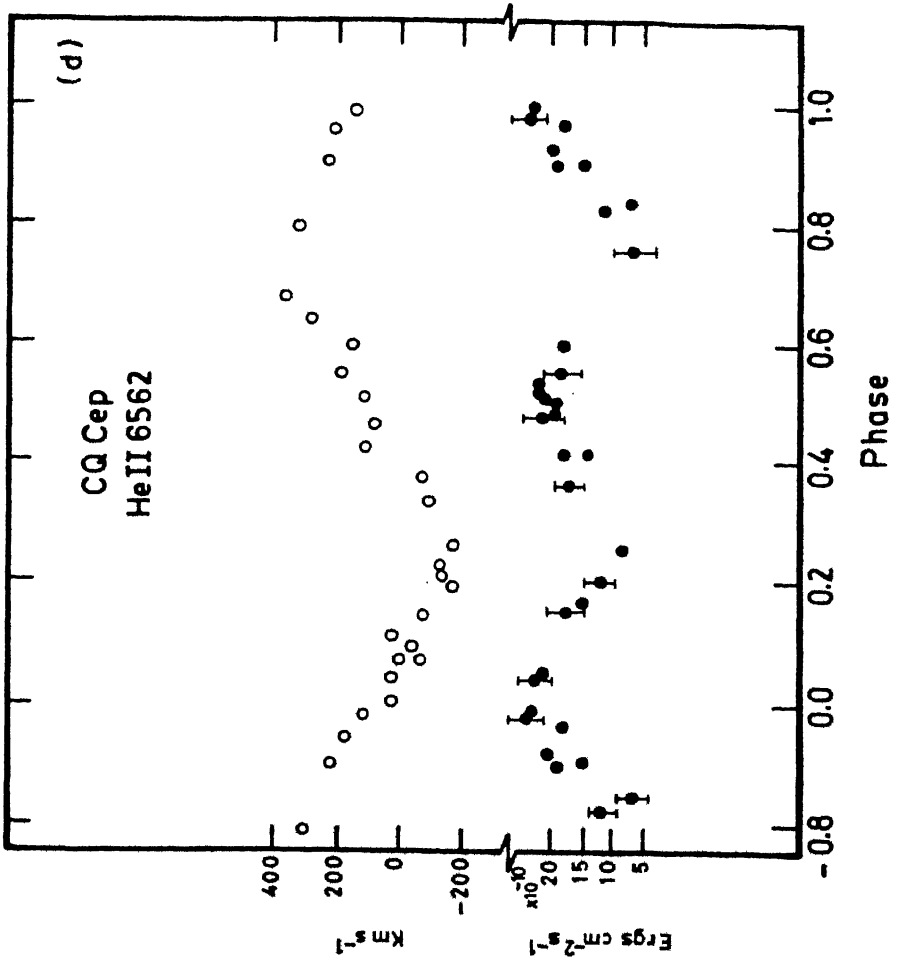


Figure 3.3 (d) 6562

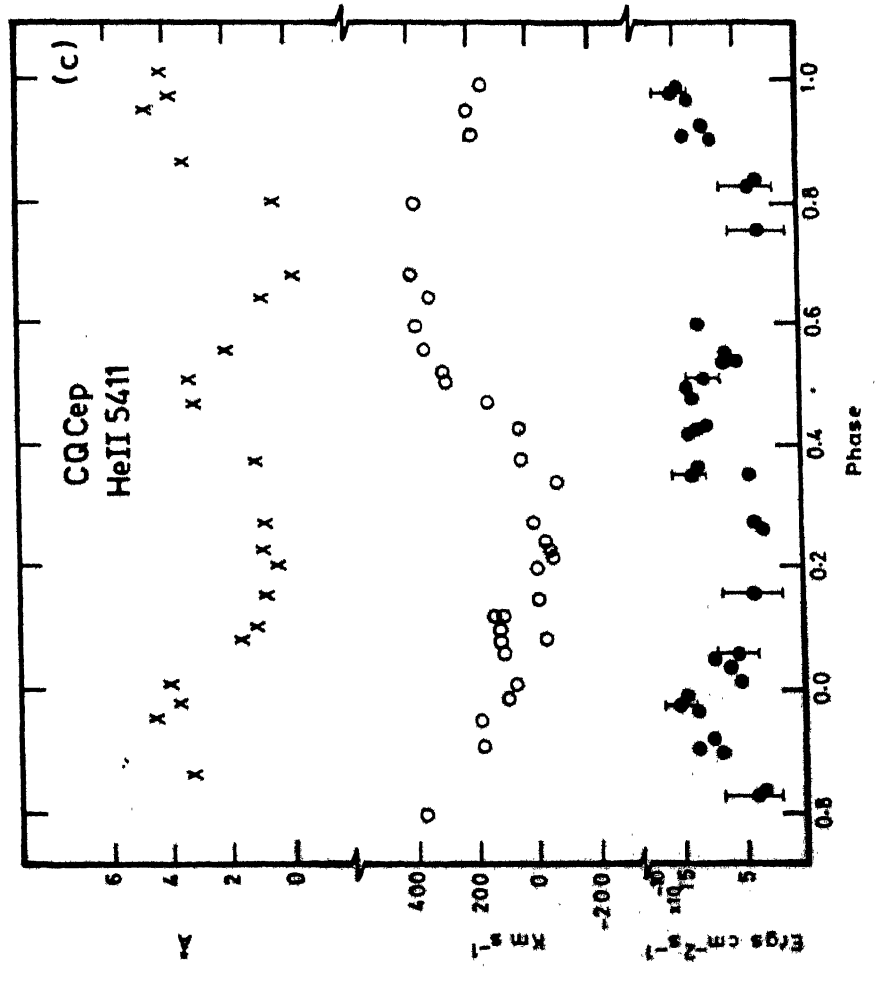


Figure 3.3 (c) 5411

are not very sharp. Thus it was possible to measure the absorption velocities only. Figure 3.7 shows this absorption RV curve as well as the flux. The RV curve displays a large scatter making it very difficult to find any orbital solution. In the same Figure 3.7 the flux of the 6678 line also are included. The behaviour of flux is similar to the other lines of helium, discussed till now, with a smaller amplitude of variation.

3.2.2 Nitrogen lines

The nitrogen lines that are studied are N III at $\lambda 4640$, N IV at $\lambda 4058$ and N V at $\lambda 4603$.

The N III line at 4640 is affected at both the wings by the He II line at 4686 and N V line at 4603. Thus the measured flux may not be very accurate. Allowing for these measures in the flux measures, it may be seen from Figure 3.4 that the flux increases at phases 0.0 and 0.5 and the total amplitude of variation is very small. Bappu (1973) had pointed out that this broad emission is probably a blend of more than 3 lines, based on high dispersion spectral studies. The radial velocities were measured with a mean center of emission and this also is shown in Figure 3.4. It appears that the amplitude is quite small compared to RV curves of other lines. An orbital solution gives almost a circular orbit with $e = 0.014$ and $\gamma = -114 \text{ kms}^{-1}$. It may be noticed that this γ value is different compared to other emission lines.

Bappu and Viswanadham (1977) emphasized that the N IV line of $\lambda 4058$ is the only line that represents the true motion of the WN component. They derived the orbital solution as $e = 0.1$ and

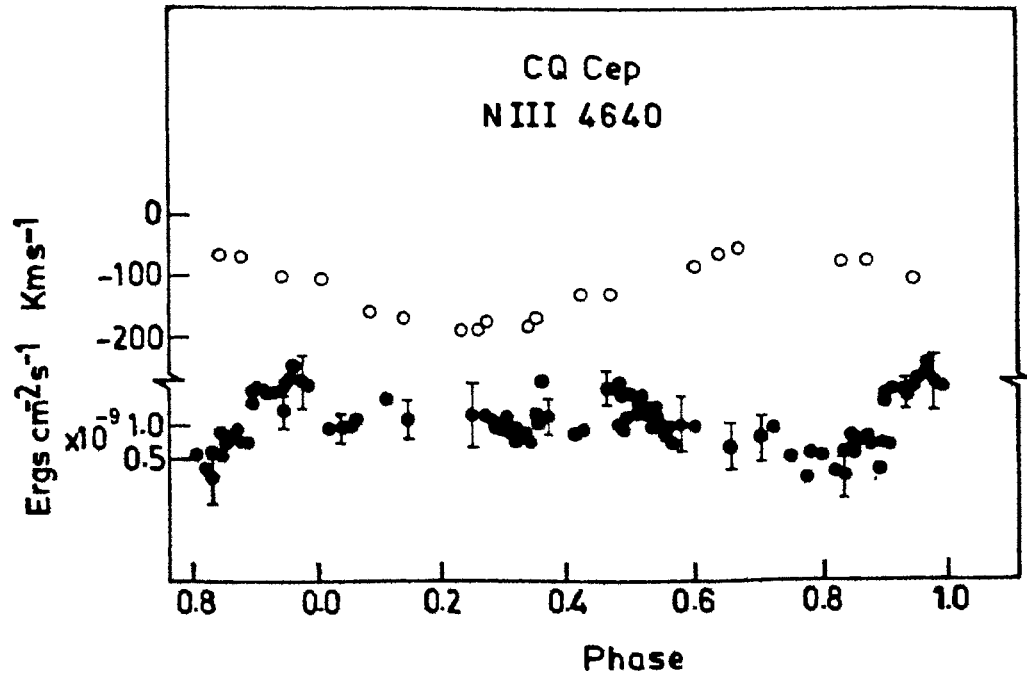


Figure 3.4 Variation of flux and RV for N III λ 4640 symbols same as in Figure 3.3.

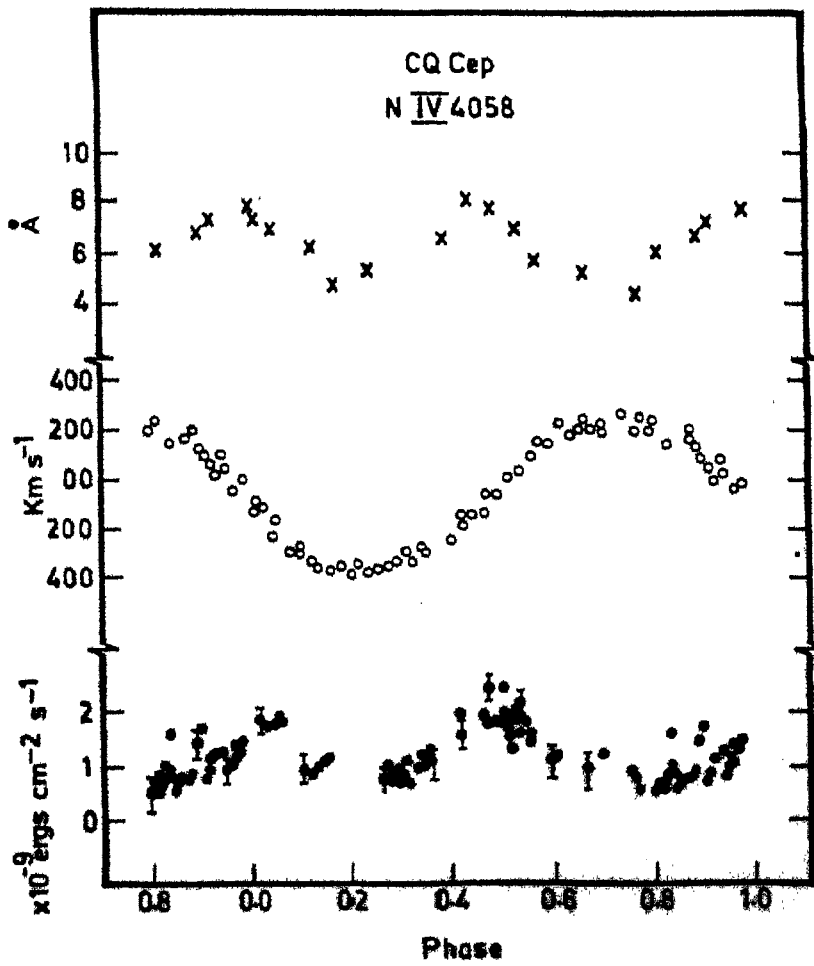


Figure 3.5 Variation of flux, RV and emission equivalent width for N IV λ 4058 symbols same as in Figure 3.3.

$\gamma = -62 \text{ kms}^{-1}$. They have shown that the profile is not affected by the absorptions and is generally symmetrical. Figure 3.5 shows the measured line flux, showing enhancement at minima, as well as the radial velocities.

Now, we turn to the N v line at $\lambda 4603$, which has a stable profile and a violet absorption is seen throughout the orbital phase. It was possible to derive the RV curves for both the emission and absorption components. These curves and the flux are shown in Figure 3.6. The flux measures are probably affected by the violet wing of the strong N III line at $\lambda 4640$, but only high dispersion can reveal this effect. The line flux above the continuum only are measured and, unlike the variation of flux of other emission lines discussed till now, these measures show a dip near phase 0.0, but for this the flux values are generally constant. Both the RV curves give almost circular orbit solutions with only the γ values shifted (Table 3.4)

3.2.3 Carbon lines

The only Carbon line that was available for measurement of flux was that of C IV at 5808 A. The measured flux show the same pattern as the other lines (Figure 3.8). The amplitude of variation is not very large. This region is covered in the density tracings of Figure 3.9b, which clearly points to the difficulty in measuring the radial velocity, at any phase. Since the spectrophotometric observations made in the red region were not as frequent as in the blue region, the number of flux measures are relatively smaller. This is true for the other lines in the region, namely 5876, 6678 lines of He I and 6562 line of He II as well.

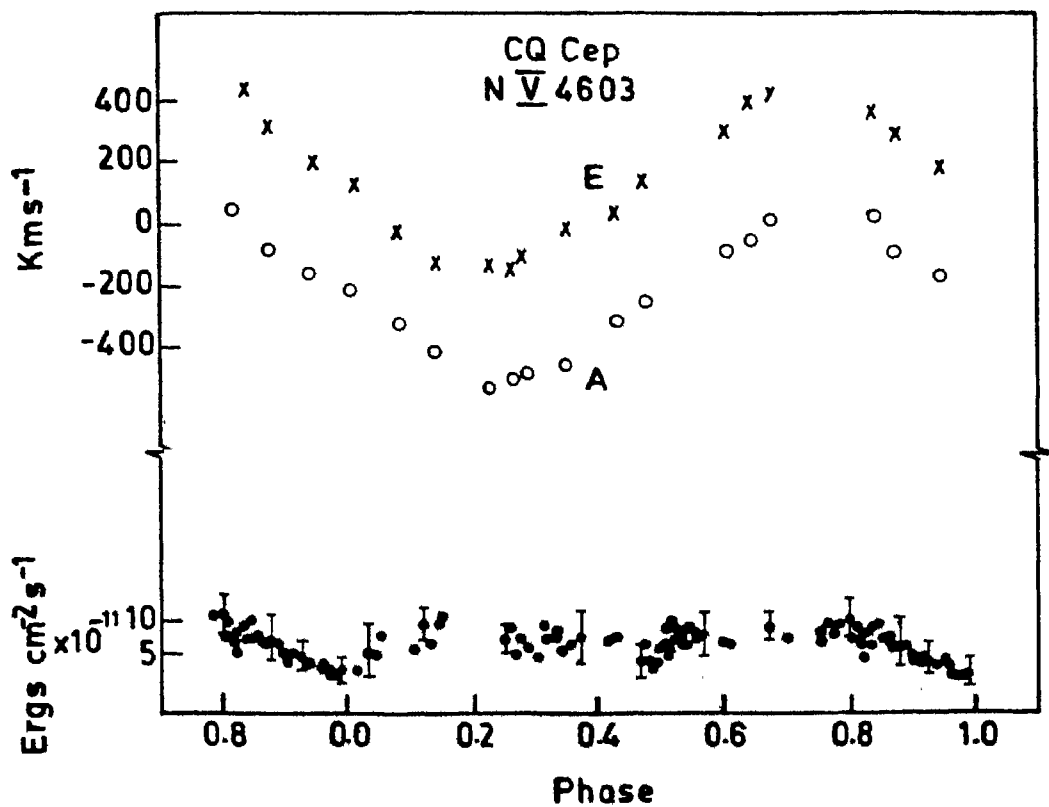


Figure 3.6 Variation of flux and RV (emission and absorption) for N V λ 4603.

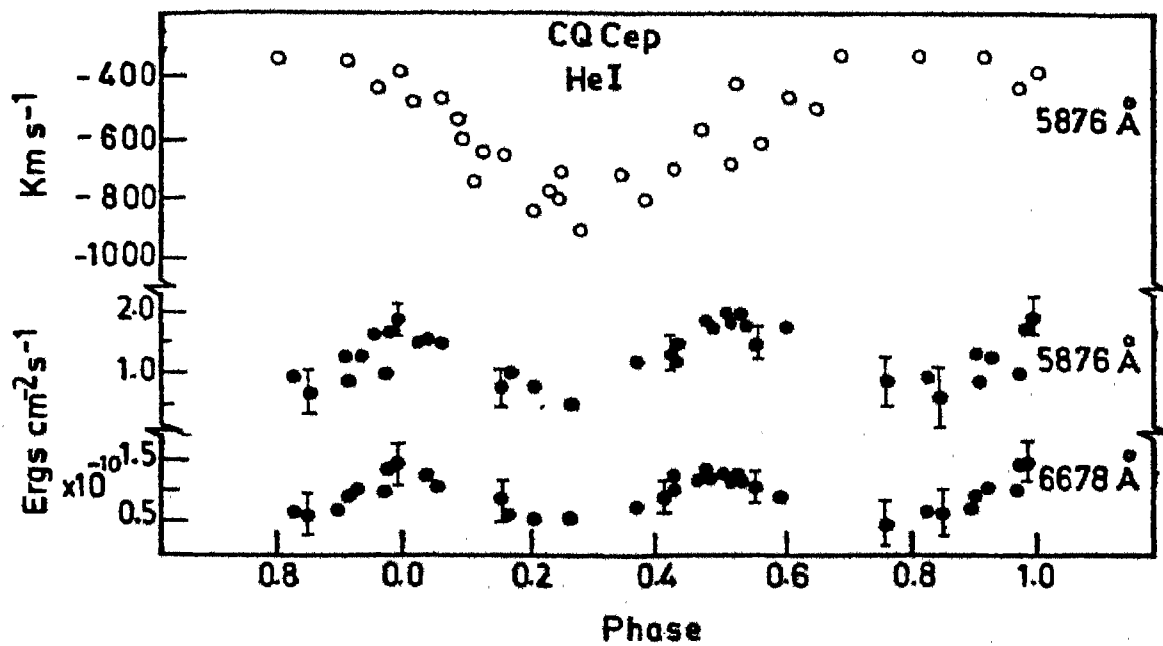


Figure 3.7 Flux variation of He I λ 6678 and λ 5876 and RV variation of λ 5876.

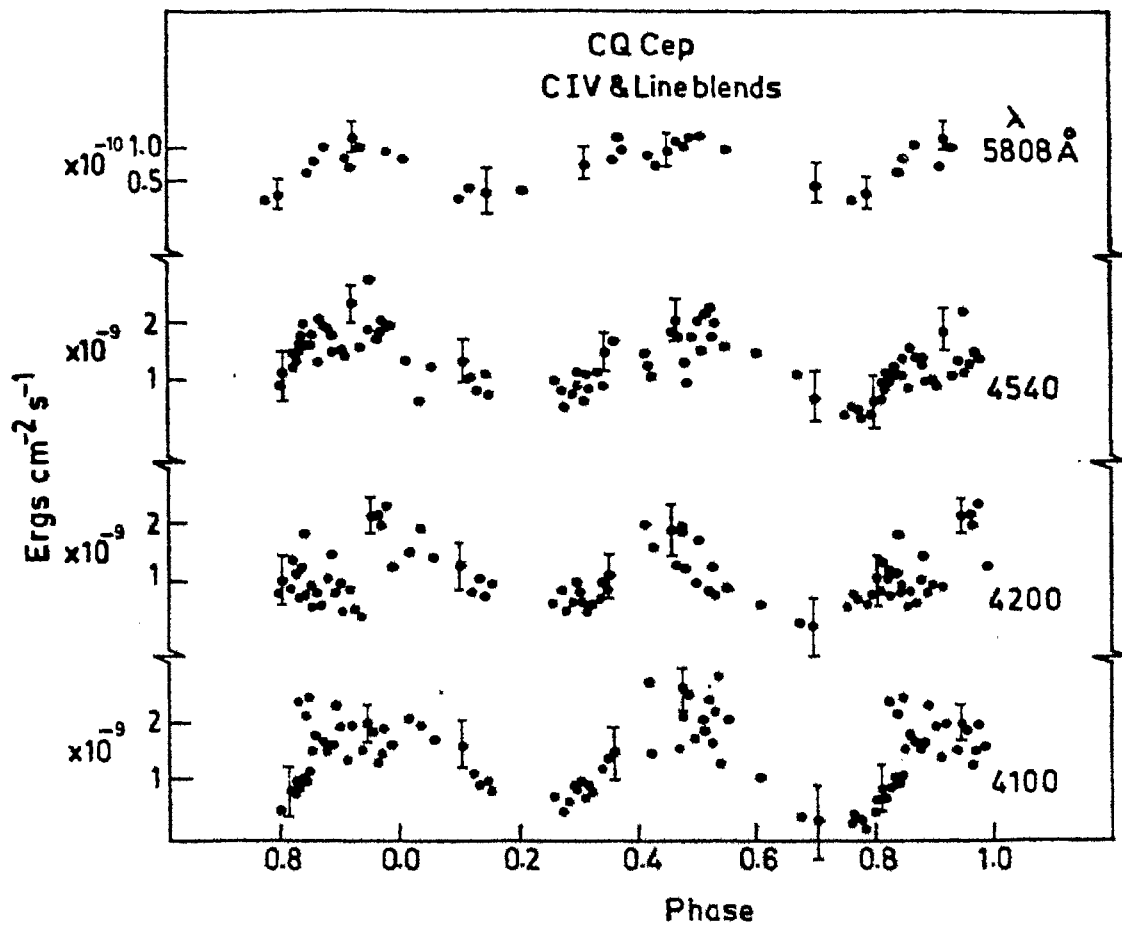


Figure 3.8 Flux variation of C IV λ 5808 and emission blends at λ 4100, λ 4200 and λ 4540.

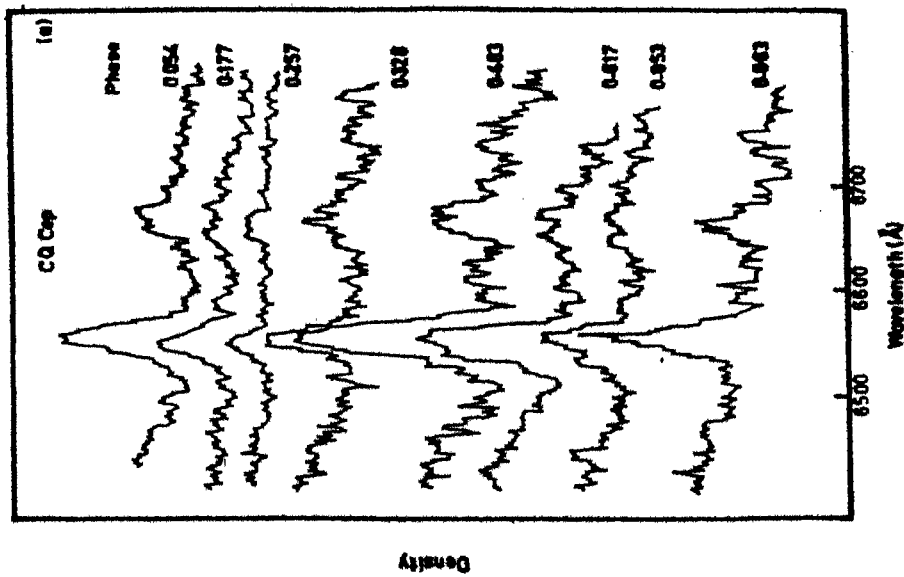
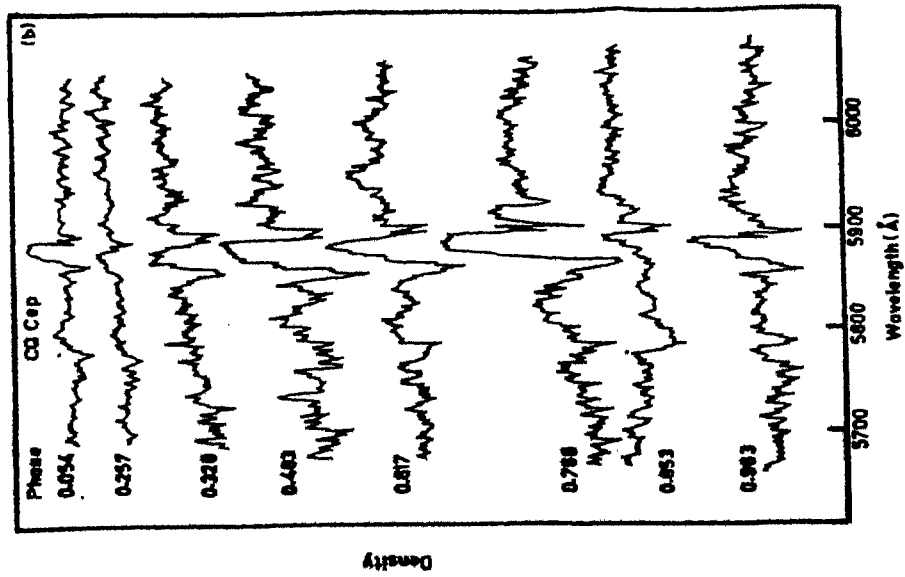


Figure 3.9 (b) λ 5900 region.

Figure 3.9 Density tracings to show the variation with orbital phase (a) λ 6600 region.

3.2.4 Line Blends

We now look at the various line blends at $\lambda 4540$, $\lambda 4200$ and 4100 . The main contributors to these lines are known to be He II and N III. These flux measurements show a variation similar to that of other He II lines (Figure 3.8), indicating that both the contributors to these blends behave in the same way. However measurements with better resolution will decide the behaviour of each component.

3.3 Model

All the solutions from different emission line RV curves (Table 3.4) and the light curve solutions can be made use of for an attempt to construct the model of CQ Cep.

3.3.1 Light curve solutions and the nature of the companion

One of the light curves at $\lambda 5300$ was solved for orbital elements using the method of Russel & Merrill (1950). The results in Table 3.6 show that the effect of tidal distortion is significant.

The light curve at 5300 , obtained by Hiltner (1950) has been solved by Leung et al. (1983) by Wilson-Devinney method. They discuss the choice of the mass ratio of 0.75 in great detail. Stickland et al. (1984) have solved the same light curve taking into account the atmospheric eclipses. They arrive at a mass ratio of 0.6 . Both the solutions necessitate a massive companion of the order of $35 M_{\odot}$. The mass of the WN component also appears large - it is $46 M_{\odot}$ from Leung et al. and $64 M_{\odot}$ from Stickland et al. - compared to other such mass derivations for WN components in binaries. For example, it is $10 M_{\odot}$ in V444 Cyg

(Kuhi, 1968), 5 to 12 M_{\odot} for CX Cep (Massey & Conti, 1981) and about 10 to 20 M_{\odot} for HD 211853 (Massey, 1981). Considering that the subgroups in these three subsystems are WN5, WN5 and WN6 respectively, the difference in the derived mass range is perhaps reasonable, since it is known that WN7 subgroups are different from other subgroups in many respects (Moffat & Seggewiss, 1980).

Thus the mass range ($35 M_{\odot} + 46 M_{\odot}$ and $38 M_{\odot} + 64 M_{\odot}$) derived for CQ Cep, implies a companion of spectral type. The energy distributions obtained at various phases were checked for any possible contribution from the companion. However, there was no evidence of change of slope of the Paschen continuum from conjunctions to quadratures (Figures 3.1 a & b).

Niemela (1980) analyzing the spectra with better dispersions (15 \AA mm^{-1}) found evidence for absorption arising from the companion. Leung et al. (1983) measured the $\lambda 3888$ line of He I and showed that it probably represents the line splitting due to companion. Stickland et al. (1984) also found this line splitting for the $\lambda 3888$ line at one epoch only and the velocity of the second component was almost a constant. Therefore, all the plates, in our collection, used for spectroscopic studies in this work, were checked carefully for detecting such absorptions. The region of $\lambda 3888$ is not well exposed for detecting such splitting up into two components. The behaviour of the He I lines at $\lambda 4471$ in the plates taken in 1951 appeared different. This definitely shows two components (Bappu & Viswanadham, 1977). The measured radial velocities of one component show a scatter similar to the 5876 line of He I, following the motion of the WN component; the other component shows a scatter about a mean velocity value of

Table 3.6

Solutions by Russell and Merrill method

Fourier Coefficients from light outside the eclipses		
$A_0 = 0.918$	$A_1 = -0.014$	$A_2 = -0.073$
$B_1 = -0.03$	$B_2 = 0.25$	
Ratio of the radii = 0.79 ± 0.1		
Fractional radius of the larger star = 0.36 ± 0.1		
Fractional radius of the small star = 0.28 ± 0.1		
Angle of inclination = 52 ± 7		
Eccentricity of the orbit = 0.078 ± 0.06		

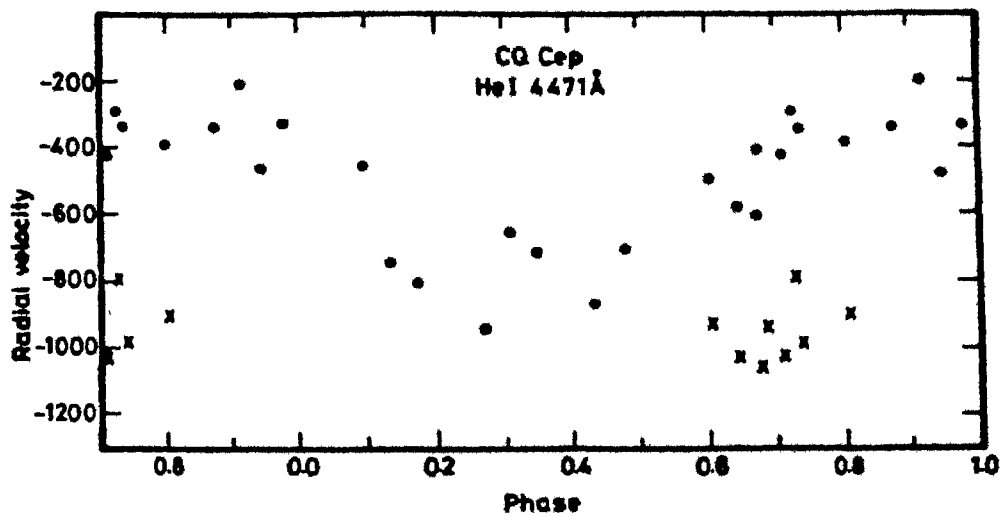


Figure 3.10 Radial velocity curve of absorption components of He I λ 4471 in 1951. The second component is indicated by crosses.

about -900 km s^{-1} (Figure 3.10). However the velocity of this absorption does not resemble the motion of the companion.

It has already been mentioned that the derived mass ratios from the light curves by either method imply a massive companion of $\sim 35M_{\odot}$. From the UV measurements of the P Cyg profiles, Stickland et al. (1984) have derived the terminal velocity, the escape velocity and the ratio $M_*/R_* = 1.2 M_{\odot}/R_{\odot}$. According to this the radius can be either $18 R_{\odot}$ (for the $20M_{\odot}$ WN component) or $38 R_{\odot}$ (for the $46 M_{\odot}$ WN component). The separation between the components in these two cases are $20 R_{\odot}$ and $25 R_{\odot}$ respectively, which conflicts with the sizes derived for stellar radii. Further, Underhill (1969) has pointed out that the atmospheres of WR systems are extended to about 5 times the core radius. In this case, even for a smaller value of $10 M_{\odot}$ for WN, the extension will be about $45 R_{\odot}$. Hence, irrespective of the method of light curve solution, the companion will be inside the stellar wind of the WN. It is also known that the the WR atmospheres are generally optically thick for helium and hydrogen lines for $n < 10$ (Smith, 1973). Hence these lines produced at the photosphere of the companion (which is completely embedded in the wind) will not be appreciably recognizable after passing through the thick atmosphere. It is difficult to check these on medium dispersion spectra, because the absorptions indicate the motion of the WN itself. Any absorption due to the companion will move in the opposite direction, in case of helium lines, well within the 10 \AA width of emission profile. At phases close to 0.0 and 0.5 , this absorption is expected to be superimposed on the emission

profiles. At phase 0.25, this absorption would have moved away and at phase 0.75 it is likely to coincide with the violet wing of the emission profile. This can add to the total absorption at this phase making the effect easily recognizable, as was seen for the He II lines $\lambda 4860$ and 6562 and to some extent $\lambda 5410$ also. Whether such an effect is present for the $\lambda 4686$ line is hard to notice not only because of its increased strength, but also because of the red wing of another strong emission of N III at $\lambda 4640$.

The radial velocity discrepancy curves (Figure 3.11) generated with reference to the N IV at $\lambda 4058$, show more positive value at all phases, reflecting mainly the shift in γ axes. Hence it is difficult to judge the possibility of any contribution of opposite moving absorption. The type of absorptions shown by the He II lines at $\lambda 4860$, 6562 and 5411 have not been observed by Stickland (private communication). This may also imply that these absorptions are probably of sporadic nature, although the observed amplitude differences (and almost circular orbit for only 5410) appears constantly at all epochs.

In the absence of any such confirmation from any spectroscopic or spectrophotometric data, other than the only one high dispersion measurement by Niemela (1980), we may assume that the companion is of spectral type O, contributing to absorption, if recognizable, only in He II and He I lines.

3.3.2 Circumstellar Matter

The radial velocity variations and flux variations may now be studied to understand the envelope structure surrounding the star.

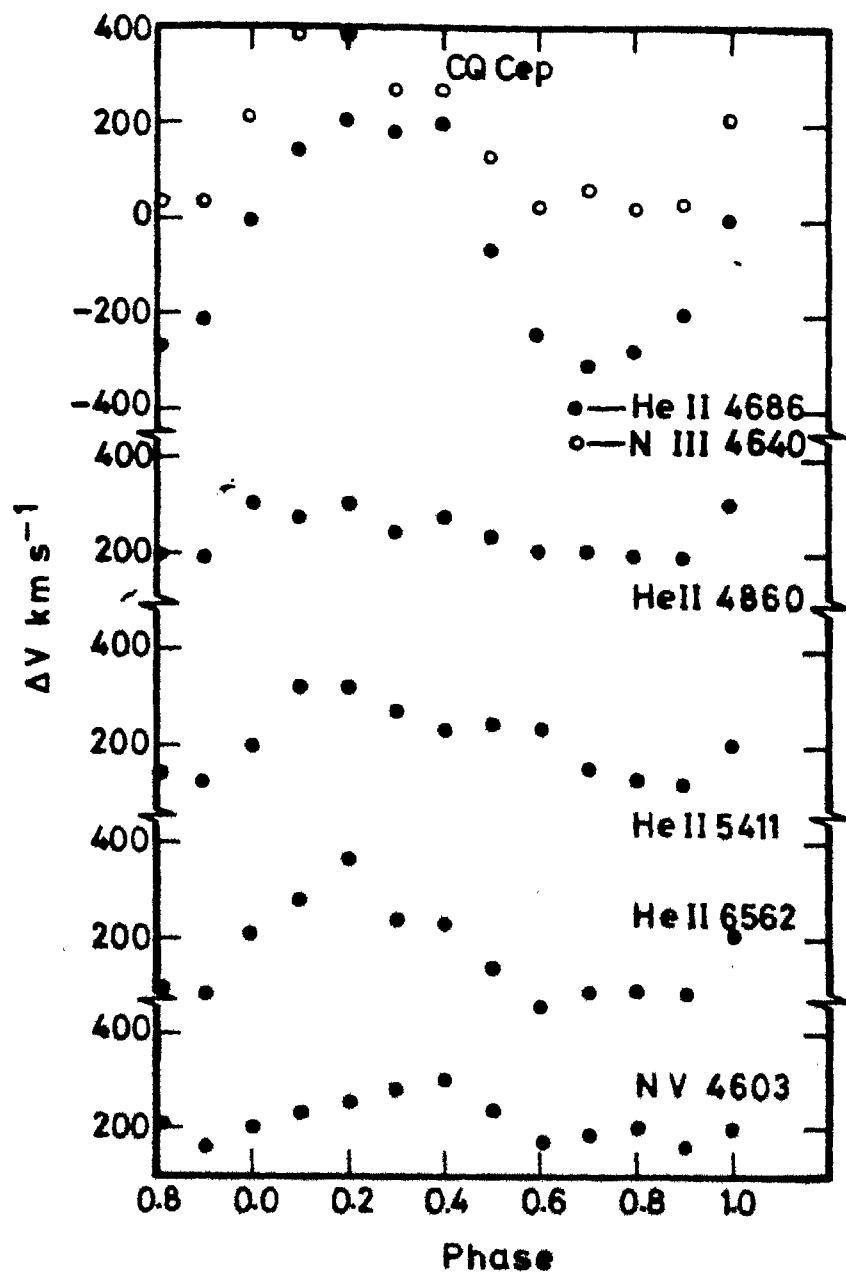


Figure 3.11 The radial velocity discrepancy curves relative to N IV $\lambda 4058$ of emission lines.

We may use the 4058 line of N IV to be representing the motion of the WN component for the following reasons

1. The spectra clearly show that this line is free of any blends.
2. It does not show asymmetry in line profile.
3. Its RV curve gives an almost circular orbit, as can be anticipated in such close binary.
4. Its γ velocity has a value very close to the systemic velocity of other members of the Cepheus Association (Stickland et al., 1984).

We may start with the nitrogen lines for understanding the WN atmosphere, since they are known to be formed in the WN atmosphere only and not in the companion. The flux variation of the N V line shows eclipse effects, implying its formation in a region closer to the WN photosphere and, therefore, an approximate size of the line emitting region may be calculated. We may also note that no eclipse effects are seen at phase 0.5, when the WN is between the observer and the O type star. Assuming that this line originates deep in the atmosphere we can think of a configuration of an eclipse of parts of this line emitting sphere at the primary minimum. The depth of the eclipse is about 25% and the duration of the eclipse is from phase 0.85 to 0.15. Then the radius of the line emitting region will be about $10 R_{\odot}$.

From the variations of the line profile we see that the absorption and emission are moving together so as to leave the profile unchanged. This further indicates that the decrease in flux at phase 0.0 corresponds to an eclipse effect only. The RV curves of this line show an interesting phenomenon; these curves

are identical but for a shift in the axes. If we assume that this line originated in a region close to the photosphere, it should follow the characteristics of N IV at $\lambda 4058$ i.e. γ axis should have been $\sim -65 \text{ kms}^{-1}$. However, because of the associated absorption there can be a positive shift of γ axis. It may be noticed that when we combine the effect of emission and absorption the net value of γ will be -56 kms^{-1} . This would imply that the red shift of γ axis is due to the associated absorption only. However, it is not possible to verify with the present data whether this effect is true for all other lines with absorptions, or whether it is just a coincidence in case of N V at $\lambda 4603$.

The N III line at $\lambda 4640$ shows a negative shift of γ viz -114 kms^{-1} . An explanation of this shift based on the associated absorptions appears to be complicated in this case because this is a blend of at least three emissions (Bappu, 1973) and also because the red wing is probably affected by the strong line of He II at $\lambda 4686$.

The behaviour of the He II lines has already been discussed in the previous section. Here the shift in γ axes may be a consequence of the absorption arising in the WN itself (like N V at $\lambda 4603$) or because of the absorption due to the companion. A situation like this, of two absorption features moving in opposite directions can also reduce the total flux at phases 0.25 and 0.75. At phase 0.75 both absorptions add to the violet wing of the profile so that the measured flux will be still smaller. This is partly true, because on some occasions at phases 0.75, the flux was too small to make any meaningful measurements. However, this cannot totally explain the observed flux increase

at phases 0.0 and 0.5.

The absence of eclipse effects for all lines other than N V at $\lambda 4603$ demands that their line emitting regions will have to be larger than at least $10 R_{\odot}$ (the value of the same for N V line). This also sets a limit on the size of the companion to be $10 R_{\odot}$. As discussed in the previous section the companion sweeps through the WN stellar wind, thus partly occulting the wind during quadrature, while at minima the entire line emitting region is visible. This geometrical effect will cause an apparent increase of flux at minima. This situation is likely to be more plausible specially in case of CQ Cep, because in V444 Cyg the companion is larger and all the lines show eclipse effects.

Thus it appears that in case of helium lines absorptions and geometric effects cause the observed flux variation, while for other lines it is mainly the geometrical effect.

4. THE BINARY NATURE OF HD 50896

HD 50896 = EZ CMa is the sixth bright star in the catalog of Wolf-Rayet Stars, with a magnitude of 6.94 (van der Hucht et al., 1981). In one of the earliest studies, Wilson (1948) reported three types of changes in line profiles -

1. The 4686 line of He II yields a variable velocity from $+120 \text{ kms}^{-1}$ to $+260 \text{ kms}^{-1}$.
2. The N V line at $\lambda 4603$ shows displacements unconnected with the He II line.
3. The line profile of the N IV line at $\lambda 4058$ varies.

In a more detailed analysis, Smith (1955) studied the line profiles of the $\lambda 4058$ line of N IV, the central absorptions of the He II lines at $\lambda 4860$, 5411 and also the He I line at $\lambda 5876$, and suspected it to be a spectroscopic binary. Ross (1961) observed photometrically and reported a systematic difference of 0.1 mag. in about five months, and also an irregular variation of 0.05 mag. in a few days. Kuhl (1967) observed it more thoroughly and suggested a period of about one day with an amplitude of about 0.04 mag. The night-to-night variations of the He II line 4686 were reported by Smith (1968), Irvine & Irvine (1973) and Schmidt (1974). However, none of these studies led to a positive conclusion on the binary nature. Serkowski (1970) reported strong polarimetric variations and this was further confirmed by McLean et al. (1979) and McLean (1980). The photometric periodic variation with a small amplitude was reported by Firmani et al. (1979) and further confirmed for the same period by Firmani et al. (1980) and Cherepas hchuk (1981),

although the shapes of the light curves did not agree. The variations of the line profiles have been discussed by Ebbets (1979), Firmani et al. (1980) and Singh (1984), in time scales of a few hours.

The most recent and detailed photometric and spectroscopic studies are provided by Ebbets (1979), Firmani et al. (1980) and Cherepas hchuk (1981), who point to the binary nature of the system with a compact companion of about 1-2 M_{\odot} mass range, although other mechanisms like non-radial pulsations and roation were offered as alternative explanations for the light and emission line behaviour. The presence of a compact companion goes in tune with the evolutionary scheme of a WR stage in a binary in a post X-ray binary stage (van den Heuvel, 1976 ; Tutukov & Yungelson, 1979) and therefore makes this an interesting system for study.

The study of emission lines offers an opportunity for understanding the envelope structure and the asymmetry, which arise as a consequence of the presence of the companion. Spectrophotometric studies of CQ Cep, a very close binary (WN 7 + O), showed that the emission line flux variations are dependent on the stellar wind structure and Roche Surfaces modified for this effect. In the present analysis of HD 50896 similar studies are made with an aim to understand the possible atmospheric stratification and the effect of the companion on it.

4.1 Observations

4.1.1 Spectrophotometry

The observations were obtained with the spectrum scanner, as explained in Chapter 2. The standard stars are listed in Table 2.1. For this study the blue observations were done in second order and the red observations, in first order.

4.1.2 Reddening corrections

Although this star is within the boundary of the open cluster Collinder 121, doubts have been expressed on its membership (cf. Firmani et al., 1980), because of the difference in the age of the cluster and other WR stars, known to be definite members of other clusters (Moffat & Seggewiss, 1979). At the same time, the reddening of the cluster members is very small, not making it a unique property of HD 50896 exclusively ($E(B-V) = 0.0$). The dereddened fluxes are derived by Kuhl (1966) and corrected for overcorrection by Smith & Kuhl (1981).

For the observations reported here, 27 CMA was used for reddening corrections. The derived energy distribution was normalized at 5000 Å and compared with those of 27 CMA also normalized at the same wavelength. A systematic difference was noticed between these values and those given by Smith & Kuhl (1981). A similar effort made with η CMA also showed a difference in the energy distribution of Smith & Kuhl (1981). We may also note from the IR observations of Hillier (1984) that the reddening corrections are small for HD 50896. Therefore, all the flux and magnitude measurements are not corrected for reddening. Figure 4.1 shows sample scans for different epochs.

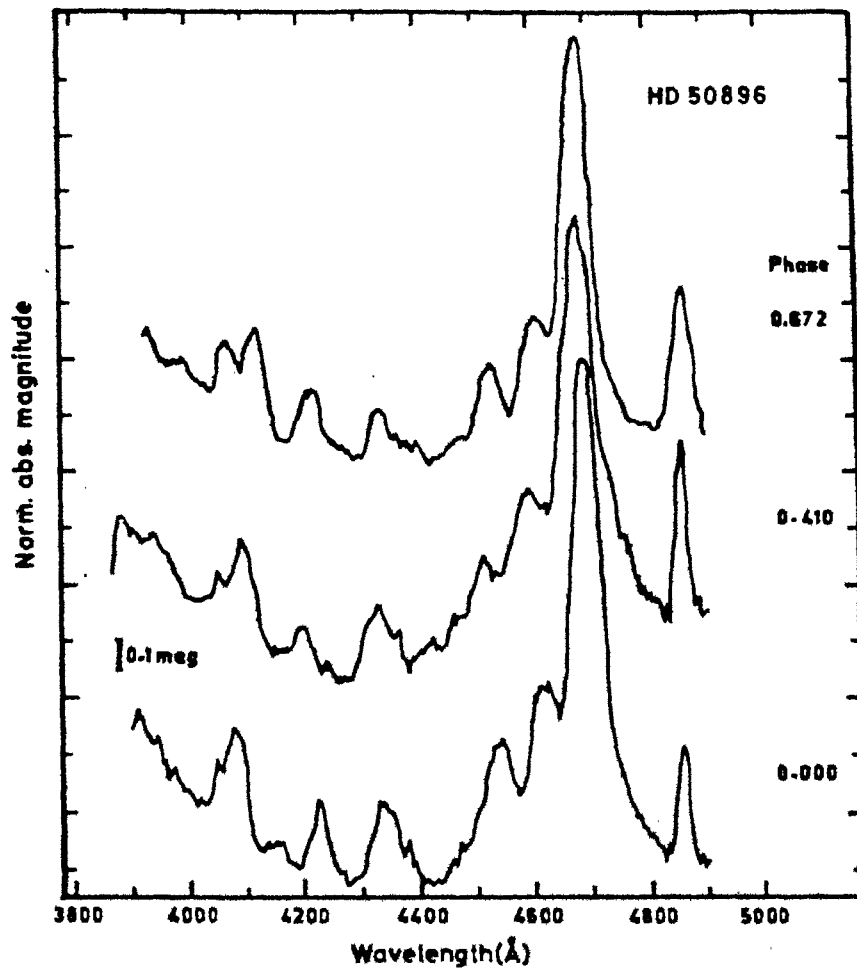


Figure 4.1 Sample scans of HD 50896 in the blue region. The derived absolute magnitudes are normalised at 5000 Å.

4.2 Results

4.2.1 Photometry

On 10 and 11 April 1982, photometric observations were obtained for monitoring the rapid variations in the visual magnitude. The same equipment was used with the exit slot increased to 100 Å and the grating position centered at 5000 Å. This technique has been used to derive the precise values of the absolute magnitudes of WR stars (details in Chapter 5, Shylaja & Bappu, 1983). HD 50646 ($m_v = 7.4$) was used as a comparison star. Continuous runs of HD 50896 for stretches of 10 minutes were obtained with the integration time of 1 sec, with similar runs of comparison and sky in between. Samples of such runs on each night are shown in Figure 4.2. It appears that the data were noisier on 11th April compared to 10th April. A similar run of HD 50646, which is of similar brightness, is also shown in the Figure. Power spectral analyses by DFT techniques of these runs (Blackmann & Tukey, 1958, choosing the number of lags as one-fifth the total number of points, which limits the detectable periodicity to 30 seconds), showed periodicities of 11 to 12 seconds with amplitudes of 0.005 mag., although other smaller periodicities of still smaller amplitudes are seen (Figure 4.3). It may also be seen that the intrinsic variations are not influenced by emission line variation described later. It is difficult to determine any other variation with this limited data.

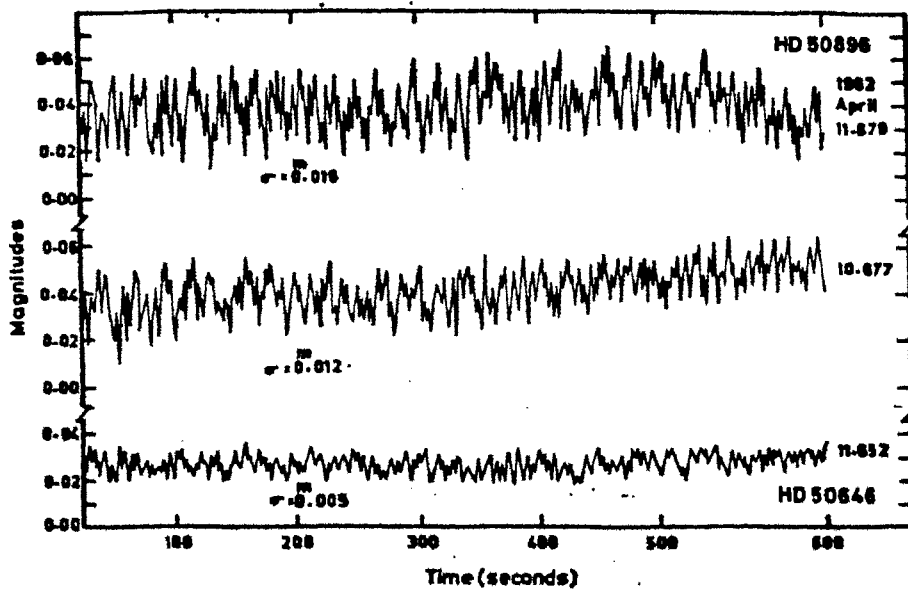


Figure 4.2 Photometric variation of HD 50896 on 10th and 11th April 1982: Comparison HD 50846 also may be seen.

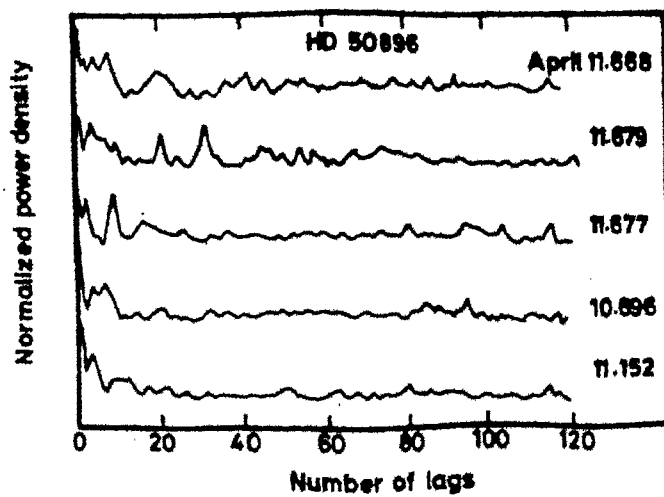


Figure 4.3 Results of power spectral analysis by DFT techniques.

4.2.2 Light Curves

From the observed energy distributions it was possible to derive the light curves. Representative light curves at 4790 and 5560 are shown in Figure 4.4. The shape of the curve does not seem to match with the broad band light curves of Firmani et al. (1980) and Cherepashchuk (1981). The available data was folded on 3.763 d period, after applying the heliocentric corrections from Landolt & Blondeau (1972). This folding was done separately for each season for reasons explained later (See also Figure 4.3, where each season is represented by separate symbol). At longer wavelengths also the data did not yield a clearly defined light variation. Table 4.1 lists the derived monochromatic magnitudes at three wavelengths. The short term variations within a night are about 0.05 mag., which is similar to the amplitudes observed by the previous investigators on broad bands. The entire data spread over three years, are shown in Figure 4.5. It may be seen there is an apparent variation of about 400 d. However, it is very difficult to find any smooth variation of period 3 to 4 d in any season individually.

4.2.3 Emission Line Flux

The flux of some emission lines of He I, He II, N IV, N V and C IV were measured from the energy distributions. The N III line at $\lambda 4640$ was too weak to make any meaningful measurements. The type of profile variations, described by the previous investigators, of He II $\lambda 4686$ and N IV $\lambda 4058$ could be clearly seen on some occasions, in spite of a resolution of 10 Å only.

Table 4.1

MONOCHROMATIC MAGNITUDES OF HD 50896

JD 2444000+	PHASE	WAVELENGTH(A)		
		4790	5000	5560
5254.375	0.684	2.275	2.375	-
5254.401	0.691	2.262	2.351	2.268
5254.432	0.700	2.287	2.395	-
5330.204	0.835	2.275	2.295	-
5330.221	0.840	2.261	2.310	-
5330.234	0.843	2.262	2.285	-
5330.246	0.847	2.229	2.290	2.277
5330.259	0.850	2.281	2.268	-
5330.309	0.863	2.230	2.278	-
5330.321	0.867	2.264	2.285	-
5330.361	0.877	2.231	2.245	2.235
5330.374	0.881	2.241	2.259	-
5330.396	0.887	2.226	2.285	2.246
5370.141	0.449	2.276	2.305	2.232
5370.162	0.454	2.271	2.355	-
5370.175	0.458	2.263	2.347	-
5370.192	0.462	2.281	2.329	-
5370.236	0.474	2.262	2.336	-
5370.251	0.478	2.251	2.370	-
5370.271	0.483	2.246	2.366	-
5370.292	0.489	2.241	2.365	2.213
5370.307	0.493	2.207	2.349	2.238
5405.128	0.746	2.218	2.295	2.241
5405.140	0.750	2.239	2.289	-
5405.156	0.754	2.228	2.280	2.235
5405.167	0.757	2.231	2.265	-
5405.183	0.761	2.252	2.315	-
5405.197	0.765	2.256	2.368	2.232
5405.210	0.768	2.226	2.320	-
5405.223	0.772	2.256	2.350	-
5452.092	0.227	2.215	2.304	-
5602.462	0.187	2.260	2.340	-
5649.421	0.665	2.280	2.277	-
5649.439	0.671	2.730	2.323	-
5649.464	0.677	2.210	2.317	2.366
5650.373	0.919	2.060	2.370	-
5650.376	0.920	2.710	2.382	-

Table 4.1 contd

MONOCHROMATIC MAGNITUDES OF HD 50896 (CONTD)

JD 2444000+	PHASE	WAVELENGTH(A)		
		4790	5000	5560
5650.380	0.921	2.750	2.360	2.275
5650.386	0.922	2.620	2.375	-
5650.390	0.923	2.590	2.368	-
5650.437	0.936	2.630	2.382	-
5650.441	0.937	2.650	2.340	-
5650.445	0.938	2.550	2.362	-
5650.458	0.942	2.810	2.310	-
5650.467	0.943	2.700	2.355	-
5650.468	0.944	2.640	2.355	2.271
5650.472	0.945	2.530	2.338	-
5651.412	0.195	2.240	2.330	-
5651.419	0.197	2.265	2.280	-
5651.439	0.202	2.310	2.262	-
5651.443	0.203	2.520	2.229	-
5651.451	0.205	2.390	2.270	2.281
5752.279	-	2.217	2.335	2.279
5790.158	0.066	2.198	2.311	2.278
5810.147	0.378	2.350	2.229	2.275
5811.139	0.641	2.390	2.312	2.225
6037.475	0.786	2.266	2.355	2.198
6047.260	0.387	2.198	2.232	2.268
6047.268	0.389	2.250	2.241	2.283
6047.277	0.391	2.222	2.236	2.277
6047.284	0.393	2.221	2.285	2.276
6047.317	0.402	2.264	2.270	2.219
6047.325	0.404	2.280	2.312	2.277
6047.349	0.410	2.255	2.240	2.282
6047.393	0.422	2.240	2.255	2.286
6047.400	0.424	2.240	2.272	2.292
6047.438	0.434	2.210	2.232	2.235
6047.446	0.436	2.200	2.259	2.292
6048.213	0.640	2.188	2.234	2.271
6048.218	0.641	2.244	2.274	2.273
6048.224	0.643	2.261	2.321	-
6048.236	0.646	2.247	2.315	2.275
6048.252	0.650	2.276	2.307	2.279
6048.261	0.653	2.254	2.315	-

Table 4.1 contd

MONOCHROMATIC MAGNITUDES OF HD 50896 (CONTD.)

JD 2444000+	PHASE	WAVELENGTH(A)		
		4790	5000	5560
6048.300	0.663	2.239	2.282	2.227
6048.309	0.665	2.269	2.300	-
6048.333	0.672	2.246	2.336	2.276
6048.341	0.674	2.272	2.391	2.268
6048.359	0.679	2.246	2.268	2.317
6048.376	0.683	2.246	2.275	-
6048.401	0.690	2.244	2.326	2.269
6048.429	0.697	2.243	2.262	2.267
6048.445	0.702	2.251	2.281	2.239
6048.466	0.707	2.232	2.365	2.305
6048.491	0.714	2.241	2.335	2.228
6072.146	-	2.209	2.317	2.283
6083.217	0.942	2.245	2.358	2.217
6083.259	0.953	2.242	2.390	2.235
6083.337	0.974	2.280	2.345	-
6083.493	0.015	2.175	2.272	-
6148.115	0.189	2.231	2.276	2.285
6148.180	0.206	2.258	2.239	-
6150.094	0.714	2.249	2.358	2.218
6150.172	0.735	2.259	2.312	2.267
6150.218	0.747	2.277	2.335	2.219
6197.102	0.207	2.268	2.236	2.273
6198.110	0.474	2.257	2.222	2.254

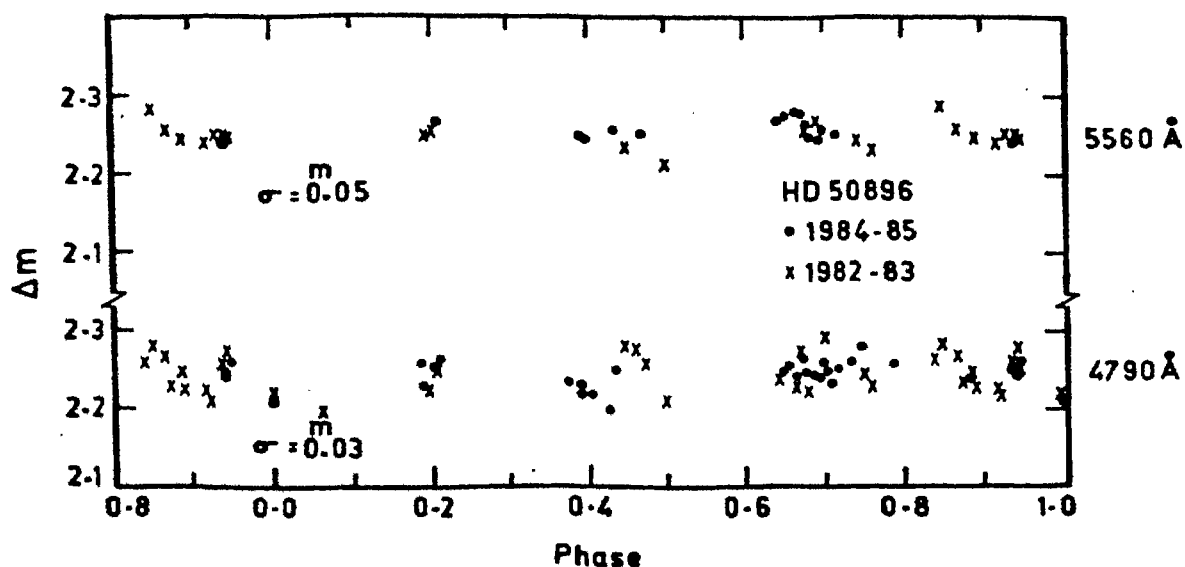


Figure 4.4 Monochromatic light curves folded over a period of 3.763 days (a) at 4790 Å (b) at 5560 Å. The zero phase is taken at JD 2,445, 752.279 and 2,446,072.146 separately for each season. The magnitude difference on the ordinate is relative to η CMa.

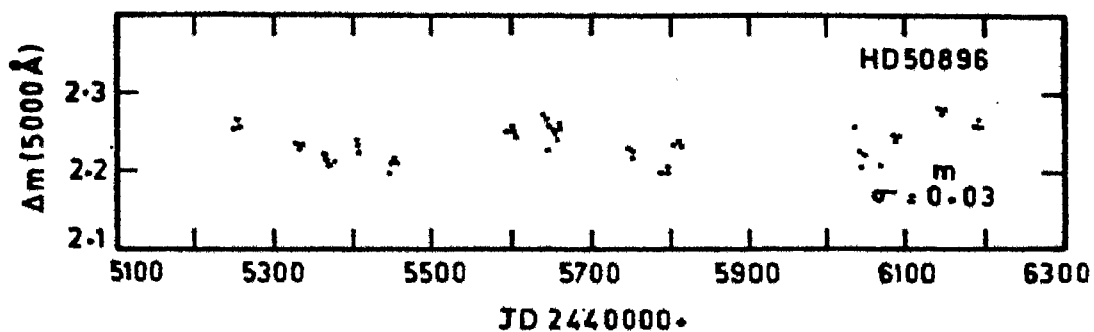


Figure 4.5 Long term variation of HD 50896 at 5000 Å during 1982-84, expressed as a difference relative to η CMa.

in the longer wavelength region flux measures, C IV λ 5808 is generally stronger than He II 5876, but only on few occasions was the latter stronger than the former. Some line blends at 4200 and 4540, were also measurable, although the individual contributors could not be resolved. Smooth profiles were drawn above the continuum to measure the area enclosed by them. The atlas of Smith & Kuhl (1981) was used for this purpose.

Hillier (1984) discusses the influence of electron scattering on He II line profiles. Bappu (1973) had attributed the red wing of the He II (7-4) line at 5411 to an unidentified transition, because this was not seen in any other member of the Pickering Series. Hillier shows that this is due to electron scattering and the effect has been shown to be present in other He II lines as well. It should be noted that these red wings can lead to erroneous continuum and line flux measurements. To avoid this, only the relative line ratios are compared (Table 4.2 and Figures 4.6 & 4.7), to see the possible effect of binarity. The He II line at λ 4860 was chosen for taking these flux ratios, because it was generally covered in both parts. The scatter in the flux of this line (Figure 4.6) may represent an intrinsic variation of flux for the system, which masks the effect of binarity.

4.3 Line Flux Variations

Many recent detailed spectroscopic investigations have established the changes in line profiles. In our scans, although it was not possible to see the profile variations very clearly, because of lower resolution, phase dependant changes in flux are

Table 4.2 Flux ratios relative to λ 4860 line

	PHASE	NIV 4058	B ₁₀₀	B ₁₀₀	HeII 4686	HeII 5410	CIV 5810	HeI 5876	HeII 6562	HeI 6678	NV 4620	HeI 7065	HeII 4860
2443300+													
5254.375	0.484	0.40	0.77	1.22	7.69	-	-	-	-	-	1.28	-	375.0
5254.401	0.491	-	-	-	-	1.59	0.76	1.15	1.76	0.31	-	2.31	391.0
5254.432	0.700	0.36	0.75	1.17	7.55	-	-	-	-	-	1.31	-	375.0
5330.204	0.835	0.39	0.84	1.15	6.88	-	-	-	-	-	1.33	-	345.0
5330.521	0.840	0.38	0.86	1.21	6.92	-	-	-	-	-	1.31	-	310.0
5330.234	0.843	0.40	0.75	1.31	7.12	-	-	-	-	-	1.29	-	335.0
5350.246	0.847	-	-	-	-	1.69	0.74	1.21	1.75	0.34	-	2.33	340.0
5330.259	0.850	0.43	0.78	1.10	7.92	-	-	-	-	-	1.38	-	308.0
5330.309	0.863	0.39	0.80	1.25	7.62	-	-	-	-	-	1.35	-	328.0
5330.321	0.867	0.36	0.86	1.15	7.42	-	-	-	-	-	1.40	-	345.0
5330.361	0.877	-	-	-	-	1.75	0.71	1.28	1.69	0.31	-	2.46	295.0
5330.374	0.881	0.34	0.82	1.11	7.37	-	-	-	-	-	1.39	-	309.0
5330.396	0.887	-	-	-	-	1.64	0.81	1.31	1.73	0.36	-	2.76	325.0
5370.141	0.449	-	-	-	-	1.69	0.81	1.35	1.62	0.29	-	2.65	305.0
5370.162	0.454	0.47	0.91	1.36	8.11	-	-	-	-	-	1.27	-	355.0
5370.175	0.458	0.45	0.88	1.29	8.07	-	-	-	-	-	1.25	-	347.0
5370.192	0.462	0.41	0.86	1.17	7.56	-	-	-	-	-	1.29	-	329.0
5370.236	0.474	0.44	0.85	1.22	7.92	-	-	-	-	-	1.31	-	336.0
5370.291	0.478	0.39	0.68	1.36	7.65	-	-	-	-	-	1.29	-	370.0
5370.271	0.483	0.45	0.71	1.28	7.55	-	-	-	-	-	1.31	-	365.0
5370.292	0.489	-	-	-	-	1.62	0.79	1.21	1.75	0.33	-	2.70	358.0
5370.307	0.493	0.49	0.82	1.32	7.12	-	-	-	-	-	1.33	-	349.0
5405.128	0.746	-	-	-	-	1.58	0.77	1.25	1.81	0.37	-	2.54	295.0
5405.140	0.750	0.48	0.95	1.36	7.53	-	-	-	-	-	1.41	-	289.0
5405.156	0.754	-	-	-	-	1.62	0.68	1.19	1.91	0.36	-	2.46	280.0
5405.167	0.757	0.47	0.87	1.22	7.89	1.81	0.59	1.06	-	-	1.36	-	265.0
5405.183	0.761	0.44	0.91	1.31	6.82	1.75	0.72	1.12	-	-	1.31	-	315.0
5405.197	0.765	-	-	-	-	1.66	0.75	1.20	1.88	0.31	-	2.59	368.0
5405.210	0.768	0.40	0.86	1.28	6.95	-	-	-	-	-	1.23	-	320.0
5405.223	0.772	0.46	0.92	1.29	7.51	-	-	-	-	-	1.26	-	350.0
5452.092	0.227	0.51	0.88	1.35	6.51	-	-	-	-	-	1.40	-	304.0
5402.462	0.187	0.54	0.54	0.86	7.58	1.41	0.77	1.08	-	-	1.38	-	340.0

Table 4.2 contd.

JD 2440000+	PHASE	NIV 4038	Blnd 4100	Blnd 4540	MeII 4686	MeII 5410	CIV 5810	MeI 5876	MeII 6562	MeI 6678	NV 4620	MeI 7069	MeII 4860
5649.421	0.665	0.47	0.82	1.34	6.43	1.58	0.85	1.17	-	-	1.32	-	246.0
5649.439	0.671	0.43	0.87	1.28	6.17	1.62	0.89	1.23	-	-	1.29	-	330.0
5649.464	0.677	-	-	-	-	1.54	0.86	1.21	1.81	0.44	-	2.69	317.0
5650.373	0.919	0.41	0.61	1.07	7.17	1.71	0.79	1.19	-	-	1.34	-	370.0
5650.376	0.920	0.48	0.59	1.13	7.32	1.68	0.77	1.06	-	-	1.36	-	382.0
5650.380	0.921	-	-	-	-	1.53	0.69	1.13	1.79	0.41	-	2.56	360.0
5650.386	0.922	0.43	0.71	1.08	7.33	1.62	0.62	1.16	-	-	1.26	-	375.0
5650.390	0.923	0.44	0.68	1.18	7.28	1.77	0.68	0.97	-	-	1.31	-	368.0
5650.437	0.936	0.43	0.63	0.97	7.53	1.59	0.73	1.03	-	-	1.29	-	382.0
5650.441	0.937	-	-	-	-	1.63	0.71	0.89	1.76	0.43	-	2.63	340.0
5650.445	0.938	0.46	0.57	1.16	7.33	1.68	0.64	0.95	-	-	1.29	-	362.0
5650.458	0.942	-	-	-	-	1.75	0.59	0.91	1.78	0.44	-	2.68	310.0
5650.468	0.944	-	-	-	-	1.80	0.61	1.11	1.76	0.41	-	2.72	353.0
5650.467	0.943	0.43	0.64	1.15	7.54	1.65	0.65	1.08	-	-	1.31	-	355.0
5650.472	0.945	0.42	0.54	0.96	7.35	1.78	0.68	1.02	-	-	1.24	-	338.0
5651.412	0.195	-	-	-	-	1.58	0.75	0.93	1.66	0.39	-	2.68	330.0
5651.419	0.197	0.39	0.64	0.86	7.41	1.49	-	-	-	-	1.28	-	275.0
5651.439	0.202	0.33	0.64	0.97	7.38	1.62	-	-	-	-	1.26	-	305.0
5651.443	0.203	0.36	0.49	0.88	7.22	1.67	-	-	-	-	1.29	-	315.0
5651.451	0.205	-	-	-	-	1.65	0.78	0.97	1.59	0.44	-	2.66	320.0
5752.279	0.000	0.36	0.58	1.03	7.81	1.51	0.61	1.05	1.91	0.41	1.14	-	278.0
5790.158	0.066	0.42	0.62	0.83	7.97	1.56	0.61	0.89	1.88	0.38	1.23	-	295.0
5810.147	0.378	0.45	0.63	1.21	6.69	1.71	0.83	1.12	1.85	0.42	1.29	-	372.0
5811.139	0.641	0.51	0.89	1.06	6.83	1.55	0.79	1.08	1.76	0.41	1.44	-	375.0
6037.479	0.786	0.44	0.85	1.17	7.06	1.56	0.76	0.98	1.98	0.37	1.47	-	355.0
6047.260	0.387	0.46	0.55	0.99	5.95	1.46	0.76	0.96	-	-	1.22	-	285.0
6047.268	0.389	-	-	1.14	6.13	1.49	0.68	1.08	1.83	0.41	1.39	2.61	276.0
6047.277	0.391	0.49	0.53	0.96	6.22	1.48	0.77	1.07	-	-	1.33	-	210.0
6047.284	0.393	-	-	-	-	1.53	0.66	1.16	1.85	0.36	-	-	255.0
6047.317	0.402	0.43	0.69	1.11	7.13	1.65	0.75	1.03	-	-	1.41	-	190.0
6047.323	0.404	0.47	0.68	1.16	6.90	1.71	0.73	1.13	-	-	1.33	-	310.0

Table 4.2 contd.

JD	PHASE	NIV 4058	Blnd 4100	Blnd 4340	MeII 4484	MeII 5410	CIV 5810	MeI 5876	MeII 6562	MeI 6678	NV 4620	MeI 7065	MeII 4860
2440000+													
6047.349	0.410	0.45	0.68	1.23	6.85	1.68	0.74	0.87	-	-	1.38	-	240.0
6047.393	0.422	0.51	0.74	1.08	6.43	1.49	0.69	0.95	-	-	1.27	-	253.0
6047.400	0.424	-	-	-	-	1.59	0.77	0.92	1.91	0.34	1.36	2.54	278.0
6047.438	0.434	0.55	0.77	0.93	6.45	1.39	0.82	0.97	-	-	1.41	-	323.0
6047.444	0.436	-	-	-	-	1.46	0.79	0.96	1.92	0.35	-	-	259.0
6048.213	0.440	0.37	0.78	1.17	5.82	1.53	0.68	0.69	-	-	1.32	-	431.0
6048.218	0.441	-	-	-	-	1.55	0.68	0.75	1.72	0.38	-	2.73	475.0
6048.224	0.443	-	-	-	-	1.58	0.59	0.73	1.68	0.33	-	2.81	520.0
6048.234	0.446	0.36	0.69	1.32	5.92	1.47	0.59	0.72	-	-	1.37	-	513.0
6048.232	0.450	-	-	-	-	1.63	0.65	0.64	1.90	0.39	-	2.79	507.0
6048.261	0.453	0.41	0.63	1.20	5.28	1.44	0.65	0.63	-	-	1.33	-	482.0
6048.300	0.463	-	-	-	-	1.47	0.56	0.69	1.65	0.34	-	2.70	475.0
6048.309	0.465	0.43	0.83	1.26	5.81	1.59	0.67	0.66	-	-	1.36	-	502.0
6048.333	0.472	0.41	0.79	1.28	5.33	-	-	-	-	-	1.39	-	486.0
6048.341	0.474	0.46	0.76	1.38	5.77	-	-	-	-	-	1.33	-	495.0
6048.359	0.479	-	-	-	-	1.46	0.59	0.81	1.93	0.42	-	2.68	506.0
6048.376	0.483	0.41	0.91	1.33	5.93	1.41	0.86	0.79	-	-	1.40	-	465.0
6048.401	0.490	0.39	0.94	1.34	5.74	1.53	0.83	0.68	-	-	1.41	-	480.0
6048.429	0.497	0.38	0.87	1.43	5.86	1.63	0.84	0.80	-	-	1.32	-	462.0
6048.445	0.702	-	-	-	-	1.58	0.78	0.82	1.55	0.39	-	2.74	481.0
6048.466	0.707	0.32	0.75	1.28	5.33	1.80	0.54	0.63	-	-	1.36	-	465.0
6048.491	0.714	-	-	1.30	5.21	1.75	0.57	0.71	1.53	0.36	1.39	2.80	335.0
6072.146	0.000	0.37	0.47	0.86	8.53	1.42	0.65	0.85	1.62	0.33	1.09	-	318.0
6083.217	0.942	0.43	0.86	0.92	8.77	-	-	-	-	-	1.21	-	358.0
6083.259	0.953	0.39	0.83	1.17	7.98	1.77	0.77	1.21	2.17	0.31	1.23	2.19	390.0
6083.337	0.974	0.33	0.81	0.85	7.97	-	-	-	-	-	1.23	-	345.0
6083.493	0.015	0.39	0.68	1.22	8.56	-	-	-	-	-	1.26	-	332.0
6148.115	0.189	0.45	0.45	0.84	8.59	0.97	0.76	0.49	-	-	1.41	-	285.0
6148.180	0.206	0.51	0.60	0.93	7.32	0.79	0.72	0.85	-	-	0.83	-	246.0
6150.094	0.714	0.48	0.91	1.05	5.89	1.49	0.86	0.71	1.81	0.34	1.43	-	358.0
6150.172	0.735	-	-	-	-	1.78	0.78	0.67	2.07	0.39	1.55	2.72	312.0
6150.218	0.747	0.44	0.88	0.94	7.40	1.81	0.84	0.60	2.12	0.38	1.46	-	335.0
6197.102	0.207	0.45	0.89	0.84	6.38	1.64	0.75	0.90	-	-	1.33	-	336.0
6198.110	0.474	0.46	0.65	0.96	7.37	1.66	0.68	1.21	1.73	0.31	1.19	-	226.0

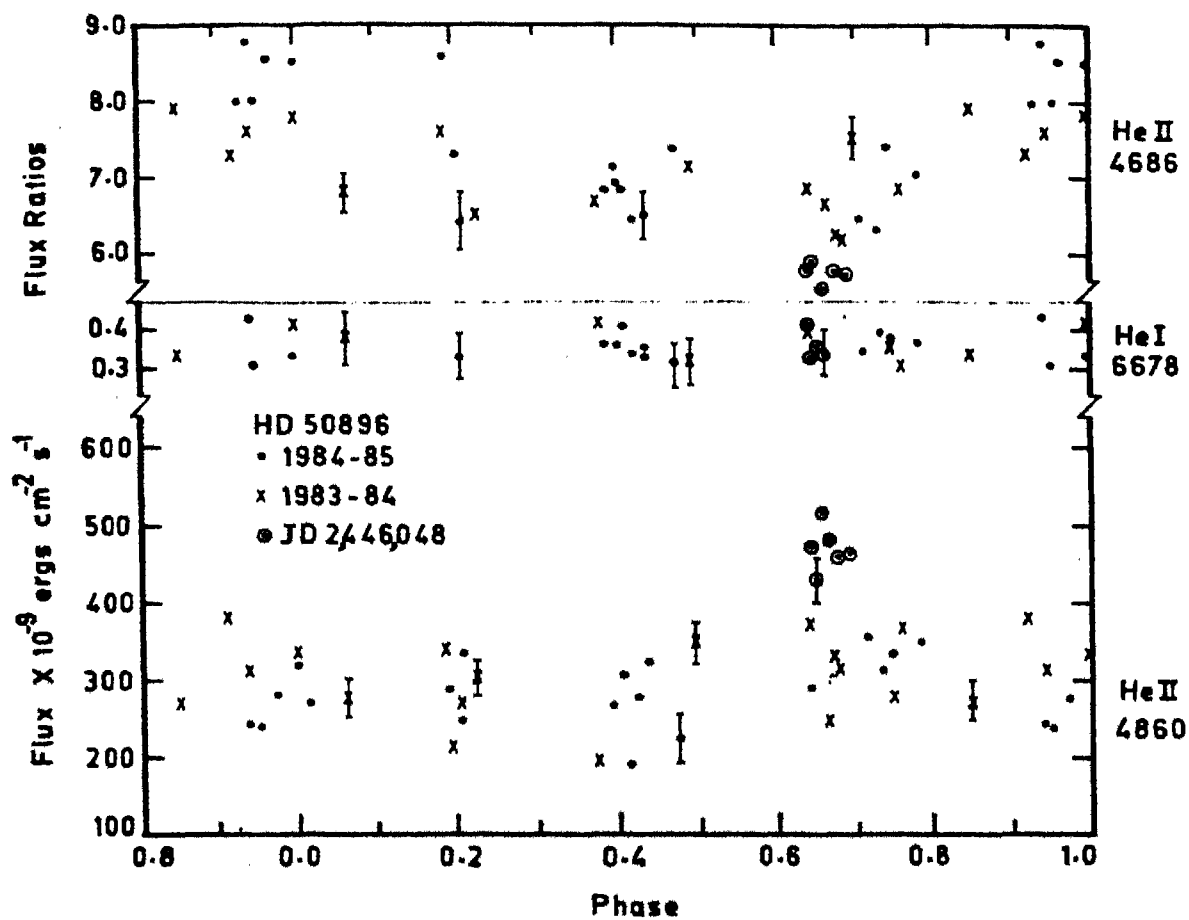


Figure 4.6 Flux variation of He II lines at 4860, and flux ratio for He II at λ 4686 Å and He I line at λ 6678. Note the sudden change in flux near phase 0.68 and its absence for λ 4686 line. Phases are calculated as described in Figure 4.4.

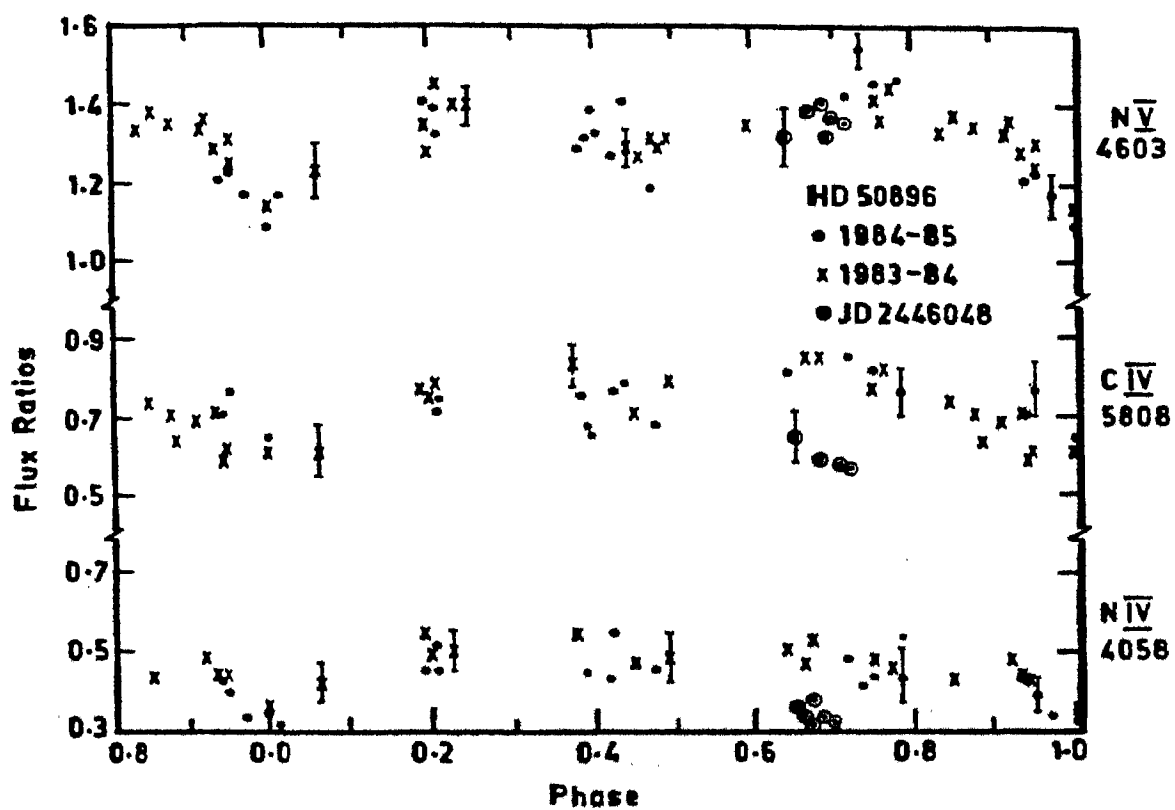


Figure 4.7 Flux variation of N V at $\lambda 4603-20 \text{ \AA}$, N IV at 4058 \AA and C IV at 5808 \AA . All are expressed as a ratio relative to $\lambda 4860$ line flux. Calculation of phases same as described in Figure 4.4.

seen. High dispersion spectra have shown the finer details of such changes (Firmani et al., 1980). The two peaks of some emission lines merge into one at phase 0.5. The line of N IV at 4058, which is very stable and deemed to represent the true motion of the WN component in CQ Cep (Chapter 3), shows large-scale structural variations in profiles (Firmani et al., 1980). However, the line of N IV at $\lambda 3483$ is very stable, although it is a blend of more number of multiplets. It may also be noticed that the N V line at $\lambda 4603$ does not undergo this kind of splitting and merging in line profiles. This line may be treated to be truly representing the variation over the period 3.763 d. Hence the phases of points have been calculated using this as the reference. As explained in the previous section, the extrapolation from JD 2,444,3199.53 (as referred to by the previous investigators) does not show meaningful variation, which is probably because of the uncertainties in fixing the time of observations. Hence the folding of the data has been done separately for each season, choosing the minimum value of $\lambda 4603$ flux to correspond to phase 0.0. Since there is an uncertainty in this point itself of about 0.001d, precise ephemeris cannot be provided.

The flux variations of various emission lines are shown in Figures 4.6 & 4.7. It may be seen that the flux of He II line 4860 is a scatter over a mean value, throughout the orbital phase. The other lines expressed as ratios relative to this line flux may be grouped in to two categories.

1. Those with no variation over the orbital period.
2. Those with small variations.

The lines of He II at $\lambda 5411$, 6562 show not much change in flux values. The line of N V at $\lambda 4603$ undergoes a decrease, with the help of which the zero phase was defined. The lines of N IV 4058 and C IV $\lambda 5808$ also indicate a similar decrease but not striking. It may be noticed that the line of He II $\lambda 4686$ flux does not get classified to any of these categories. The variations show larger scatter and it appears that the flux is slightly more at phase ~ 0.9 . The line blends at $\lambda 4540$ and 4200 have flux similar to the He II lines, which may be because the main contributor is He II itself.

4.4 Model

As was seen in case of CQ Cep (Chapter 3), if one were to assume that N V originates closest to the core, the reduction in flux at phase 0.0 can be immediately attributed to the eclipse effects. This requires that the size of the companion be large enough to partly cover the line emitting region. However, the estimated mass from the mass function of the RV curve for the companion is very small. The argument holds for the line emitting regions of N IV and C IV lines also.

One may attempt to explain these variations on the basis of asymmetric distribution of material and intrinsic variations. The intrinsic variation is apparent in the scatter of the measured flux of lines eg. $\lambda 4860$, which cannot be definitely established from the monochromatic magnitudes, since the long term variations of the comparison stars η CMa and 27 CMa are

not definitely known. Thus the variations of the line flux ratios may be deemed to represent the orbital variation (the intrinsic variations getting cancelled).

One may start with the model suggested by Firmani et al. (1980), which is based on precise RV measurements. Only the N V line 4603 gives a smaller eccentricity in the RV solutions; others indicate an eccentric orbit. Since the applicability of Roche surfaces is questioned, the precise values of the orbital parameters cannot be derived (discussed in Chapter 6). However, the small amplitude variations of the fluxes of the high excitation lines like N V, C IV and N IV put their source closer to the photosphere itself.

The phase dependent variation of the flux ratios of the lines of He II and He I is not quite apparent from the flux ratios, except the line of $\lambda 4686$, which shows an increase in flux. This is possible only if their line emitting regions are varying continuously or if the asymmetry is caused by the companion. The same argument holds for the He I lines also, which show insignificant variations relative to the He II lines. It may also be inferred that these He I lines originate in a region which surrounds both the stars, not participating in the orbital motion. Generally all the He I lines are associated with violet absorption edges with high V_{∞} , implying their origin in the outermost parts of the envelope.

With the RV curve solutions, one may derive that the mass of the compact star as $1 - 2 M_{\odot}$, assuming the mass of the WN component as $10 M_{\odot}$ and the small mass function with the orbital

inclination as $i = 70^\circ$, as derived from the polarimetric measurements. If we adopt the measurements of the WN5 component of V444 Cyg for this case also (Cherepashchuk et al., 1984), the extension of the atmosphere will be about that of the separation itself. The compact star although considerably distant from the WN5 core in this case, is not detectable by its spectral features or the change in the energy distribution. The accretion onto it can produce detectable X-rays, but they can get degraded to lower energies because of the dense electron envelope. (Moffat & Seggewiss, 1979). Recently Vanbeveren et al. (1982) have considered the production mechanism as well as the absorption of X-rays and discussed the different reasons for non-detection of X-rays.

Thus the binary model proposed by Firmani et al. can explain the flux variations of emission lines. N V, N IV and C IV have their origin close to the WN5 core, similar to other systems (Moffat & Seggewiss, 1978, 1979; Sahade, 1980). As sketched by Firmani et al., the lines of He II at 5410, 6562 and 4860 originate in a region farther from the core. This region is distorted by the companion and therefore, the flux show a scatter. The region of the He I line formation is the outermost, probably enclosing the companion and therefore, the flux measures reflect only the intrinsic variations only.

5. THE MEMBERS OF THE CLUSTER NGC 6231

The open cluster NGC 6231 is considered to be belonging to the Sco OB1 Association. Many detailed investigations like the determination of the H-R diagram, the distance modulus and the reddening have been carried out extensively (Struve, 1944; Schild et al., 1969; 1971; Graham, 1965; Crawford et al., 1971; Garrison & Schild, 1979; Lundstrom & Stenholm, 1980). There are two WR stars in this cluster, HD 152270 (WC 7 + 0) is at the central region of the cluster, whereas HD 151932 (WN 7) is situated 22' west of the center. The membership of these two to the cluster has been discussed in detail (Seggewiss, 1974 a & b; Seggewiss & Moffat, 1979; Lundstrom & Stenholm, 1980).

HD 152270 (MR 65, WR 79) is one of the four binaries with WC component and was established as a spectroscopic binary with O type companion by Struve (1944). Radial velocity curves were studied by Seggewiss (1974b), who improved the period to 8.893 days. Proper motion measures Braes (1967) and RV measures of the interstellar lines (Seggewiss, 1974b) have confirmed the membership to the cluster. Line profiles have the absorptions due to the companion, as well as the violet shifted absorptions moving with the WC component (Seggewiss, 1974b). The profile of the C III line at $\lambda 5696$ has been particularly studied in great detail (Schumann & Seggewiss, 1975; Schmidt & Seggewiss, 1976; Neutsch et al., 1981; Neutsch & Seggewiss, 1985) and a cone model explanation has been offered for the double peaked profile. Polarimetric observations (Luna, 1982) have been used for deriving the angle of inclination of the orbit to be 35° .

HD 151932 (MR 64, WR 78) was classified as WN 7A by Hiltner & Schild (1966) because of the narrow emission lines. The membership to the cluster itself has been debated about not only because of its location 22' west of the center, but also because of the large reddening it displays. The radial velocity and the proper motion deviate not very significantly from the mean values for other cluster members. Based on the interstellar line velocities and interstellar diffuse band equivalent widths, Seggewiss & Moffat (1979) have included it into the cluster.

Schild et al. (1969) studied the radial velocity measures of Struve (1944) and suspected that there is an unseen companion and the orbital period is about 3.3 d. Bappu (1973) attributed the excess reddening to a late type companion. Seggewiss (1974a) studied the RV curves and found that the 3.3d periodicity was spurious because even the interstellar lines showed the same period. Hill et al. (1974) also did not find any orbital motion. A further detailed investigation by Seggewiss & Moffat (1979) showed that the excess reddening can be explained by normal interstellar reddening and an unseen companion need not be provoked.

These two objects are important for study because of the following reasons-

1. Although HD 152270 is not an eclipsing binary, based on the previous studies of CQ Cep and HD 50896 (chapters 3 & 4), we may expect to see atmospheric eclipses, which by virtue of angle of inclination may be partial.

2. In case of HD 151932 any similar effect of flux variation may throw some light on the possibility of a companion.

5.1 Observations

5.1.1 Spectrophotometry

These observations were done as described in chapter 2, the wavelength range was 4000 to 6000 Å in first order (later this was extended to 8500 Å for measuring the continuum distribution only). The standards from the list of Hayes (1970), Breger (1976) and Kuan & Kuhi (1976) were used for estimating the instrumental corrections. Sample scans are shown in Figure 5.1

5.1.2 Photometry

The same equipment was used for the photometric observations also. A central wavelength of 5560 Å, close to the center of the conventional V band was chosen and 100 Å exit slot was used. This system is similar to the v of Smith (1968b). In the 230 Å bandwidth used by Smith, a number of emission lines contributed (Table 5.1). After examining the spectra of WN 7 and WC 7 stars (Bappu, 1973), we chose a slit width of 100 Å such that the emission contribution is minimum.

Along with the cluster members, including these two Wolf - Rayet stars, ten spectrophotometric standards (Breger, 1976; Landolt, 1973) were also obtained for the calibration of the system. These values derived for the cluster members, when compared with the V magnitudes obtained by Schild et al. (1969) show a standard deviation of 0.01 mag (Figure 5.2).

In order to get the distribution of colour excess across the cluster we have selected the regions $4300 \pm 10 \text{ Å}$ and $5000 \pm 10 \text{ Å}$

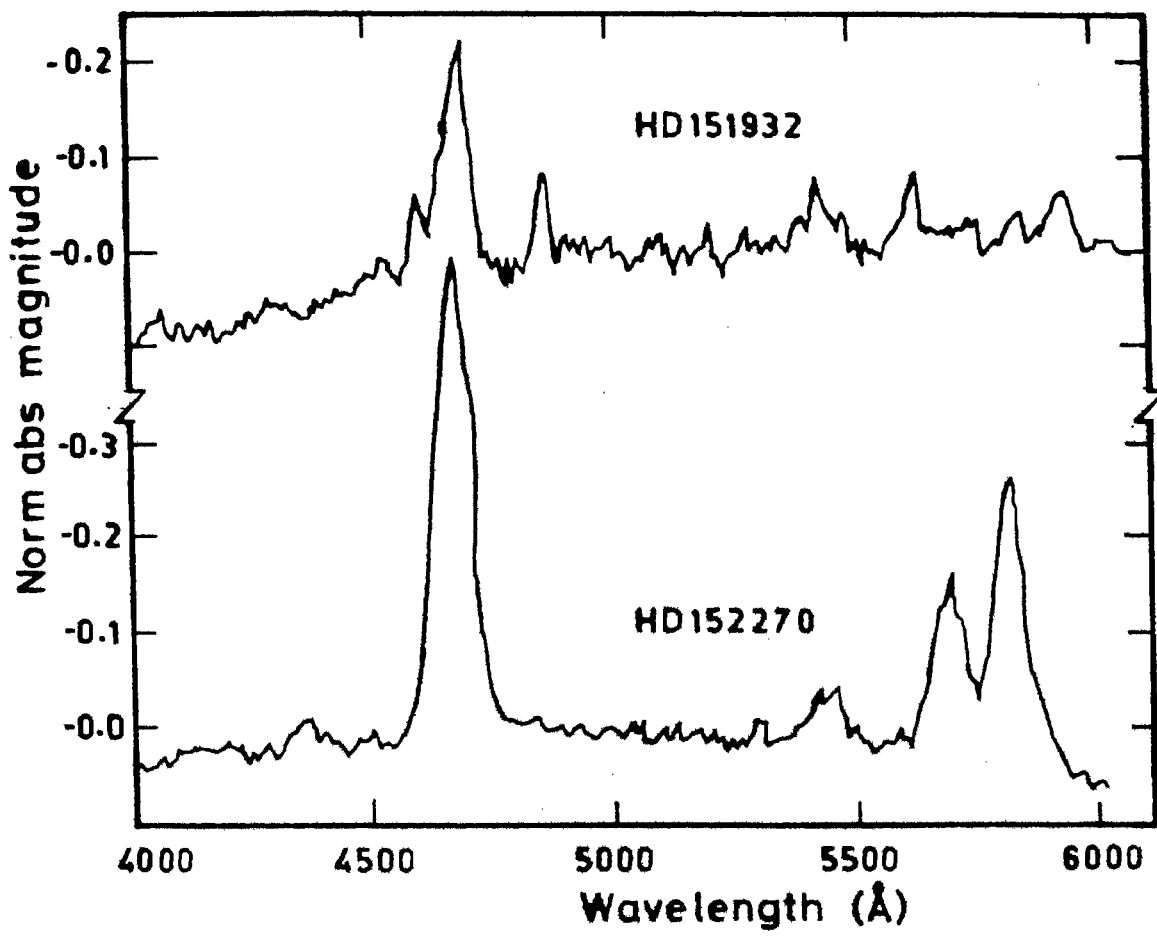
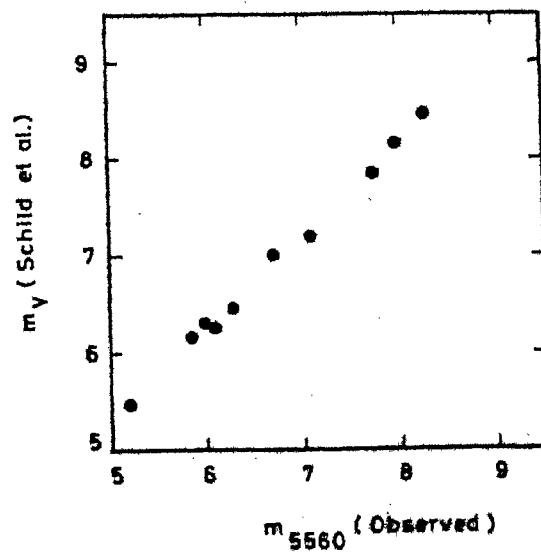


Figure 5.1 Sample scans of HD 151932 and HD 152270.

Table 5.1 Filters used by Smith (1986b) for determination of absolute magnitude and the emission lines included in the pass bands.

Indices	Central λ	Width	Lines included	
			W N	W C
u'	3500	80	N $\overline{\text{IV}}$ 3481	O $\overline{\text{II}}$ 3471 O $\overline{\text{V}}$ 3501
u	3650	100		C $\overline{\text{III}}$ 3609 C $\overline{\text{IV}}$ 3689 O $\overline{\text{VI}}$ 3622
b	4270	70		C $\overline{\text{II}}$ 4267
v	5160	130		C $\overline{\text{II}}$ 5145 O $\overline{\text{V}}$ 5114 O $\overline{\text{VI}}$ 5112
v'	5560	230	He $\overline{\text{II}}$ 5412	C $\overline{\text{IV}}$ 5411 C $\overline{\text{IV}}$ 5471 O $\overline{\text{V}}$ 5597 O $\overline{\text{VI}}$ 5410 He $\overline{\text{II}}$ 5412
r	6000	80		

Figure 5.2 Comparison of V magnitudes (Schild et al 1969) with monochromatic magnitudes.



since they are relatively free of emission lines in both in WN 7 and WC 7 (Smith, 1973; Bappu, 1973), and we have designated them as b and v respectively. These are similar to the b and v bands of Smith (1968), (centered at 4270 Å and 5160 Å with bandwidths of 70 Å and 130 Å respectively). For this purpose a few bright members within the spectral range O8 to B3 were scanned from 4000 Å to 5100 Å with a slit width of 20 Å.

Assuming the colour variation with the spectral type is very small in the range O8 to B3, the colours of the unreddened star 10 Lac, O9 V (Kuhi, 1965), have been used to estimate the colour excess $E(b-v)$ of the WR and a few other cluster members.

The values of the colour excesses $E(B-V)$ obtained by Schild et al. (1969) and $E(b-v)$ obtained here show a linear (Figure 5.3) relationship for the normal members of the cluster. With the help of this relationship the colour excesses of the WR stars can be obtained. In case of HD 151932, we get $E(B-V)=0.42$, which is very close to the value 0.44 estimated by Schmutz & Smith (1980) independently from the observations of $\lambda 2200$ feature. Hence using these values of $E(b-v)$, the intrinsic magnitudes have been obtained.

A distance modulus of 11.6 has been derived for the cluster by Garrison & Schild (1979) as well as by Levato & Malorada (1980). This value is used to get the absolute magnitudes of the WR members and are given in Table 5.2

The Table includes the results from other sources as well. All the estimates have been corrected for a distance modulus of 11.6 mag. for uniformity. The notes that follow the Table show

Figure 5.3 Comparison of colour excesses.

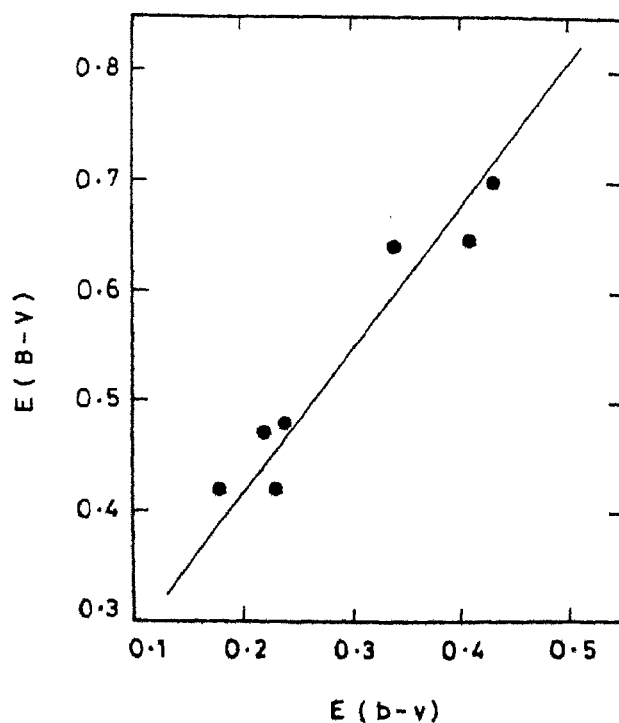


Table 5.2 Absolute Magnitudes of HD 152270 and HD 151932 from various investigation.

HD	Sp. type	Crawford (1971)			Graham (1965)	Seggeweiss (1974)	Schild et al. (1969)	Smith (1968)		Present work with	
										E(B-V)	E(b-v)
151932	WN 7	-5.7	-6.4	-6.3	-6.5	—	-6.3	-6.3	-6.6	-6.5 ± 0.3	-6.4 ± 0.3
152270	WC7+05-8	—	-6.3	-6.3	-6.1	-6.0	-6.3	-5.4	-5.7	-5.4 ± 0.3	-5.2 ± 0.3

that for most of the estimates no corrections have been applied for the emission line contributions. The eleventh column gives the results from this work. No correction has been applied for the presence of companion in case of HD 152270, although its presence has been established.

The monochromatic magnitudes derived from the energy distributions are tabulated in Table 5.3 for the objects.

5.2 Results

5.2.1 HD 152270

The phases have been calculated from an initial epoch of JD 2,441,160.826 and a period of 8.893d, following Seggewiss (1974b). Although the photometric results at 5560 Å show a small dip near phase 0.4 there is too much of scatter to be attributed to eclipse effects.

Spectrophotometric results were used to derive the line flux of the broad features like (C III + He II) near λ 4650, C IV 5470, (C IV λ 5808 + He I λ 5876) and also C III 5696, all these measurements are listed in Table 5.5 and indicated in Figures 5.5.

5.2.2 HD 151932

The photometric data of HD 151932 was searched for any possible periodicities by the method of least squares (Raveendran et al., 1982) between 1 and 10 d. This showed that there is an indication of a period of about 6 d, but the amplitude of variation is very small 0.05 mag. However, such a period determination is not completely free of alias effects and further continuous monitoring only can establish this. The

Table 5.3 Monochromatic magnitudes of HD 151932 and HD 152270.

JD 2440000+	MAGNITUDES		JD 2440000+	MAGNITUDES	
	HD 151932	HD 152270		HD 151932	HD 152270
4711.331	0.731	-	4740.317	0.710	-
4711.396	0.739	-	4740.300	-	0.819
4711.475	0.718	-	4740.330	-	0.823
4711.383	-	0.815	4740.356	-	0.814
4711.454	-	0.820	5065.426	-	0.831
4711.480	-	0.829	5065.436	-	0.714
4712.325	0.714	-	5068.443	0.702	-
4712.349	0.727	-	5068.454	0.711	-
4712.475	0.722	-	5068.466	0.705	-
4712.350	-	0.822	5068.434	-	0.826
4712.425	-	0.829	5068.461	-	0.815
4712.461	-	0.826	5068.476	-	0.822
4713.335	0.708	-	5069.446	-	0.821
4713.366	0.717	-	5069.466	-	0.819
4713.373	-	0.827	5069.450	0.719	-
4713.443	-	0.816	5069.475	0.708	-
4739.386	0.705	-	5070.426	-	0.824
4739.446	0.716	-	5070.450	-	0.817
4739.459	0.725	-	5070.474	-	0.822
4739.393	-	0.822	5070.434	0.735	-
4739.419	-	0.815	5070.456	0.729	-
4739.468	-	0.812	5070.478	0.732	-
4740.308	0.718	-	5071.348	0.724	-
4740.313	0.728	-	5071.359	-	0.821

Table 5.4 Flux of emission lines of HD 151932.

JD 2440000+	NV 4603	NIV 4058	CIV 5808	HeII 4860	HeII 5411	HeII 4686	Blend 4540	HeI 5876
4663.430	190.0	182.0	146.0	324.0	298.0	724.0	249.0	174.0
4663.461	198.0	177.0	143.0	308.0	279.0	717.0	236.0	163.0
4664.435	182.0	174.0	135.0	318.0	272.0	769.0	268.0	212.0
4665.451	186.0	178.0	141.0	307.0	284.0	748.0	258.0	203.0
4684.467	172.0	174.0	135.0	281.0	241.0	641.0	222.0	151.0
4685.403	183.0	182.0	152.0	294.0	263.0	669.0	241.0	172.0
4685.428	180.0	177.0	143.0	286.0	256.0	658.0	236.0	164.0
4711.406	205.0	181.0	156.0	327.0	268.0	707.0	249.0	170.0
4711.436	209.0	170.0	168.0	306.0	274.0	725.0	268.0	186.0
4712.441	212.0	185.0	155.0	291.0	289.0	758.0	292.0	192.0
4713.424	196.0	174.0	141.0	308.0	275.0	741.0	297.0	214.0
4714.333	192.0	176.0	146.0	332.0	296.0	707.0	276.0	168.0
4739.383	202.0	172.0	154.0	294.0	271.0	695.0	213.0	206.0
4740.277	211.0	184.0	162.0	319.0	289.0	727.0	285.0	177.0
4780.200	191.0	178.0	164.0	325.0	327.0	746.0	291.0	211.0
4780.236	206.0	162.0	147.0	341.0	311.0	728.0	276.0	237.0
5065.370	208.0	196.0	147.0	311.0	289.0	684.0	241.0	176.0
5066.353	197.0	181.0	159.0	319.0	265.0	709.0	268.0	192.0
5068.353	184.0	174.0	138.0	276.0	247.0	651.0	218.0	159.0
5069.416	194.0	170.0	149.0	309.0	275.0	674.0	231.0	172.0
5070.380	207.0	176.0	138.0	294.0	299.0	695.0	242.0	199.0
5071.454	191.0	184.0	145.0	299.0	286.0	676.0	259.0	175.0
5405.428	190.0	176.0	140.0	291.0	296.0	681.0	257.0	176.0
5406.431	207.0	199.0	154.0	315.0	280.0	694.0	232.0	195.0
5407.411	195.0	186.0	147.0	274.0	265.0	658.0	241.0	162.0
5407.419	211.0	212.0	144.0	299.0	257.0	645.0	211.0	149.0
5408.419	200.0	207.0	155.0	326.0	249.0	676.0	250.0	168.0
5409.456	217.0	195.0	149.0	311.0	274.0	668.0	227.0	184.0
5451.360	203.0	207.0	155.0	302.0	276.0	675.0	245.0	177.0
5452.317	187.0	192.0	141.0	277.0	245.0	646.0	212.0	151.0
5811.434	201.0	203.0	152.0	295.0	260.0	641.0	198.0	142.0
5964.125	212.0	215.0	163.0	342.0	311.0	717.0	257.0	185.0

Table 5.5 Flux of emission lines of HD 152270.

JD 2440000+	PHASE	Blend 4340	CIV 5808	Blend 5450	Blend 4650	CIII 5696
4663.468	0.865	93.0	530.0	305.0	795.0	506.0
4664.442	0.975	95.0	558.0	330.0	655.0	418.0
4665.458	0.089	82.0	460.0	286.0	722.0	457.0
4684.467	0.226	119.0	475.0	238.0	797.0	465.0
4711.429	0.258	106.0	492.0	285.0	642.0	371.0
4712.332	0.360	89.0	544.0	272.0	758.0	408.0
4713.336	0.473	97.0	461.0	280.0	801.0	362.0
4714.344	0.586	135.0	550.0	372.0	983.0	565.0
4739.397	0.403	65.0	422.0	182.0	835.0	382.0
4740.281	0.503	115.0	506.0	297.0	852.0	483.0
4780.208	0.992	130.0	590.0	375.0	849.0	520.0
5065.392	0.061	110.0	570.0	352.0	907.0	545.0
5068.421	0.401	98.0	462.0	210.0	875.0	430.0
5069.417	0.513	146.0	545.0	342.0	982.0	535.0
5070.399	0.624	115.0	536.0	315.0	915.0	470.0
5071.478	0.745	140.0	587.0	368.0	995.0	561.0
5405.461	0.307	109.0	585.0	262.0	815.0	440.0
5406.441	0.411	95.0	412.0	150.0	785.0	370.0
5406.462	0.413	78.0	445.0	168.0	760.0	335.0
5406.476	0.415	84.0	430.0	155.0	735.0	348.0
5407.427	0.522	110.0	490.0	255.0	830.0	435.0
5407.437	0.523	96.0	465.0	283.0	797.0	407.0
5408.429	0.603	76.0	487.0	382.0	753.0	396.0
5408.440	0.636	82.0	481.0	285.0	827.0	456.0
5409.448	0.749	88.0	562.0	300.0	930.0	516.0
5451.369	0.463	110.0	490.0	275.0	938.0	430.0
5451.404	0.467	102.0	475.0	262.0	900.0	415.0
5451.415	0.468	113.0	453.0	248.0	927.0	442.0
5452.325	0.571	120.0	530.0	335.0	910.0	470.0
5811.393	0.947	107.0	558.0	361.0	927.0	590.0

scanner observations were used for estimating the flux values of N IV 4058, N V 4603, C IV 5808, He II 4860, 5410, 4686, He I line of λ 5876 and the blend of 4540. The line of N III could not be resolved to measure the flux accurately. All the measured fluxes are listed in Table 5.4.

5.2.3 Interstellar Reddening

For a study of the colour excesses of the various members of the cluster, previous investigators have pointed out that the interstellar reddening across the face of the cluster is not very smooth and therefore a single value of $E(B-V)$ is not applicable for all the members of the cluster (Schild et al. 1971; Garrison & Schild, 1979). This aspect is made clear in Figure 5.3 which shows the observed (normalized at 5000 Å) energy distributions of a few cluster members. Therefore, it became necessary to derive the colour excesses separately for the two WR stars (Shylaja & Bappu, 1983).

The excess of reddening, which was attributed to a possible late type companion (Bappu, 1973) was explained as a consequence of anomalous reddening (Seggewiss & Moffat, 1979). This is apparent in Figure 5.3 also. It may be noticed that HD 151932 and HD 152003, which are located 20' away from the nucleus of the cluster, have similar distributions and somewhat different from the other members of the cluster. Therefore, it may be inferred that there is some source of excess reddening in this region.

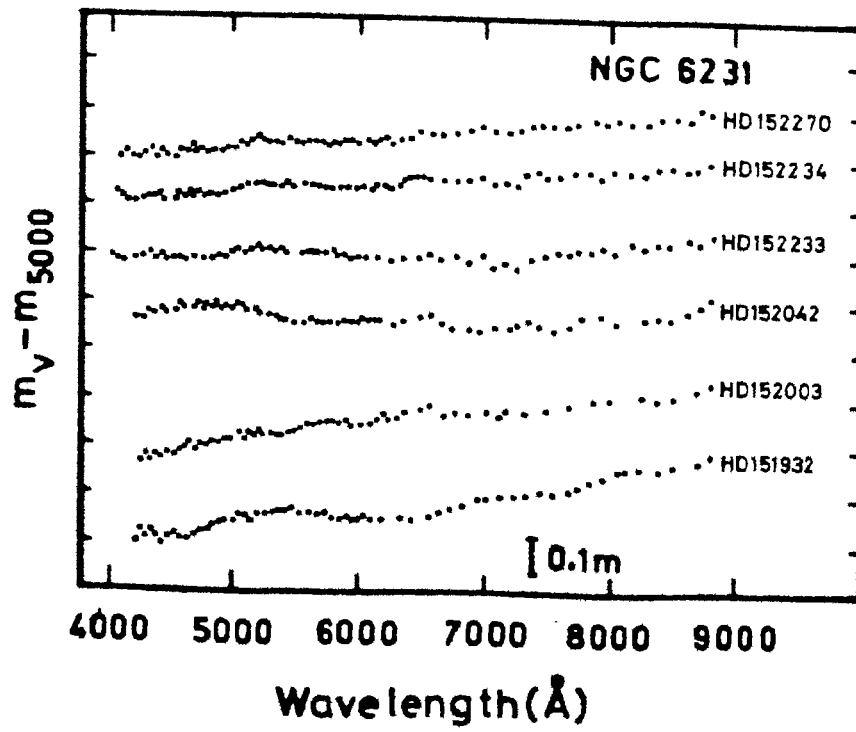


Figure 5.5 Energy distribution of some cluster members uncorrected for reddening. The difference of HD 152003 and HD 151932 is apparent.

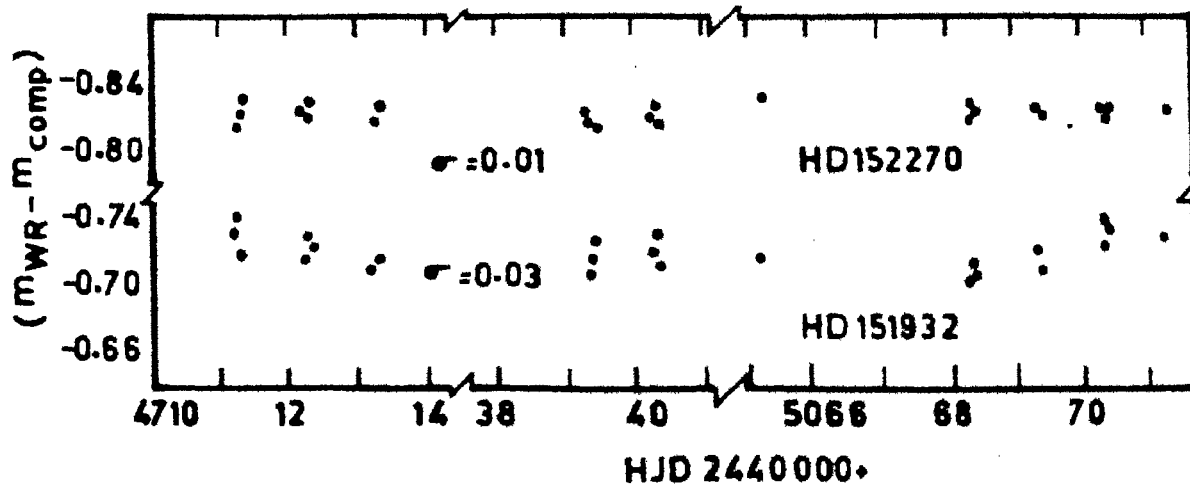


Figure 5.4 Variation of $m(5560)$ during 1981-83.

5.3 Possibilities of a Companion for HD 151932

The evolutionary calculations of de Loore (1980) for the WR phase in a binary show that a late type companion is not possible. Therefore, in the light of the explanation of anomalous reddening near HD 151932, the possibility of other type of companion may be sought.

The detailed spectroscopic investigation by Seggewiss (1974a) has clearly shown that there is no apparent RV variation. Based on the 6d period derived from the photometry, it was attempted to fold the absorption line RV measures of (Moffat & Seggewiss, 1979), which did not yield any meaningful RV curve for any line. The other emission lines show smooth RV variation and therefore it is unlikely that the compact companion, if present, can be detected by such velocity curves.

The existence of a compact companion implies a very high mass ratio of $q > 10$, assuming the WN7 to be $\sim 20 M_{\odot}$ and the compact star to be about $2 M_{\odot}$. However, in case of CQ Cep, another binary with WN7, the mass derived is about $35 M_{\odot}$ (Stickland et al., 1984; Leung et al., 1983). Therefore, the mass ratio in this case can be still higher. To estimate the approximate amplitude of the RV curve, we may assume $q = 10$ and period 6 d then the amplitudes will be less than 30 km s^{-1} . Such small amplitudes are difficult to detect with medium dispersion spectra.

the presence of the compact companion represents the second WR phase in the evolution of a binary, which in other cases like HD 50896, has many other characteristics like the nebulosity etc.

Figure 5.6 Variation of flux of HD 152270.

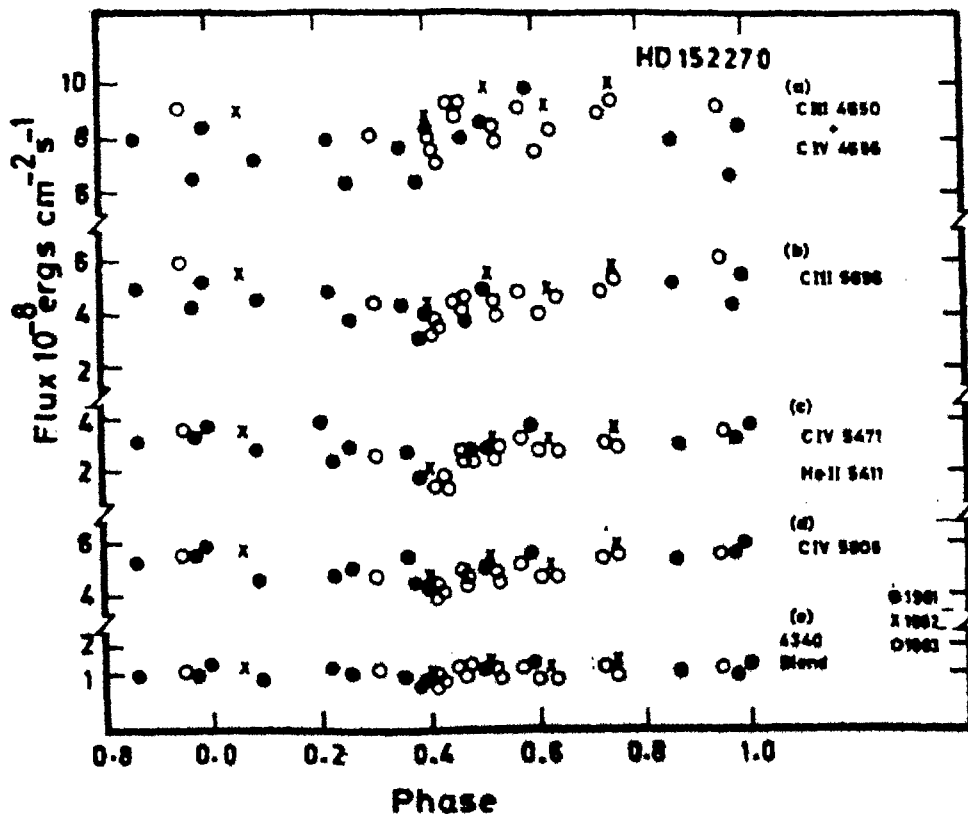
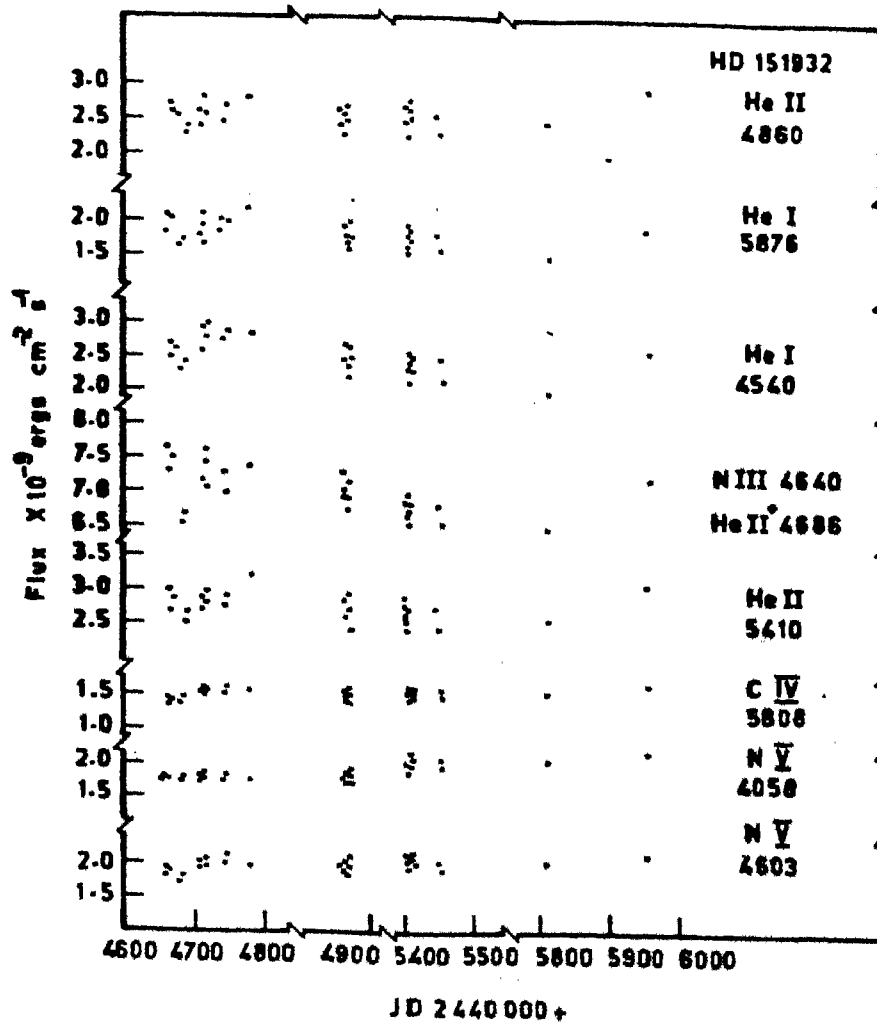


Figure 5.7 Flux of HD 151932 during 1982-83.



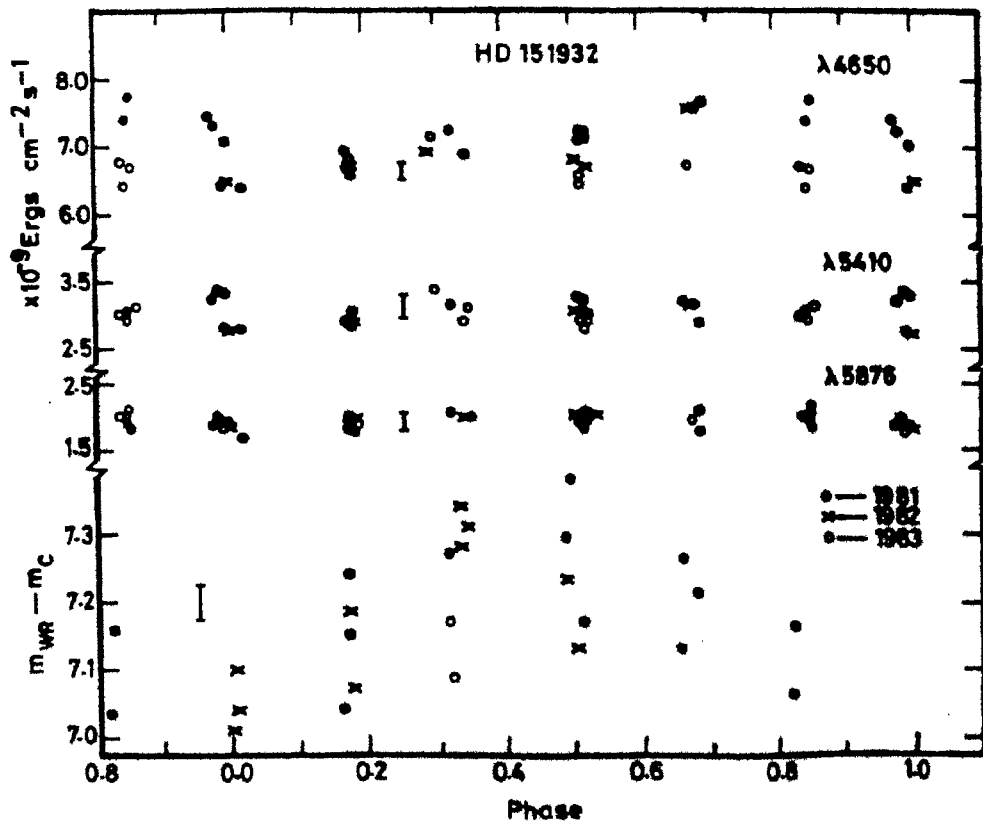


Figure 5.8 Flux and monochromatic magnitude of HD 151932 folded over a 6 days period.

associated. HD 151932 being a member of the relatively young cluster does not fit into this scheme.

5.4 Line Emitting Regions in HD 151932

The violet shifted absorptions clearly indicate an expanding envelope, following the excitation potential versus velocity relation like other systems (Seggewiss, 1974a). Therefore, it is implied that higher excitation like N V, N IV & C IV originate closer to the photosphere. The variations shown by the observed flux may be interpreted with this criterion. The He I lines, which are formed in the outermost regions of the atmosphere show large scatter of flux. Their RV curves also show a large scatter (Seggewiss, 1974a) compared to other lines. Such RV changes were attributed to changes in the particle density by Seggewiss & Moffat (1979). They have shown that small changes in particle density (the source for this is not known) can lead to large changes of ion density in the outermost regions where the He I lines are formed.

The observed photometric variations of period $\sim 6d$, which represents the asymmetry in the envelope, can also be explained by the variable density hypothesis. Further, the intrinsic variations of WRs are not uncommon, which, in the present study, might have produced the observed apparent periodic variation. Continuous photometry with simultaneous spectroscopic measurements only can establish this aspect.

5.5 Possible Atmospheric Eclipses in HD 152270

This is one of the 4 stars with WC component, with an established period of about 8.89d. Seggewiss (1974b) obtained

the RV curves with better resolutions and noticed the central absorption of the 5696 line of C III. The absorptions lines of the companion also were easily detectable because of the phase difference of 0.5 relative to the emission lines at λ 5696, 5808 and 5471. Therefore it was possible to improve the period to 8.893d. The velocities and the amplitudes of the RV curves show different values corresponding to different emission lines. Based on the RV curve of the unblended line of C IV λ 5471, which shows the systemic velocity, Seggewiss (1974b) has obtained the masses of the components.

The violet displaced absorptions also have been studied by Seggewiss (1974b); they all follow the behaviour of emission lines. Higher excitation lines like C IV have smaller velocities compared to He I lines. However, the relation of the EP versus velocity is not as strong as in case of WN systems. Further, the RV amplitudes of He I λ 5876 and C III λ 4650 are nearly same implying that they both have similar motion in binary system.

The origin of gas streams in this has also been discussed in detail (Seggewiss, 1974b). Further detailed investigations by Schmidt & Seggewiss (1976) have clearly shown the effect of central absorption with phase. This was attributed to a 'hole' near the Lagrangian point by Neutsch & Seggewiss (1977) and Neutsch et al. (1985)

The flux measures in Figure 5.6 show a dip at phase 0.4 for some lines. The zero phase corresponds to the WC in front and the angle of inclination is 35° as determined by the polarization measures of Luna (1982). Therefore, one may assume

that at phase 0.4 part of the line emitting region is covered only for some lines. then this represents the case of an atmospheric eclipse, since at the corresponding phase there is no change in the continuum (Figure 5.4). It may also be noticed that He II and I lines do not show this dip.

The effect of the central absorption on the total flux may not be significant in the resolutions of this equipment. Further, some lines appear as blends here. The C III λ 4650 and He II λ 4686 form one such blend. Similarly He II λ 5410 and C IV 5471 also form a blend. Smooth gaussian profiles may be drawn, but the total measured area only are indicated in the Figures. The lines at λ 4340 result in a single blend, making it difficult to resolve the individual contributors.

The dip at phase 0.4 in some cases is broad enough to cover up to phase 0.5, which corresponds to the O star in the front. To determine the variation of the contribution of the He II to the total value of the measured flux, other lines of He II were examined. Most of them are again blends and are expected to have central absorptions from the companion. Figure 5.6 includes one measure at λ 4340, where flux appears to be constant relative to other lines. This, perhaps, implies that it is free of any orbital effects. This may also be because, He II lines have contributions from both the components and the variation of the central absorption leaves the total flux unaltered. Extending the same argument to λ 4686, although even high dispersion spectra (Seggewiss, 1974b) were unable to resolve the possible central absorption, one may say that the contribution to the

total flux measured is constant. Then the variation seen in Figure 5.6 can be attributed to C III λ 4650 itself.

5.6 Line Emitting Regions in HD 152270

The masses derived by Seggewiss (1974b) as $35 M_{\odot}$ for the O star and $13 M_{\odot}$ for the WC star, may be used for estimating the distance of L_1 , the inner Lagrangian point, from the Tables of Plavec & Kratochvil (1964). For a separation of about $66 R_{\odot}$, this will be about $43 R_{\odot}$ from the center of mass. Since the angle of inclination is about 35° , and since the observed eclipse is very broad, quantitative derivations are not possible. The Roche surface calculations probably may not be valid for these stars with strong winds. The eclipse effects on C III and C IV imply that they are formed closer to the photosphere than the He II or He I lines. Since the line profiles do not reflect the asymmetry directly as seen in V444 Cyg (Ganesh et al. 1968) and θ Mus (Moffat & Seggewiss, 1979), the extension of the C III and C IV line emitting material may be taken as the inner Roche surface itself.

From the interferometric measurements of WC7 binary γ^2 Vel ($P = 78$ d), Brown et al. (1970) have derived that the extension of the C III line emitting region is 5 times larger than the continuum emitting region. However, the dimensions derived by them cannot be used directly here because of the difference in the subgroup.

The large velocities associated with the violet absorptions of emission lines indicate that the winds in the envelopes are strong enough to complicate the structure of He II and He I

lines, which are probably formed in the outermost parts of the envelope. Very high dispersion spectra only can reveal this aspect, since it is known that, even in a well separated binary like γ^2 Vel the line profiles are affected by the presence of the companion (Ganesh, 1966).

6. THE LINE EMITTING REGIONS

The earliest study of the atmospheres of the WR stars was by Beals (1929), as mentioned in Chapter 1. Menzel (1929) supported the idea of the broad emission lines originating in a simple expanding shell. Wilson (1942) raised questions on the validity of this hypothesis based on the non-detection of 'transit time effect' in a binary like V444 Cyg. Later studies have shown that this simple picture of expanding shell cannot explain all the observed spectral features of WR atmospheres. Various other mechanisms are investigated as possible causes for the observed broad emission features. Munch (1950) showed that electron scattering could increase the width of the emission lines, considerably. Later theories included effects of varying velocity fields and density gradients. Chandrasekhar (1934) showed that an expanding envelope can produce occultation effects. The variation of emission intensity with latitude has been discussed by Bappu & Menzel (1954). The problem of radiative transfer in moving atmospheres has been dealt with, by Sobolev (1947) and Rottenberg (1952). However, it is difficult to infer these aspects from observations directly.

Bappu (1951a) showed that rotational instability could explain large widths of emission lines. He also derived that an excitation gradient in the atmosphere would produce large widths for the highest excitation lines. Limber (1964) postulated that continuous gravitational contraction in a post main sequence stage causes the forced rotational instability, which in turn is

responsible for the large widths of the emission lines. Recent studies by Castor & van Blerkom (1973) have taken into account the electron envelopes associated with the atmospheres.

In the context of CQ Cep, various models have been put forward to explain the emission line flux behaviour by earlier investigators. The common envelope model proposed by Bappu (1951a) explain the occultation effects; however, the He I lines are assumed to be originating deeper in the envelope, which contradicts the velocity versus EP relation, derived from the UV line profiles (Stickland et al., 1984). Sahade proposed a stream towards the companion from WN to be responsible for enhancement of line flux (cf. Hack & Struve, 1970). Leung et al. (1983) explained the behaviour of some lines at phase 0.8 by assuming that the line emitting material has a maximum velocity towards the observer at that phase. The latest model by Stickland et al. (1984) takes into account the difficulties encountered in fitting a simple model, and provides a hot zone between the two stars and an enhanced outflow.

6.1 Roche Surface

The only emission line which shows eclipse effects is that of N V at $\lambda 4603$. If this may be used for estimating the line emitting region, the size will be almost equal to the inner Roche surface calculated from the Tables of Plavec & Kratochvil (1964, see Figure 6.1). The use of these Tables needs many assumptions to be made about the components. Considering the large wind velocities of the WN component and the large extension of the atmosphere, this picture of Roche surface will

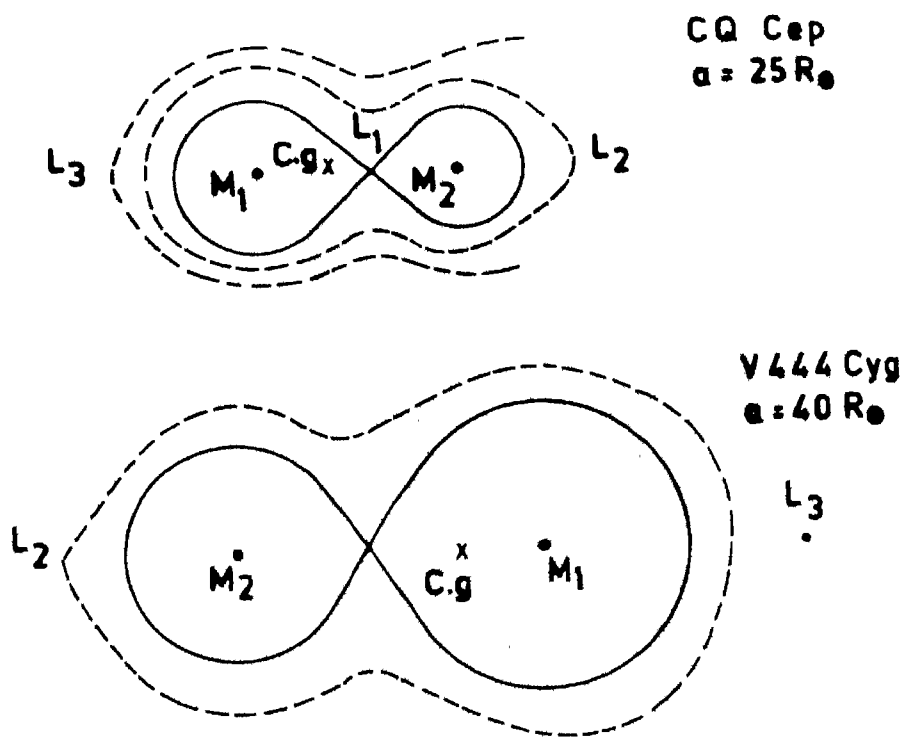


Figure 6.1 (a) Classical Roche surfaces for CQ Cep.

(b) Classical Roche surfaces for V444 cyg.

probably have to be revised. Schuerman (1972) introduced these effects into calculations of Roche surfaces and effectively used them in case of massive X-ray binaries. Zorec & Niemela (1980) considered the radiation pressure from both the components and applied it to the case of V444 Cyg (cf. Sahade & Wood, 1978). Vanbeveran considered X-ray heating, deviations from synchrotron rotation and a different rate of synchronization for the two components (1977). From all these studies, it is clear that the classical Roche surface calculations are not applicable here. The Roche surface will extend towards the companion with lower radiation pressure, making the distribution highly asymmetric and distorting the spherical shape of both the components into ellipsoids.

A sample Roche surface can be chosen for determining asymmetries, from Vanbeveran (1977), reproduced in Figure 6.2. Only hemispheres are considered for determining the ratios of line emitting material at four phases, because it is established that generally the helium lines (considered in this work) are optically thick (Smith, 1973). These ratios at phases 0.0, 0.25, 0.5 and 0.75 are 9:6.3:7.6:6.3 respectively. Thus at phase 0.0, the phase can be the highest, although the companion occults a small portion of the atmosphere. This kind of flux distribution is seen for the 4686 line of He II. For the N IV line at 4058 and the other He II lines the flux at 0.0 and 0.5 are almost equal. This may imply that their distribution may not be as asymmetric as that of λ 4686. The difference in the optical thickness of the different lines also plays a significant role in deciding this.

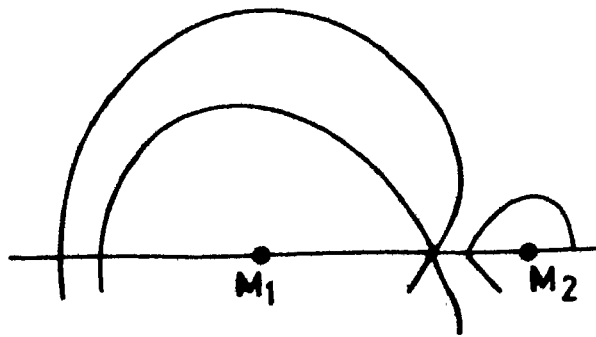


Figure 6.2 Sample Roche surface from Vanbeveren (1977).

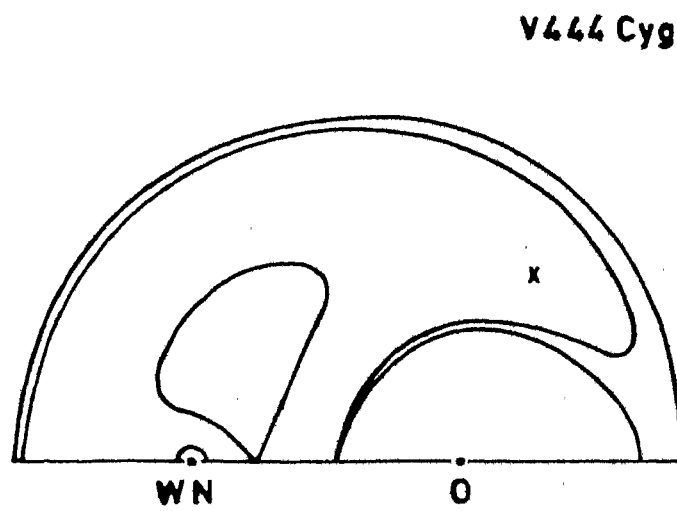


Figure 6.3 Roche surfaces for V444 cyg from Niemela (cf Sahade & Wood, 1978) taking into account the effect of wind.

Kuhi (1968b) suggested a hot zone between the two components in case of V444 Cyg, since the eclipse effects were seen for all the emission lines here. The distribution of emitting material, in such a situation, shows concentration towards the inner Lagrangian point. This will be recognizable in the line profiles (Ganesh et al., 1967; Sahade, 1958) of the He II line λ 4686. Similar observations have been available for θ Mus, (Moffat & Seggewiss, 1977) for the C III line at λ 5696. The absence of such profile variations in CQ Cep, signifies the importance of the modified Roche surfaces.

The binary nature of HD 50896 is confirmed not only by the radial velocity (RV) curves but by the moderate eclipse effects shown by the emission lines of N V, N IV and C IV as well. A quantitative derivations of the orbit is not possible because of the eccentric nature of the orbit and also the scatter observed in the flux. From the available RV measurements, it appears that the companion is a compact star. Comparison with other binaries shows that the atmospheric structures are similar. The He II lines probably arise from a region distorted by the companion. The He I lines generally show constant value of flux, indicating their formation in a region outside the influence of the companion.

From the small amplitude of the light variation it is not possible to deduce any information regarding the nature and type of components. Only the N V line at λ 4603 can be used as an indicator of eclipse effects. Detailed spectroscopic and simultaneous spectrophotometric measurements can throw some light on this phenomenon.

The variation of the total flux of HD 151932 (Chapter 5) may be a consequence of variable particle density or a possible unseen companion. Considering that there is a variation in the continuum, the latter possibility of a companion cannot be completely eliminated, because a compact companion may show RV variations $< 25 \text{ kms}^{-1}$. However, the other characteristic features of such WR + compact system are yet to be detected, which, if established, necessitates a rethinking on the membership of this star to the cluster.

For the spectroscopic binary HD 152270 (Chapter 5), the total flux variation show possible atmospheric eclipses of some higher excitation lines like C III and C IV. However, the flux of the He II lines appear to be unaffected by the orbital motion, which may be a consequence of the variable contribution from the companion to the flux either as absorption or emission. Although, the C III line at $\lambda 5696$ shows a variable profile, the measured flux shows eclipse effects.

6.2 Inferences from IR and UV studies

The earliest IR measurements were made by Hackwell et al. (1974) and Cohen et al. (1975), who showed that the observed IR excess, in many cases, can be explained by either free free emission or black body radiation. However, in case of CQ Cep only a free free fit was possible. Stickland et al. (1984) obtained the IR light curves of CQ Cep and showed that the amplitude of the light curve decreases towards the IR region. Hence the presence of a 'third source' could be recognized. The asymmetry in the distribution of the third source is similar to that of other emission lines.

The flux of different emission lines in the UV also have been measured by Stickland et al. (1984). The behaviour is similar to the variation seen in the present study in the optical region. Thus, the emissions lines both in the optical and UV region show enhancements of flux at phases 0.0 and 0.5. Stickland et al. (1984) have also measured one unidentified line in the UV region whose behaviour is similar to that of N V at 4603 in the optical, showing moderate eclipse effects. The equivalent widths of some absorptions also have been measured and they appear to have larger values at quadratures.

Ganesh et al. (1967) pointed out that the absorptions from O type star look widened at the primary eclipse, which is probably because they are seen through the electron envelope. Such an effect is difficult to see in systems like CQ Cep, because the absorptions from the companion are not at all detectable. Further, the IR excess measurements (Hackwell et al., 1974) have shown that both the free free or blackbody fit very well.

6.3 Comparison with other eclipsing systems

There are only four eclipsing systems according to the catalog of van der Hucht et al. (1981) and all the four have WN companions. They are CQ Cep, CX Cep, V444 Cyg and HD 211853.

For CX Cep the components are WN5 and O8 and the orbital period is about 2.1 d. This system has not been studied in great detail because of the faintness ($m_v \sim 12$). The eclipses are shallow, because the angle of inclination of the orbital plane is not favourable for sharp eclipses. The estimated mass range is 5 to 12 M_{\odot} for the WN component (Massey & Conti, 1980c).

V444 Cyg is the only binary with more detailed studies on line profiles and RV measurements. Here the O component is larger and more massive. Kuhl (1968b) studied the secondary eclipses using the passage of the O type star as an occulting disc in front of the WN atmosphere. He mentions about the highly individualistic behaviour of these emission lines.

The line profiles indicate the concentration of line (Ganesh et al., 1967) emitting material towards the inner Lagrangian point. Following the stratification seen in CQ Cep (Chapter 3), the secondary eclipse observations of V444 Cyg by Kuhl (1968b) may be interpreted. N V lines, being formed closer to the photosphere should show deepest eclipses. However, this is only partly true because the deepest eclipse is that of N IV at 7112 and the N V line is only next to it; then follow the other N IV lines.

The other peculiarity is that the eclipses do not occur at 0.5 but slightly earlier than that. This can be partly explained by considering the Roche surface calculations of Niemela, which is reproduced in Figure 6.3. At phase 0.5, when the O star is in front, the line emitting region is still visible, but for a small portion getting occulted, where as a larger portion will be occulted just before or after the phase 0.5, depending on the orbital inclination.

The separation of the components is $40 R_{\odot}$, from the light curve analysis (Kuhl, 1968b). Further, all the line emitting material will be within the Roche lobe and of the order of the size of the secondary ($10 R_{\odot}$) so that the eclipse effects are

seen. Since no information is available on the He I lines it is not possible to deduce anything on their line emitting region.

Thus, it appears that there is a difference in the sizes of the atmospheres of CQ Cep and V444 Cyg. For CQ Cep all the emission zones had to be larger than $10 R_{\odot}$ whereas for V444 Cyg they had to be smaller than $10 R_{\odot}$. Observing the difference between the subgroups WN5 and WN7 in masses, abundances, absolute magnitudes and ionization structures (Moffat & Seggewiss, 1980) this change in the size of the atmosphere is understandable.

The fourth eclipsing binary is HD 211853, which shows irregular variations of light. Earlier investigators classified this into an eclipsing system of period 6.7 d. Ganesh & Bappu (1967) derived the RV curves for N IV line at $\lambda 4058$ and He II line at $\lambda 4686$. However, the absorption measurements resulted in a scatter. Recently Massey (1981) studied this system in greater detail and arrived at an important conclusion: this is a quadruple system - pair A consists of WN6 and O and has a period of 6.7 d; pair B has both O type stars and a period of 3.5 d. Based on this the estimated mass of the WN component is derived as 10 to 20 M_{\odot} . From the line profiles, it appears that this also shows enhancement of flux at minima; however, the complications arise because it is a quadruple system.

The well studied binary V444 Cyg has an orbital period close to that of HD 50896. Direct comparison between the two is not possible because of the difference in the type of companion. The influence of the small companion is detectable only as a

distortion in the atmosphere where the higher excitation lines originate. Other lines show scatter.

There are some similarities between the two systems. None of the RV curves give identical solutions in either case. Both show variation of polarization with phase, which implies a dense electron envelope.

The wind dominant Roche surface can explain the flux variation, to some extent, for CQ Cep and V444 Cyg. In case of HD 50896 there is a complication introduced by the eccentricity of the orbit. The value of $e = 0.34$ is based on the RV measures of N IV λ 3483 and He II λ 4686, while N V gives a still smaller value of e .

6.4 Peculiarities of some emission lines

From a study of WNL systems, it has been shown that the motion of the WN component in binaries is best represented by the N IV line at λ 4058 (Moffat & Seggewiss, 1979). This assumption has been extended to all binaries, so that the differences in the behaviour of some emission lines can be understood, as a consequence of the differences in the dynamics of the line emitting regions.

Although hydrogen deficiency is an established phenomenon in WR stars (Sahade, 1980), in some binaries the Balmer lines of hydrogen in absorption have been detected. Therefore, it is difficult to estimate the contribution of the companion to some lines like those at λ 4100, 4340, 4860 and 6562. Therefore, although these lines can be considered as due to He II, their behaviour appears to be different relative to other lines.

6.4.1 Total Flux Variations

The flux of the two systems CQ Cep and HD 50896 are shown in Figures 3.5, 4.6 & 4.7 for the lines λ 4058 and 4686. It may be seen that the flux of λ 4686 shows an increase at orbital phase 0.0 and 0.5, corresponding to the eclipse and transit of the components. In case of CQ Cep, not only the N IV 4058 line, but all the other He II lines also showed a similar behaviour, which were attributed to the complicated structure of the atmosphere, arising as a consequence of the proximity of the companion. In case of HD 50896, the N IV line at λ 4058 and lines of He II except 4686 show a scatter of flux. Similar flux measures of other binaries are not yet available. However, the line profiles of HD 186943 (Ganesh & Bappu, 1967) show a large difference in the profiles from conjunctions to quadratures, from which it may be inferred that there is an increase in flux at eclipse and transit.

In case of V444 Cyg (Kuhi, 1968b) all the emission lines show eclipse effects. Again, the eclipse depth of λ 4686 is markedly different from those of other lines. This may imply that at phases corresponding to the eclipse and transit, the total flux increases relative to other lines, so that the net effect is to reduce the eclipse depth. There are some other systems, which also indicate increase of flux indirectly. In case of HD 90657 ($P = 8.26$ d), a dip in the light curve at λ 4680 is observed (Niemela & Moffat, 1982) at phase 0.1, which is attributed to the asymmetric line emitting region. However, the light curve can be interpreted as showing an increase in flux at

phase 0.5, corresponding to the WN4 component behind the companion.

The line profile studies of V444 Cyg have shown the multiple component structure of the λ 4686 line, attributed to the concentration of the material between the two stars. A similar possibility exists for HD 90657, for explaining the dip near phase 0.1, when the contribution from the region between the two stars is minimum. In case of HD 5980 ($P = 19.27$ d), Breysacher et al. (1982) have explained the profile by a larger amount of material towards the hemisphere facing the O star.

6.4.2 Radial Velocities

The RV curves from various sources are reproduced in Figures 6.4 a & b. The sources are indicated in the Table 6.1. The following points are immediately apparent -

1. Considering that the N IV line of λ 4058 represents the true motion of the WN component, there is a red shift of in γ the velocity of the center of mass in all cases.
2. The amplitudes of the RV curves $K(4686)$ and $K(4058)$ vary from system to system. The variation of the difference is shown in Figure 6.5 [$\Delta K = K(4058) - K(4686)$]. For CQ Cep, ΔK is largest and positive, while it reaches zero for systems with orbital period near 4 d. For still longer orbital periods, it appears that ΔK will remain zero or take negative values.
3. The solutions derived from the λ 4686 RV curve generally give eccentric orbit, while the solutions from other lines may be circular.

Table 6.1 Binaries chosen for study of the behaviour of $\lambda 4686$ line.

Name / HD	P (d)	Sp type	$\lambda 4686$		$\lambda 4058$		Ref.
			amp k	c.m. γ	amp k	c.m. γ	
CG Cep	1.34	WN 7.07	134	165	297	-53	Stickland et al 1984
			148	118	313	-61	Bappu & Viswandham 1977
			165	137	295	-75	Hiltner 1944
					285	-85	Niemela 1980
			181	77	310	-60	Leung et al 1983
HD 50896	3.76	WN5 (SB)	25	147		Firmani et al 1980	
V444 Cyg	4.21	WN5.06	283	16	303	-42	Ganesh et al 1967
HD197406	4.32	WN7(SB)	57	-95	82	-126	Bracher 1979
HD311884	6.34	WN6.05	310	-10	297	-89	Niemela et al 1980
HD 90657	8.26	WN4.0B	246	20	221	-33	Niemela & Moffat 1982
HD186943	9.56	WN4.09	146	239			Massey 1981
			212	107	187	70	Ganesh & Bappu 1967
HD193928	21.64	WN6(SB)	147	60	135*	-64*	Ganesh & Bappu 1967

All velocities in km s^{-1}

* Approximate

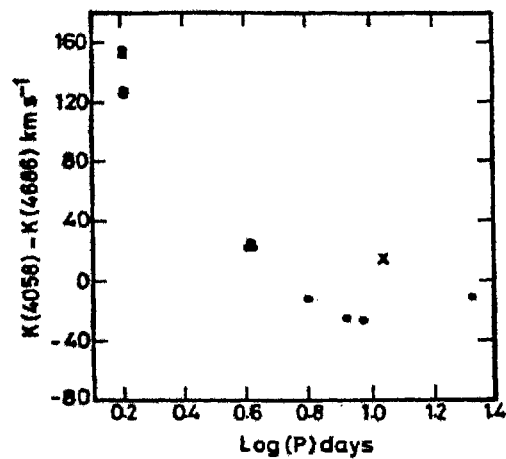


Figure 6.5 The variation of ΔK , the difference in amplitude of RV curves of $\lambda 4686$ and $\lambda 4058$ with the orbital period. The cross corresponds to HD 228766.

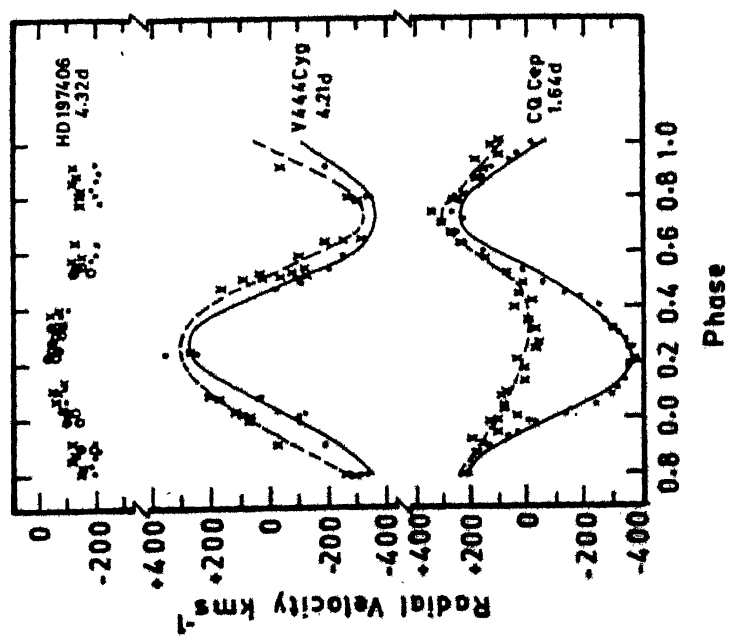
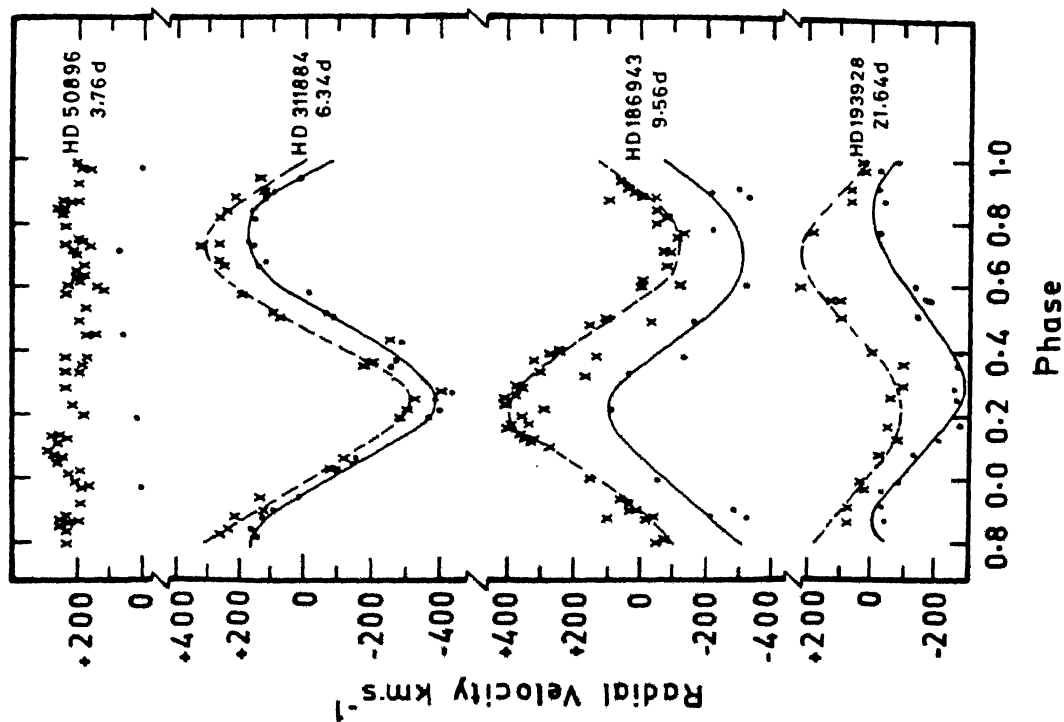


Figure 6.4 Radial velocity curves of the λ 4686 and λ 4058 lines for various binaries from Table 6.1.

In the context of the short period binary CX Cep ($P = 2.1$ d), the amplitude differences of the two RV curves have been discussed (Massey & Conti, 1981) and they have assumed that the two are equal. However, their RV curve excludes the possibility of $K(4058) < K(4686)$, while there is a suggestion that $K(4058)$ may be greater than $K(4686)$. From Figure 6.5, it may be inferred that the value of ΔK may be about $+ 60 \text{ km s}^{-1}$. This can be established by only a better RV curve for $\lambda 4058$. The cross in the Figure corresponds to that of HD 228766 ($P = 10.74$ d), which does not agree with the smooth curve. However, the available RV curve does not correspond to $\lambda 4058$ only (Massey & Conti, 1977), because the 'narrow emission' corresponds to an average of the velocities of N III, N IV and Si IV lines. Similarly for another binary HD 311884 (Niemela et al., 1980), the RV curve of $\lambda 4686$ cannot be separated from the mean of all He II lines. In case of HD 97950 ($P = 3.77$ d), the mean of $\lambda 4686$ and 4058 only is available (Moffat & Niemela, 1984). Other systems have only one of the two RV measurements available (eg. HD 5980, Breysacher et al., 1982; HD 86161, Moffat & Seggewiss, 1982) and therefore these systems are not included in the discussion.

6.4.3 Effects of Companion

In general, the established companions in many binaries are of spectral type O. Therefore, it is possible that there is an absorption component superposed on the emission profile. Any such absorption component, if present, will move in the opposite direction to indicate the movement of the companion. Attempts made to search for this, revealed that such absorptions are not

clearly noticeable. The profiles of $\lambda 4860$, for V444 Cyg, show this type of absorption but $\lambda 4686$ line profiles do not. (Ganesh & Bappu, 1967). However, one may interpret the double hump profile as being caused by an absorption rather than two emissions. In case of HD 193928 ($P = 21.64$ d), there is an indication of double hump structure but not very well separated.

If one postulates a companion of type Of, the contribution to the emission itself becomes considerable. This has been discussed in case of HD 5980 (Breysacher et al., 1982), where three contributors to the emissions are considered.

1. the WN component
2. the companion and
3. the region between the two stars.

By means of such a multicomponent profile, they are able to analyze the variation of the half-intensity widths of the line. At phase 0.0 and 0.5, probably the contribution (3) is not very significant, causing a decrease in the half-intensity widths.

The observational evidence, thus, clearly indicates that there are additional contributors to $\lambda 4686$ relative to $\lambda 4058$. One may consider the other possibilities such as the differences in optical depths and the asymmetric distribution of emitting material.

In case of binaries with Of companions, therefore, it is possible to have significant contribution from all the above mentioned three parameters. In medium dispersion spectra, however, the line profiles get smoothed resulting in an error in fixing the center of the profile. This can cause a net reduction in the amplitude of the RV curve.

In case of binaries, with compact companions, although the contributions from the companion is not very significant, the accretion disk can contribute. However, not many samples are available for verifying this aspect. HD 197406 (P = 4.17 d) fits in to Figure 6.5 very well, but the contribution from the disk cannot be distinguished in the profile. In case of HD 50896, the 4058 line profile is complicated and therefore a comparison is not possible.

The red shift of the γ value is a general feature in all binaries. This aspect has been discussed by many previous investigators (Sahade, 1958; Ganesh & Bappu, 1967). The effects of electron scattering in an expanding envelope was investigated by Auer & van Blerkom (1972), who showed that the velocity field preferentially scatters the photons to the red. Thus electron scattering is mainly responsible for the red wing of the He II line profile asymmetry and this has been confirmed by Hillier (1984) by both observations and theoretical deductions in case of HD 50896. Thus, this effect adds to the asymmetry making it difficult to fix the line center and hence adding to the errors in the RV measurements.

The above discussed effects of the companion and the electron scattering are probably common to all WR systems. Therefore the reduction of ΔK , the amplitude difference, with the orbital period cannot be explained by these two factors only.

It is known that classical Roche surfaces are not applicable to the WR systems, which have asymmetric line emitting regions.

Further, it is also known that $\lambda 4686$ has the largest optical depth amongst all He II lines (Hillier, 1983) and therefore we are seeing the emission from the outermost parts of the line emitting region. Thus the flux variations of $\lambda 4686$ reflect the asymmetries in the line emitting regions directly. However, the exact distribution of the line emitting material in such a surface will be decided by the density distribution, the velocity law and also the temperature gradient. A qualitative analysis of the asymmetry can lead to the deduction that short period systems show more complicated line profiles and larger flux variations. As the companion goes farther and farther, (i.e. period longer and longer) this effect reduces.

Therefore, long period systems may not show increase of flux at phases corresponding to eclipse and the amplitude reduction of $\lambda 4686$ RV curve. It may also be seen in Figure 6.5 that not many samples are available for longer period range. It is possible that the amplitudes do not differ greatly in this range.

The effect of the O or Of companion on other emission lines may be also considered. The line of N III at $\lambda 4640$ is a possible contributor. However, because there are three unresolved components, the additional contributor cannot be resolved. However, in case of CQ Cep the behaviour of this line was different from other lines.

Therefore it appears that the contribution from the companion either as emission or absorption to the line profile is partly responsible for the observed difference in the

behaviour relative to $\lambda 4058$. The large optical depth and the asymmetric distribution in the atmosphere also can cause the observed variation. Since the proximity of the companion is responsible for the distortion of line emitting regions and therefore the line profiles, the inequality $K(4686) < K(4058)$ may be valid for very short period binaries only. Thus there is an emphasis on the study of the other short period systems like CX Cep and HD 97950 more thoroughly for both RV and flux variations.

The peculiarity of the central absorption in the line profile of C III $\lambda 5696$ is a unique feature, not seen in any other line. The cone model of Neutsch & Schmidt (1985) which explains this satisfactorily, can be extended to other systems too. However, not many samples are available for this. The other binary with WC7 component θ Mus ($P = 18$ d) also has a peculiar feature about the C III $\lambda 5696$ line; however, this has been explained in terms of the concentration of emitting material towards the inner Lagrangian point (Moffat & Seggewiss, 1977). As an effect of the extension of this cone model, one may expect to see such 'hole' effects in the lines which are formed in the outer regions of the atmosphere. This is a difficult task because the He II and He I lines are complicated by the contribution from the companion. In case of shorter period binaries the effect may become noticeable for other higher excitation lines as well. Therefore, a study of the absorptions in line profiles of other binaries can throw some light on whether only the $\lambda 5696$ line is a special case or, other lines

also show this behaviour. It is possible that this line is emitted in an extended region similar to the $\lambda 4686$ line in WN binaries, in which case all the four binaries may be expected to share special behaviour of this line.

6.5 Sporadic Events

It may be mentioned that there are many reports of sporadic brightenings of many emission lines. A change in the strength of the $\lambda 4686$ line will not result in a corresponding change of $\lambda 4860$ line in many cases. The cause of this may be the effect of absorption line or the small difference in the upper level of excitation or the optical depths or the differences in the sizes of the line emitting regions.

A brightening of the order of 0.03 mag was noted by Hiltner (1950) for CQ Cep. Later Kartasheva (1976) reported variations up to about 0.1 mag in 10 months. Both these observations were for the continuum only. However, in 1950 Hiltner also noticed a sudden change in the strength of He II at $\lambda 4686$. It is possible that we have a similar situation in our observations in 1982. The sudden increase in flux at phase ~ 0.9 corresponds to the observations made only in one season. Hence if this corresponds to a sporadic brightening of the $\lambda 4686$ line, its behaviour otherwise is similar to the other He II lines. It may be also noted that the corresponding observations of other lines do not show any increase.

The behaviour of the He I lines also has been changing for CQ Cep at some epochs, as has already been discussed (Chapter 3). The line at $\lambda 4471 \text{ \AA}$ split into two components in Hiltner's plates taken in 1943. Bappu's collection of the plates of 1952 showed similar line splitting. In 1978, Leung et al. (1983) also noticed such double peaks for the $\lambda 3888$ line. Therefore, it is likely that some transient phenomenon like the enhancement of mass loss (Stickland et al., 1984) may be responsible for such line splitting. High dispersion spectra can reveal these aspects and the possible effect due to the companion.

In case of HD 50896, there is an evidence of the brightening of the He II line at $\lambda 4860$. On JD 2,446,048 this enhancement of flux is noticeable for only this line and not for $\lambda 4686$. This is represented by different symbol in the Figure 4.6 and 4.7.

6.6 Evolution

Smith (1973) suggested that all population I WR stars have $10 M_{\odot}$ and therefore, they all evolved from more massive stars. Recently, Massey (1981) has shown that the mean value of the WR mass is $20 M_{\odot}$. Since hydrogen deficiency is a general feature of all WR stars (Sahade, 1981), it was also postulated that the outer hydrogen material is being lost. The evolutionary scheme of de Loore (1980) invokes two stages of WR phase in a binary. The first phase corresponds to the more widely known (WR + OB) phase: the second is (WR + compact star) phase, through a supernova explosion. In such a binary, it is possible that the mass from the WR gets accreted onto the companion, making it more massive and readily detectable (Paczynski, 1967). However, the

winds are so fast that the accretion may be negligible. When the companion is not detectable, the material is lost to the surroundings which may appear like a nebula. Therefore Wendker et al. (1975) attributed the presence of the nebula in NGC 6888 to the material ejected from HD 192163, which was considered to be single. Recently this object also has been discussed for possible binarity (cf. van der Hucht et al., 1981; Vreux, 1985).

The observations reported in Chapters 4 and 5 present many interesting features about the companion. For HD 151932, it may be seen that the variation in the total flux is very little, unlike the continuum; while in HD 50896, the variation of flux is more compared to the continuum. This can be a consequence of the asymmetric distribution of the line emitting material. If the cone model (Neutsch & Seggewiss, 1985) for HD 152270, can be extended to WN7 systems, the change in the line profile will become noticeable for different ionization levels depending on the period. This also leads to an apparent variation of flux for some lines only. At the same time, it should be remembered that the extension of the WN7 systems is larger compared to any other subgroup. Therefore the absence of flux variation in HD 151932 for higher or lower excitation lines may indicate an undisturbed atmosphere. This, again, does not eliminate the possibilities of a companion completely embedded in the atmosphere, or a longer orbital period system.

In case of HD 50896, the binary nature is arrived at through the RV variations and flux variations, although intrinsically varying single WR stars are known. The presence of a compact

companion puts this to the second WR phase in the scenario proposed by de Loore (1980). Another characteristic feature which would facilitate the confirmation of this aspect is the space velocity. It is generally believed that the binary pulsars with high space velocities are results of supernova explosions in a binary with unidentical components. It is also derived that depending on the mass lost, the circular orbit changes to one with high eccentricity, without getting completely disrupted and thus a close binary may get separated out (van den Heuvel, 1976; Shylaja & Kochhar, 1983). The large distance of HD 50896 from the galactic plane and the non circular orbit also favour this idea. The association with the ring nebula S308 (Chu et al., 1982) puts its origin to the WN itself (Kwitter, 1984), since the [N(II)] lines from the nebula probably indicate nitrogen enrichment. Recently a large interstellar structure has been detected in the line of sight of HD 50896 (Heckathorn & Fesen, 1984).

The question of compact companion has led to many new type of observations. Many features like the high space velocity, associated nebula, rapid light variations and the RV variations are likely to be helpful in the detection of such compact companions, since it has been shown that pulsations also can cause light variations of short periods (Vreux et al., 1985). Many candidates like HD 192163, are being reobserved in this context.

The system of HD 76536, which is suspected to be having a compact companion (Bromage et al., 1982) was observed, to find

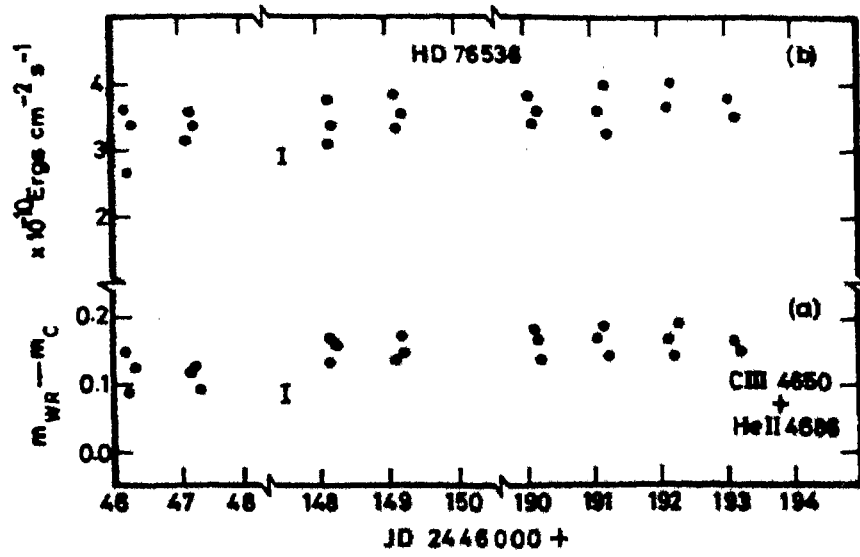


Figure 6.6 Magnitude and flux (C III 4650 He II 4686) variation of HD 76536 relative to HD 76556.

evidence of flux and magnitude variations. Figure 6.6 shows the flux of (C III + He II 4686) and the monochromatic magnitude at 5000 Å. As can be seen, the scatter of the data prevents any conclusion to be drawn. The variation in magnitude resembles the variations of cataclysmic variables. However, because of the faintness of the star, variations of other emission line flux could not be derived. Further detailed observations may reveal the characteristic features mentioned above. The flux variation may mean only the asymmetric distribution of the emitting material and not necessarily the companion.

Although twenty binaries with WR components are known, it has not been possible to establish any correlation between the binary nature and the evolution associated with it. Generally, it is observed that WC have smaller mass compared to WN, which probably implies the former evolving from the latter. However, it remains uncertain as to how the different subgroups evolve. The type of atmospheric structure seems to be similar in all these cases and therefore, the relation between subtype, mass and ionization cannot be established. Further, it has not been possible to understand whether the single WRs evolve in a significantly different way compared to their counterparts in binaries (Conti et al., 1983) based on their different chemical compositions. As remarked earlier, perhaps the Roche lobe overflow is not able to alter the mass loss rates significantly.

There are many massive semidetached binaries, eg. UW CMa, with O8 components, which are considered as probable progenitors of WR binaries. The mass loss rates, period and the masses of

the companions indicate that they are in the contact phase of evolution (Parthasarathy, 1978).

Thus a study of these systems provides indirect evidence on the stratification of the line emitting regions prevalent in these atmospheres. The distortions in these atmospheres are reflected as flux variations, which depict the nature of orbital parameters and the companion. Similar detailed investigations to include the H and He I lines may throw light on the complete structure of the atmospheres. The chemical compositions are considered normal (Underhill, 1980) and hydrogen deficiency is treated as an apparent effect of their origin deep in the atmosphere closer to the photosphere (Sahade, 1980). These aspects can be understood in a better way by the study of such binary systems since 'the variable phenomenon discloses more of its nature than a steady one'.

SUMMARY AND FUTURE PROSPECTS

The aim of this study was to understand the effect of the companion on the extended atmosphere of the Wolf-Rayet stars and to examine the stratification prevalent in them. The technique of spectrophotometry has been utilized for deriving not only the absolute flux but the monochromatic magnitudes as well. Such a detailed examination of the behaviour of the flux and magnitudes have yielded as a by-product, the study of the seasonal variation of the atmospheric extinction at the Observatory and the effect of the minor constituents in the atmosphere on the transparency. The monochromatic light variations in the systems studied here, reveal different characteristics of the respective companions. In the first system under study, CQ Cep ($P = 1.64d$), only one line namely N V $\lambda 603$, shows eclipse effects, based on which, qualitative deductions of the atmospheric stratification was done. The other lines clearly demonstrate the effect of the asymmetric distribution of the line emitting source. The second system HD 50896, with a compact companion, shows emission flux variation, which again reflect the asymmetric distribution. Photometric measurements indicate possibilities of mass transfer and accretion.

The detection of atmospheric eclipses for the higher excitation lines in case of the spectroscopic binary HD 152270, also indicate the possibility of stratification prevalent in the atmosphere. Such eclipses are not detectable in He II and He I lines. The scatter in the measured flux over the orbital period for these lines may be interpreted as due to either

unfavourable angle of inclination or non-participation in the orbit. The apparently single star, HD 151932, shows irregular variation of flux, while the emission free continuum measurements display a periodicity of about 6d. Although the possibility of a companion cannot be completely eliminated, the confirmation also is not possible from these techniques only.

The distortion of the line emitting region due to the presence of the companion is evident in all these cases. The maximum distortion is seen in case of the shortest period system CQ Cep, where almost none of the emission lines displays effect of eclipses. Their behaviour of increase of flux at phases corresponding to eclipses can be partly explained by the wind dominant Roche surfaces. Similar variations in HD 50896 with a compact companion reflect the stratification (i.e. N V, N IV and C IV originating closer to the photosphere) and hence the moderate eclipse effects are seen. The He II and He I lines, which arise in the outer regions show a scatter of flux, implying the distortion of their line emitting regions. The stratification is almost similar in case of the WC component of HD 152270, since only the C III and C IV lines show possibility of eclipse effect, whereas the He II lines show an irregular variation. Similar variations of flux are not apparent in case of HD 151932, whose binary nature is yet to be established. A comparison of all these inferences with some indirect evidences in case of other binaries bring out the following points -

1. Wind dominant Roche surfaces play an important role in the distribution of line emitting material.

2. These effects are probably true for the lines in the UV and IR regions as well.
3. All the four eclipsing binaries show indirect evidences of similar stratification although the extension of the atmosphere appears to be more in case of WN7 subgroup.
4. Some of the emission lines like λ 4686 of He II in WN and C III λ 5696 behave in a different way compared to other members of the same group. This may be because of the differences in the line emitting regions, or the contribution from the companion in emission or absorption, or optical depth differences.

Sporadic brightening of continuum as well as selected emission lines and sudden changes in the line profiles appear to be present in almost all systems.

It has been deduced theoretically that there are two WR phases in the evolution of a close massive binary, the first one is the more common (WR + O) phase. The detection of a compact companion puts any WR system to the more evolved, second WR phase. However, the stratification in the atmosphere does not seem to have changed significantly during this evolution. Thus, in spite of the differences in evolution, mass, effective temperatures and chemical abundances, the stratification of atmosphere appears to be similar, in the various subgroups.

FUTURE PROSPECTS

Thus the study of Wolf-Rayet binaries in a few selected regions clearly shows the effect of the companion on the extended atmosphere. As such, it emphasizes the need of the

individual attention to selected spectral lines. Thus, the technique of spectrophotometry used here may be well utilized to study of atmospheric eclipses, even in case of spectroscopic binaries, especially when combined with simultaneous high dispersion studies. This is also expected to be helpful in understanding the long term variation of the orbital parameters.

The main limitations of the technique are the poor spectral and time resolution, especially for faint, short period systems. However, the detector sensitivity can be improved by better substitutes. This technique itself is not self-sufficient in some aspects of study - for eg. in case of HD 50896 or HD 151932 the existence of a compact companion cannot be established by only the spectrophotometric measures of flux and monochromatic magnitudes.

There are many massive binaries, whose understanding may be improved by supplementing spectrophotometric data on their atmospheric structure (eg UW CMA). Many other systems with suspected compact companions also need to be monitored.

There is a possibility of extension of this technique to a few other types of binaries as well. For example, the RS CVn systems have late type components and the complications of their chromospheric activities may be better understood by mainly such studies. On the other hand, the cataclysmic binaries are generally believed to be sources of continuous mass accretion from a late type star onto a white dwarf companion. However, their faintness and short orbital period necessitate larger telescopes along with more sophisticated, efficient detectors

like the Reticon and the CCD. At the same time, it is important to have the UV observations of these binaries to understand the fineness of the line profile variations. The IR studies also are essential to study some aspects like the dust shell evolution of the novae, which form one important subgroup amongst cataclysmic variables. Finally, it is necessary to have good theoretical models, because only then it would be possible to explain the ultimate evolutionary aspects of these binaries.

REFERENCES

- Allen, C.W. 1976, in Astrophysical Quantities, Athlone Press, London, p. 127.
- Antokhina, F.A., Lipunova, N.A., Cherepashchuk, A.M. 1982, Soviet Astr., 26, 429.
- Appenzeller, I. 1970, Astr. Astrophys., 5, 355.
- Auer, L.H., van Blerkom, D. 1972, Astrophys. J., 178, 175.
- Babu, G.S.D., Shylaja, B.S. 1981, Astrophys. Space Sci., 79, 243.
- Babu, G.S.D., Shylaja, B.S. 1982a, Astrophys. Space Sci., 81, 269.
- Babu, G.S.D., Shylaja, B.S. 1982b, Astrophys. Space Sci., 83, 367.
- Babu, G.S.D., Shylaja, B.S. 1983, Astrophys. Space Sci., 89, 341.
- Bappu, M.K.V. 1951a, Ph.D. Thesis, Harvard Univ.
- Bappu, M.K.V. 1951b, Astr. J., 56, 120.
- Bappu, M.K.V. 1952, Astr. J., 57, 6.
- Bappu, M.K.V. 1973, in IAU Symp. 49: Wolf-Rayet and High Temperature Stars, Eds M.K.V. Bappu & J. Sahade, d.Reidel, Dordrecht, p. 59.
- Bappu, M.K.V. 1977, Kodaikanal Obs. Bull. Ser. A, 2, 64.
- Bappu, M.K.V., Viswanadham, P. 1977, Kodaikanal Obs. Bull. Ser. A, 2, 89.
- Bappu, M.K.V., Menzel, D.H. 1954, Astrophys. J., 119, 508.

- Bappu, M.K.V., Mohin, S., Unnikrishnan, K.G. 1978, Kodaikanal Obs. Bull. Ser. A, 2, 168.
- Bappu, M.K.V., Sinhal, S.D. 1959, Observatory, 79, 140.
- Bappu, M.K.V., Sinhal, S.D. 1955, Astr. J., 60, 152.
- Bappu, M.K.V., Parthasarathy, M., Sivaraman, K.R., Babu, G.S.D. 1980, Mon. Not. R. astr. Soc., 192, 641.
- Barbon, R., Bertola, F., Ciatti, F., Morgan, R. 1965, Inf. Bull. Var. Stars, No. 109.
- Beals, C.S. 1929, Mon. Not. R. astr. Soc., 90, 200.
- Beals, C.S. 1938, Trans. IAU, 6, 248.
- van den Bergh, S., Henry, R.C. 1963, Publ. David Dunlop Obs., 2, 281.
- Blackman, R.B., Tukey, J.W. 1958, in The Measurement of Power Power Spectra, Dover, NewYork, p.52.
- Bracher, K. 1979, Publ. astr. Soc. Pacific, 91, 827.
- Braes, L.L.E. 1967, Bull. astr. Inst. Netherl. Suppl., 2, 1.
- Breger, M. 1976, Astrophys. J. Suppl., 32, 1.
- Breysacher, J., Moffat, A.F.J., Niemela, V.S. 1982, Astrophys. J., 257, 116.
- Bromage, G.E., Burton, W.M., van der Hucht, K.A., Macchetto, F., Wu, C.C. 1982, in Third European IUE Conf. Eds E.Rolfe, A.Heck, B.Battrick, ESA SP 176, ESTEC, p 269.
- Brown, R.H., Davis, J., Herbison-Evans, D., Allen, L.R. 1970, Mon. Not. R. astr. Soc., 148, 103.
- Chandrasekhar, S. 1934, Mon. Not. R. astr. Soc., 94, 522.
- Cherepashchuk, A.M., Khaliullin, Kh.F. 1976, Soviet. Astr., 19, 727.

- Cherepashchuk, A.M. 1981, Mon. Not. R. astr. Soc., 194, 755.
- Cherepashchuk, A.M., Eaton, J.A., Khaliullin, Kh.F. 1984,
Astrophys. J., 281, 774.
- Chiosi, C., Nasi, E., Srinivasan, S.R. 1978, Astr. Astrophys.,
63, 103.
- Chu, Y.H., Gull, T.R., Treffers, R.R., Kwitter, K.B., Troland,
T.H. 1982, Astrophys. J., 254, 562.
- Code, A.D. 1960, in Stellar Atmospheres : Stars and Stellar
Systems VI Eds G.D.Kuiper & B.M.Middlehurst, Univ.
Chicago Press, p. 50.
- Code, A.D., Liller, W.C. 1962 in Astronomical Techniques :
Stars and Stellar Systems II Ed. W.A.Hiltner,
Univ. Chicago Press, p. 281.
- Cohen, M., Barlow, M.J., Kuhi, L.V. 1975, Astr. Astrophys., 40,
291.
- Conti, P.S., Massey, P. 1981, Astrophys. J., 249, 471.
- Conti, P.S. 1982, in IAU Symp 99: Wolf Rayet Stars:
Observations, Physics and Evolution, Eds C.W.H.de
Loore & A.J.Willis, D.Reidel, Dordrecht, p.3.
- Conti, P.S. 1976, Mem. Soc. R. Sci. Liege, Ser. 6e, tome IX,
193.
- Cowley, A.P., Hiltner, W.A., Berry, C. 1971, Astr. Astrophys.,
11, 407.
- Crawford, D.L., Barnes, J.V., Hill, G., Perry, C.L. 1971,
Astr. J., 76, 1948.
- de Loore, C., De Greve, J.P. 1975 Astrophys. Space Sci., 35,
241.

- de Loore, C.W.H. 1980, Space Sci. Rev., 26, 113.
- Dunkelman, L., Scolnik, R. 1959, J. Opt. Soc. America, 49, 356.
- Ebbets, D. 1979, Publ. astr. Soc. Pacific, 91, 104.
- Fay, T.D., Stein, W.L., Warren Jr., W.H. 1974, Publ. astr. Soc. Pacific, 86, 772.
- Firmani, C., Koenigsberger, G., Bisiacchi, G.F., Ruiz, E., Solar, A. 1979, in IAU Symp. 83: Mass Loss and Evolution of O stars, Eds P.S. Conti & C.W.H. de Loore, D. Reidel, Dordrecht, p. 421.
- Firmani, C., Koenigsberger, G., Bisiacchi, G.F., Moffat, A.F.J., & Isserstedt, J. 1980, Astrophys. J., 239, 607.
- Ganesh, K.S. 1966, Ph.D. Thesis, Karnataka Univ.
- Ganesh, K.S., Bappu, M.K.V., Natarajan, V. 1967, Kodaikanal Obs. Bull. Ser. A, 184.
- Gaposchkin, S. 1944, Astrophys. J., 100, 242.
- Garmany, C.D., Conti, P.S., Massey, P. 1980, Astrophys. J., 242, 1063.
- Garrison, R.F., Schild, R.E. 1979, Astr. J., 84, 1020.
- Giridhar, S. 1978, Kodaikanal Obs. Bull. Ser. A, 2, 164.
- Giridhar, S., Bappu, M.K.V. 1978, Kodaikanal Obs. Bull. Ser. A, 2, 161.
- Graham, J.A. 1965, Observatory, 85, 196.
- Hack, M., Struve, O. 1970, in Stellar Spectroscopy: Peculiar Stars, Osser. Trieste, p. 129.
- Hackwell, J.A., Gehrz, R.D., Smith, J.R. 1974, Astrophys. J., 192, 383.
- Hall, J.S. 1936, Astrophys. J., 84, 369.

- Hardie, R.H. 1962, in Astronomical Techniques : Stars and Stellar Systems II Ed. W.A. Hiltner, Univ. Chicago press p. 178.
- Hayes, D.S. 1970, Astrophys. J., 159, 165.
- Hayes, D.S., Latham, D.W. 1975, Astrophys. J., 197, 593.
- Heckathorn, N., Fesen, R.A. 1984, in Future of UV Astronomy Eds J.M. Mead, R.D. Chapman & Y. Kondo, NASA CP - 2349, p. 207.
- van den Heuvel, E.P.J. 1976, in IAU Sump. 73: Structure & Evolution of Close Binaries, Eds P.Eggleton, S. Mitton & J.A.J. Whelan, D. Reidel, Dordrecht, p.35.
- Hill, P.W., Kilkenny, D., Van Breda, I.G. Mon. Not. R. astr. Soc., 168, 451.
- Hillier, D.J. 1983, Astrophys. J., 271, 222.
- Hillier, D.J. 1984, Astrophys. J., 280, 744.
- Hiltner, W.A. 1950, Astrophys. J., 112, 477.
- Hiltner, W.A. 1944, Astrophys. J., 99, 273.
- Hiltner, W.A., Schild, R.E. 1966, Astrophys. J., 143, 770.
- Hjellming, R.M., Hiltner, W.A. 1963, Astrophys. J., 137, 1080.
- Hoffleit, D. 1964, in The Catalog of Bright Stars, Yale Univ. Publ.
- Hua, C.T., Woo, J.O., Nguyen, H.D. 1982, Astr. Astrophys. Suppl., 53, 407.
- van der Hucht, K.A., Conti, P.S., Lundstrom, I., Stenholm, B., 1981, Space Sci. Rev., 28, 227.
- Irvine, C.E., Irvine, N.J. 1973, Publ. astr. Soc. Pacific., 85, 403.

- Kartasheva, T.A. 1976, Soviet Astr. Lett., 2, 197.
- Khaliullin, Kh.F. 1974, Soviet Astr., 18, 229.
- Kuan, P., Kuhi, L.V. 1976, Publ. astr. Soc. Pacific, 88, 128.
- Kuhi, L.V. 1966a, Astrophys. J., 143, 753.
- Kuhi, L.V. 1966b, Astrophys. J., 145, 715.
- Kuhi, L.V. 1967, Publ. astr. Soc. Pacific, 79, 57.
- Kuhi, L.V. 1968, Astrophys. J., 152, 89.
- Kwitter, K.B. 1984, Astrophys. J., 287, 840.
- Landolt, A.U., Blondeau, K.L. 1972, Publ. astr. Soc. Pacific,
84, 784.
- Landolt A.U. 1973, Astr. J., 78, 959.
- Leung, K.C., Moffat, A.F.J., Seggewiss, W. 1983, Astrophys. J.
265, 961.
- Levato, H., Malorada, S. 1980, Publ. astr. Soc. Pacific, 92,
323.
- Lundstrom, I., Stenholm, B. 1980, Rep. Lund Observatory, No. 16.
- Luna, H.G. 1982, Publ. astr. Soc. Pacific, 94, 695.
- Lynds, C.R., Aitkin, R.I. 1965, Publ. astr. Soc. Pacific, 77,
347.
- Maeder, A. 1983, Astr. Astrophys., 120, 113.
- Massey, P. 1980, Astrophys. J., 236, 526.
- Massey, P. 1981a, Astrophys. J., 244, 157.
- Massey, P. 1981b, Astrophys. J., 246, 153.
- Massey, P. 1985, Publ. astr. Soc. Pacific, 97, 5.
- Massey, P. 1977, Astrophys. J., 218, 431.
- Massey, P., Conti, P.S. 1981a, Astrophys. J., 242, 638.
- Massey, P., Conti, P.S. 1981b, Astrophys. J., 244, 169.

- Massey, P., Conti, P.S. 1981c, Astrophys. J., 244, 173.
- Massey, P., Niemela, V.S. 1981, Astrophys. J., 245, 195.
- Massey, P., Conti, P.S., Niemela, V.S. 1981, Astrophys. J., 246, 145.
- McLean, I.S., Coyne, G.V., Trecker, J.E., Serkowski, K. 1979, Astrophys. J. Lett., 231, L 141.
- McLean, I.S. 1980, Astrophys. J. Lett., 236, L 149.
- Menzel, D.H. 1929, Publ. astr. Soc. Pacific, 41, 344.
- Moffat, A.F.J., Seggewiss, W. 1977, Astr. Astrophys., 54, 607.
- Moffat, A.F.J., Seggewiss, W. 1978, Astr. Astrophys., 70, 69.
- Moffat, A.F.J., Seggewiss, W. 1979, Astr. Astrophys., 77, 128.
- Moffat, A.F.J., Seggewiss, W. 1980 in IAU Symp. 83: Mass loss & Evolution of O Type Stars, Eds. P.S.Conti & C.W.H.de Loore, p. 447.
- Moffat, A.F.J. 1982 in IAU Symp. 99: Wolf Rayet Stars: Observations, Physics and Evolution, Eds A.J.Willis & C.W.H. de Loore ,p. 263.
- Moffat, A.F.J., Seggewiss, W. 1982, Astr. Astrophys., 108, 326.
- Moffat, A.F.J., Seggewiss, W. 1983, Astr. Astrophys., 86, 87.
- Moffat, A.F.J., Niemela, V.S. 1984, Astrophys. J., 284, 631.
- Munch, G. 1950, Astrophys. J., 112, 266.
- Neutsch, W., Schmidt, H., Seggewiss, W. 1981, Acta. Astr., 31, 197.
- Neutsch, W., Schmidt, H. 1985, Astrophys. Space Sci., 109, 249.
- Niemela, V.S. 1973, Publ. astr. Soc. Pacific, 85, 220.

- Niemela, V.S. 1973, in IAU Symp. 88: Close Binary stars : Observations and Interpretations, Eds M.J.Plavec, D.M.Popper & R.K.Ulrich, D.Reidel, Dordrecht, p. 177.
- Niemela, V.S., Moffat, A.F.J. 1982, Astrophys. J., 259, 213.
- Niemela, V.S., Conti, P.S., Massey, P. 1980, Astrophys. J., 241, 1050.
- Niemela, V.S., Sahade, J. 1980, Astrophys. J., 238, 244.
- Oke, J.B. 1964, Astrophys. J., 140, 689.
- Oke, J.B. 1965, A. Rev. Astr. Astrophys., 3, 23.
- Paczynski, B. 1967, Acta Astr., 17, 355.
- Parthasarathy, M. 1978, Mon. Not. R. astr. Soc., 185, 485.
- Plavec, M., Kratochvil, P. 1964, Bull. astr. Inst. Csl., 15, 165.
- Radhakrishnan, V. 1985, Pulsars , Invited talk at the IAU General Assembly, New Delhi, Nov. 1985.
- Raveendran, A.V., Mohin, S., Mekkaden, M.V. 1982, Mon. Not. R. astron. Soc., 199, 707.
- Ross, L.W. 1961, Publ. astr. Soc. Pacific, 73, 354.
- Rottenberg, J.A. 1952, Mon. Not. R. astr. Soc., 112, 125.
- Sahade, J. 1958, Mem. Soc. R. Sci. Liege, Ser 4e, 20, p. 46.
- Sahade, J. 1980, Astr. Astrophys., 87, L 7.
- Sahade, J. 1981, Rev. Mex. Astr. Astrofis., 6, 189.
- Sahade, J. & Wood, F.B. 1978, in Interacting Binary Stars, Pergamon, p. 101.
- Schild, R.E., Hiltner, W.A., Sanduleak, N. 1969, Astrophys. J., 156, 609.

- Schild, R.E., Neugebauer, G., Westphal, J.A. 1971, Astr. J.,
76, 237.
- Schmidt, G.D. 1974, Publ. astr. Soc. Pacific, 86, 767.
- Schmidt, H., Seggewiss, W. 1976, in Multiple Periodic Variable Stars Ed. W.S.Fitch, Akademiai, Budapest, p. 311.
- Schmutz, W., Smith, L.J. 1980, in Proc. Second. European IUE Conf., Eds B.Battrick & J.Mort, ESA - SP 157, p. 249.
- Schuerman, D.W. 1972, Astrophys. Space. Sci., 19, 351.
- Schumann, J.D., Seggewiss, W. 1975, in IAU Symp. 67: Variable Stars and Stellar Evolution Eds V.E.Sherwood & L.Plaut, D. Reidel, Dordrecht, p. 299.
- Seggewiss, W. 1974a, Publ. astr. Soc. Pacific, 86, 670.
- Seggewiss, W. 1974b, Astr. Astrophys., 31, 211.
- Seggewiss, W., Moffat, A.F.J. 1979, Astr. Astrophys., 72, 332.
- Semeniuk, I. 1968, Acta. Astr., 18, 313.
- Serkowski, L. 1970, Astrophys. J., 160, 1083.
- Singh, M., 1984, Inf. Bull. Var. Stars, No. 2508.
- Sivaraman K.R., Babu, G.S.D., Bappu, M.K.V., Parthasarathy, M. 1979, Mon. Not. R. astr. Soc., 189, 897.
- Smith, H.J., 1955, Ph.D. Thesis, Harvard Univ.
- Smith, L.F., 1968a, in Wolf-Rayet Stars, Eds K.G.Gebbie & R.N.Thomas, NBS SP - 307, p. 21.
- Smith, L.F. 1968b, Mon. Not. R. astr. Soc., 138, 109.
- Smith, L.F. 1968c, Mon. Not. R. astr. Soc., 140, 409.
- Smith, L.F. 1973, in IAU Symp. 49: Wolf-Rayet and High Temperature Stars, Eds M.K.V.Bappu & J.Sahade, D.Reidel, Dordrecht, p. 15.

- Smith, L.F., Kuhl, L.V. 1981, An Atlas of WR Line Profiles
 JILA Report No. 117.
- Sobolev, V.V. 1947, in Moving Envelopes of Stars, Leningrad
 Univ.
- Shylaja, B.S. 1983, Observatory, 103, 203.
- Shylaja, B.S. 1984, Astrophys. Space Sci. 104, 163.
- Shylaja, B.S. 1985, in Workshop on Recent Research on
 Cataclysmic Variables, ESA SP - 236, p. 183.
- Shylaja, B.S., Babu, G.S.D. 1985, Mon. Not. R. astr. Soc.,
 (in press).
- Shylaja, B.S., Bappu, M.K.V. 1983, Kodaikanal Obs. Bull., 3, 72.
- Shylaja, B.S., Bhattacharyya, J.C. 1985, Kodaikanal Obs. Bull.
 (in press)
- Shylaja, B.S., Kochhar, R.K. 1984, Astrophys. Space Sci., 97,
 121.
- Shylaja, B.S., Prabhu, T.P. 1979, Kodaikanal Obs. Bull., 3,
 213.
- Stickland, D.J., Bromage, G.E., Budding, E., Burton, W.M.,
 Howrath, I.D., Jameson, R., Sherrington, M.R.,
 Willis, A.J. 1984, Astr. Astrophys., 134, 45.
- Struve, O. 1944, Astrophys. J., 100, 189.
- Taylor, B.J. 1984, Astrophys. J. Suppl., 54, 167
- Trodahl, H.J., Sullivan, D.J., Beaglehole, D. 1973, Publ. astr.
 Soc. Pacific., 85, 608.
- Tug, H., White, N.N., Lockwood, G.W. 1977, Astr. Astrophys., 61,
 679.

- Tutukov, A.V., Yungelson, L.R. 1979, in IAU Symp. 83: Mass Loss and Evolution of O type Stars, D.Reidel, Dordrecht, p. 401.
- Underhill, A.B. 1968, A. Rev. Astr. Astrophys., 6, 39.
- Underhill, A.B. 1969, in Mass Loss from Stars, Ed. M.Hack, D. Reidel, Dordrecht, p. 17.
- Vanbeveren, D. 1977, Astr. Astrophys., 54, 877.
- Vanbevereven, D., Van Rensbergen, W., de Loore, C. 1982, Astr. Astrophys., 115, 69.
- de Voucouleurs, G. 1965, Publ. astr. Soc. Pacific, 77, 5.
- Vreux, J.M. 1985, Publ. astr. Soc. Pacific, 97, 274.
- Vreux, J.M., Andrillat, Y., Gosset, E. 1985, Astr. Astrophys., 199, 337.
- Walker, E.N., Lloyd, C., Pike, C.D., Stickland, D.J., Zuiderwijk, E.J. 1983, Astr. Astrophys., 128, 394.
- Wendker, H.J., Smith, L.F., Israel, F.P., Habing, H.J., Dickel, H.R. 1975, Astr. Astrophys., 42, 173.
- Willis, A.J. 1980, in Proc. second European Conf. Eds B.Battrick & J. Mort, ESA - SP 157, p. 11.
- Wilson, O.C. 1939, Publ. astr. Soc. Pacific, 51, 55.
- Wilson, O.C. 1942, Astrophys. J., 95, 402.
- Wilson, O.C. 1948, Publ. astr. Soc. Pacific, 60, 383.
- Wright, K.O. 1962, in Astronomical Techniques : Stars and Stellar Systems II, Ed. W.A.Hiltner, Univ. Chicago Press p. 83.
- Zorec, J., Niemela, V.S. 1980, in C.R.Acad. Sci. Paris, Tome 290, Ser B, p. 95.

List of Publications

(* refers to the matter incorporated in the thesis)

1. 'Recent Outburst of U Scorpii'
(with T.P.Prabhu) 1979, Kodaikanal Obs. Bull. Ser A, 2, 213.
2. 'A compilation of the physical parameters of Ap & Am stars'
(with G.S.D.Babu) 1981, Astrophys. Space Sci., 79, 243.
3. 'Spectrophotometric Studies of Ap stars'
(with G.S.D.Babu) 1982, Astrophys. Space Sci., 81, 269.
4. 'Spectrophotometric Studies of Am Stars'
(with G.S.D.Babu) 1982, Astrophys. Space Sci., 83, 367.
5. 'On the radii of Ap and Am Stars'
(with G.S.D.Babu) 1983, Astrophys. Space Sci., 89, 341.
- *6. 'The Absolute Magnitudes of Wolf-Rayet Stars'
(with M.K.V.Bappu) 1983, Kodaikanal Obs. Bull., 3, 104.
7. 'Spectrophotometry of nova Muscae, 1983'
1983, Observatory, 103, 203.
8. 'Comments on the White Dwarf Collapse in Binaries'
(with R.K.Kochhar) 1984, Astrophys. Space Sci., 103, 199.
9. 'Spectrophotometry of nova Corona Austrinae, 1981'
1983, Astrophys. Space Sci., 104, 163.
10. 'Photometry of EX Hydra'
1985, Astrophys. Space Sci., 111, 407.
11. 'The Variation of the 5200 feature in HD 34452'
(with G.S.D.Babu) 1985, Mon. Not. R. astr. Soc., (in press).
12. 'Effective Temperatures of Southern Am Stars'
(with G.S.D.Babu, T.Ghosh, K.Indumathi, P.S.Joarder, S.Shanbag, S.N.Karbelkar)
1985, Bull. astr. Soc. India, 13, 87.
13. 'Spectrophotometry of Comet Crommelyn'
(with G.S.D.Babu, K.R.Sivaraman) 1986, IHW Newsletter, No.8, 25.
14. 'Spectrophotometry of nova Vulpeculae, 1984 No.1'
1985, Recent Results on Cataclysmic Variables, ESA-SP 236, p.183.

- *15. 'Atmospheric Extinction at Kavalur during 1980-85'
(with J.C.Bhattacharyya) 1985, presented at the Commission 50
Meeting of the IAU Assembly, New Delhi, Nov. 1985, submitted
to Kodaikanal Obs. Bull.
- *16. 'Spectrophotometric Studies of CQ Cep'
1986, J. Astrophys. Astr., 7, 171.
- *17. 'Behaviour of $\lambda 4686$ line in WN binaries'
1986, in IAU Symp. 122 Circumstellar Matter (in press).
- 18. 'Photometry of BD -7° 3007'
1986, in IAU Coll. 93 Cataclysmic Variables (in press).
- *19. 'Spectrophotometric Studies of HD 50896'
1986, submitted to J.Astrophys. Astr.
- *20. 'The $\lambda 4686$ line of He II in WR binaries '
1986, submitted to J.Astrophys.Astr.